9
CHAPTER 9
USE OF THE CEUS SSC MODEL IN PSHA

9.1 Overview

This section is intended to provide the reader with information about the future use of the CEUS SSC model for purposes of PSHA. Much of the guidance provided in this section is pragmatic and aimed at assisting the user such that the subsequent calculational process is optimized but the accuracy of the SSC model is maintained. The CEUS SSC model was developed within the framework of a SSHAC Level 3 process, and all the required steps were taken to implement the letter and the spirit of the SSHAC guidelines (Budnitz et al., 1997). Chapter 2 describes those process steps in some detail. A key step in achieving this goal has been the careful consideration of alternative data, models, and methods, and—using the hazard-informed approach discussed in Section 4.1.3.1—incorporating the center, body, and range of technically defensible interpretations into the SSC model. In this sense, the SSC model has been "optimized" to include only those assessments that capture present knowledge and uncertainties and are believed to be significant to hazard. Once this level of uncertainty treatment was reached, there was no further attempt to optimize or reduce the complexity of the model for purposes of subsequent calculational efficiency.

The CEUS SSC model is a regional model, developed explicitly to calculate seismic hazard at nuclear facilities. For site-specific applications—consistent with the applicable regulatory guidance for the nuclear facility of interest—local data sets will need to be reviewed and possible site-specific refinements made to the model to account for local information. This could include consideration of local geologic structures or local seismic sources that were not considered in this regional SSC model. In addition, the SSC model will need to be paired with a comparable ground-motion characterization (GMC) model to perform hazard calculations. The SSC model was developed with due consideration of the likely types of information that would be needed for these GMC models (see Section 5.4). For example, each seismic source is characterized by its style of faulting and likely future rupture geometries.

The end product of the SSHAC process—and the deliverable for PSHA calculations—is the hazard input document (HID), which is discussed below in Section 9.2 and is provided in Appendix H. Instructions for implementing the HID are given in Section 9.3, with an eye toward simplifications that can be made for future applications without sacrificing accuracy. Section 9.4 discusses approaches to define the level of precision incorporated into a hazard analysis. The purpose of this analysis is to identify the changes in hazard that can be considered significant. One application of this concept would be to provide a basis for assessing whether future changes to the model would lead to significant changes in hazard, which in turn would require that the model be updated.

9.2 Hazard Input Document (HID)

The seismic source characterization of the CEUS presented in this report consists of a large and complex model. The report has been structured to give the reader an understanding of the reasoning for the structure of the model and the basis for all the model components. When the time comes for a hazard analysis to implement the model, there is a tremendous amount of material to go through in order to obtain all the model components and link them together for a hazard calculation. One of the innovations of the PEGASOS project (NAGRA, 2004) was creation of the concept of the HID. The purpose of the HID is to provide the analyst with a complete description of how to build the source model and a listing of all the model components in one place. The HID does not contain any discussion of the bases for the model structure and model components (that is, the purpose of the entire report). Rather, the intent of the HID is to provide a clear and unambiguous description of how to implement all the SSC model components that are described in this report.

The HID for the CEUS SSC model is presented in Appendix H. This version of the HID includes references to data files for aspects such as seismic source coordinates, gridded seismicity parameters, and the like. These components of the HID will be made part of the CEUS SSC Project website and will be provided in a suitable structure to provide the analyst access to the volumes of data that constitute these model components.

9.3 Implementation Instructions

The seismic source model developed in this project is based on interpretations over a broad region of eastern North America. Implementation for a specific site in that region, as an input to a PSHA, requires that the local region around the site be examined for additional or alternative interpretations. These might show, for example, evidence for a small geologic feature near the site that might be tectonically active. As another example, a site located near the boundary of two seismic sources described here might be affected by the uncertainty in that boundary, to ensure that its effect on seismic hazard has been properly characterized. This section gives guidance on what simplifications might be made, and on what additional studies might be undertaken, to properly represent seismic hazard.

9.3.1 Simplifications to Seismic Sources

In the HID for seismic sources (Appendix H), the specification includes ranges for thickness of the seismogenic crust, fault dip, orientation of fault strike, geometry of the source, and so on. For example, to calculate seismic hazard, hypocenters are distributed uniformly over the specified seismogenic crustal thickness. Ranges in the above parameters have been included to ensure a complete description of uncertainties in parameters. However, not all variations of parameters for a given source will be influential on seismic hazard at every site. For example, for a site located a great distance from a source, small variations in source geometry (including the extent of the source vertically in the crust) will have a small influence on seismic hazard, compared with other sites.

This section describes several simplifications to seismic sources that can be made to increase efficiency in seismic hazard calculations. These simplifications are recommended on the basis of sensitivity studies of alternative hazard curves that represent a range of assumptions on a parameter's value. Sensitivities are presented using the test sites in the CEUS SSC Project (see

Figure 8.1-1 for a map of these test sites). For applications of the seismic sources from the CEUS SSC Project, similar sensitivity studies should be conducted for the particular site of interest to confirm these results and to identify additional simplifications that might be appropriate. For the seismic sources below, only parameters that can be simplified are discussed and presented graphically.

The sensitivity studies consisted of determining the sensitivity of hazard to logic tree branches for each node of the logic tree describing that source. The purpose was to determine which nodes of the logic tree could be collapsed to a single branch, to achieve more efficient hazard calculations without compromising the accuracy of overall hazard results. The sensitivity calculations were performed at the project test sites for 1 Hz, 10 Hz, and PGA; the results for 1 Hz and 10 Hz are shown below.

For many comparisons in this section, a difference in hazard of 25% is mentioned as a threshold. Many comparisons show less sensitivity of less than 25%. Section 9.4 gives a more detailed and quantitative description of what constitutes a significant difference in hazard.

9.3.1.1 Charleston RLME

A sensitivity study was performed at the Savannah test site using Appendix H. Note that any sensitivities to alternative geometries in the Charleston RLME source model will be accentuated at Savannah because it lies close to the Charleston RLME source. Sites more distant to this source will show less sensitivity to alternative geometries.

Level: Rupture Orientation

For the regional source, there are two rupture orientations outlined in the Charleston RLME source model HID logic tree. Ruptures are oriented either parallel to the long axis of the source (northeast) or parallel to the short axis of the source (northwest), with weights of 0.8 and 0.2, respectively. The results from the sensitivity analysis show that, at the 10^{-5} ground motion, the difference in hazard between the two curves representing these two orientations is less than 25% (Figures 9.3-1 and 9.3-2). At the 10^{-5} ground motion, the percent difference between the weighted mean average hazard and the selected northeast orientation is less than 5%, indicating that mean hazard at Savannah is not significantly affected by having two alternative rupture orientations for the regional source. The northeast rupture orientation was selected as the orientation that will represent this level of the logic tree for three reasons: it was assigned the highest weight, the two other alternative geometries in the Charleston RLME source model also have northeast rupture orientations, and the northeast rupture orientation gives slightly more conservative hazard than the northwest rupture orientation, at least for the Savannah site.

9.3.1.2 Charlevoix RLME

A sensitivity study was performed at the Manchester test site using Appendix H.

Level: Seismogenic Thickness

For the Charlevoix area source, there are two seismogenic thicknesses outlined in the Charlevoix RLME source model HID logic tree. The seismogenic thicknesses are 25 and 30 km (15.5 and 18.6 mi.), with weights of 0.8 and 0.2, respectively. The results from the sensitivity analysis show that, at the 10^{-5} ground motion, the difference in hazard between the two curves representing the seismogenic thicknesses is less than 10% (Figures 9.3-3 and 9.3-4), indicating that hazard at Manchester is not significantly affected by having two alternative seismogenic thicknesses for the area source. A thickness of 25 km (15.5 mi.) was selected as the seismogenic thickness that will represent this level of the logic tree because it has the highest weight and is the more conservative of the two thicknesses.

Level: Rupture Orientation

For the Charlevoix area source, there is a range of fault dips outlined in the Charlevoix RLME source model HID logic tree. The dips of the faults range from 40° to 60° (modeled as 40°, 50°, and 60°, with weights of 0.333, 0.334, and 0.333, respectively, in the sensitivity analysis). The results from the sensitivity analysis show that, at the 10^{-5} ground motion, the difference in hazard between the three curves representing the three fault dips is less than 10% (Figures 9.3-5 and 9.3-6), indicating that mean hazard at Manchester is not significantly affected by having three alternative fault dips for the area source. The 50° dip was selected as the orientation that will represent this level of the logic tree because it is the average of the three dips.

9.3.1.3 Cheraw RLME

A sensitivity study was performed at the Topeka test site using Appendix H.

Level: Seismogenic Thickness

For the fault source, there are three seismogenic thicknesses outlined in the Cheraw RLME source model HID logic tree. The seismogenic thicknesses are 13, 17, and 22 km (8, 10.6, and 13.7 mi.), with weights of 0.4, 0.4, and 0.2, respectively. The results from the sensitivity analysis show that, at the 10^{-5} ground motion, the total range in hazard among the three curves representing these three seismogenic thicknesses is less than $\pm$20% (Figures 9.3-7 and 9.3-8). The weighted mean average hazard, at the 10^{-5} ground motion, from these three hazard curves is within 2% of the central curve (17 km, or 10.6 mi.), indicating that the mean hazard at Topeka (using three alternative seismogenic thicknesses) is not significantly different from the hazard using the central curve only. Therefore, the thickness of 17 km (10.6 mi.) was selected as the seismogenic thickness that will represent this level of the logic tree. It is worth pointing out that the thickest crustal assumption indicates the highest hazard because some specifications of fault activity for the Cheraw fault are made using fault slip rate. For a given slip rate, a thicker seismogenic crust implies more fault area, which results in more seismic activity and higher seismic hazard.

Level: Rupture Orientation

For the fault source, there are two rupture orientations outlined in the Cheraw RLME source model HID logic tree. The dip of the fault is either 50°NW or 65°NW, with weights of 0.6 and 0.4, respectively. The results from the sensitivity analysis show that, at the 10^{-5} ground motion, the difference in hazard between the two curves representing these two orientations is less than 10% (Figures 9.3-9 and 9.3-10), indicating that hazard at Topeka is not significantly affected by having two alternative rupture orientations for the fault source. The 50°NW dip was selected as the orientation that will represent this level of the logic tree because it was assigned the highest weight and is the more conservative of the two dips.

9.3.1.4 Commerce Fault Zone RLME

A sensitivity study was performed at the Jackson test site using Appendix H.

Level: Seismogenic Thickness

For the area source, there are three seismogenic thicknesses outlined in the Commerce Fault Zone RLME source model HID logic tree. The seismogenic thicknesses are 13, 15, and 17 km (8, 9.3, and 10.6 mi.), with weights of 0.2, 0.5, and 0.3, respectively. The results from the sensitivity analysis show that, at the 10^{-5} ground motion, the difference in hazard between the three curves representing these three seismogenic thicknesses is less than 10% (Figures 9.3-11 and 9.3-12), indicating that mean hazard at Jackson is not significantly affected by having three alternative seismogenic thicknesses for the area source. A thickness of 15 km (9.3 mi.) was selected as the seismogenic thickness that will represent this level of the logic tree because it is approximately the average of the three thicknesses.

9.3.1.5 Eastern Rift Margin North RLME

A sensitivity study was performed at the Jackson test site using Appendix H.

Level: Seismogenic Thickness

For the area source, there are three seismogenic thicknesses outlined in the ERM-N RLME source model HID logic tree. The seismogenic thicknesses are 13, 15, and 17 km (8, 9.3, and 10.6 mi.), with weights of 0.2, 0.5, and 0.3, respectively. The results from the sensitivity analysis show that, at the 10^{-5} ground motion, the difference in hazard between the three curves representing these three seismogenic thicknesses is less than 10% (Figures 9.3-13 and 9.3-14), indicating that mean hazard at Jackson is not significantly affected by having three alternative seismogenic thicknesses for the area source. A thickness of 15 km (9.3 mi.) was selected as the seismogenic thickness that will represent this level of the logic tree because it is approximately the average of the three thicknesses.

9.3.1.6 Eastern Rift Margin South RLME

A sensitivity study was performed at the Jackson test site using Appendix H.

Level: Seismogenic Thickness

For the area source, there are three seismogenic thicknesses outlined in the ERM-S RLME source model HID logic tree. The seismogenic thicknesses are 13, 15, and 17 km (8, 9.3, and 10.6 mi.), with weights of 0.2, 0.5, and 0.3, respectively. The results from the sensitivity analysis show that, at the 10^{-5} ground motion, the difference in hazard between the three curves representing these three seismogenic thicknesses is less than 20% (Figures 9.3-15 and 9.3-16). At the 10^{-5} ground motion, the percent difference between the weighted mean average hazard and the central value (15 km, or 9.3 mi.) is less than 1%, indicating that mean hazard at Jackson is not significantly affected by having three alternative seismogenic thicknesses for the area source. A thickness of 15 km (9.3 mi.) was selected as the seismogenic thickness that will represent this level of the logic tree because it is approximately the average of the three thicknesses.

9.3.1.7 Marianna RLME

A sensitivity study was performed at the Jackson test site using Appendix H.

Level: Seismogenic Thickness

For the area source, there are three seismogenic thicknesses outlined in the Marianna RLME source model HID logic tree. The seismogenic thicknesses are 13, 15, and 17 km (8, 9.3, and 10.6 mi.), with weights of 0.2, 0.5, and 0.3, respectively. The results from the sensitivity analysis show that, at the 10^{-5} ground motion, the difference in hazard between the three curves representing these three seismogenic thicknesses is less than 20% (Figures 9.3-17 and 9.3-18). At the 10^{-5} ground motion, the percent difference between the weighted mean average hazard and the central value (15 km, or 9.3 mi.) is less than 1%, indicating that mean hazard at Jackson is not significantly affected by having three alternative seismogenic thicknesses for the area source. A thickness of 15 km (9.3 mi.) was selected as the seismogenic thickness that will represent this level of the logic tree because it is approximately the average of the three thicknesses.

9.3.1.8 Meers RLME

A sensitivity study was performed at the Topeka and Houston test sites using Appendix H.

Level: Seismogenic Thickness

For both the Meers fault source and Oklahoma Aulacogen (OKA) area source that make up the Meers RLME source, there are two seismogenic thicknesses outlined in the Meers RLME source model HID logic tree. The seismogenic thicknesses are 15 and 20 km (9.3 and 12.4 mi.), each with a weight of 0.5. The results from the sensitivity analysis show that, at the 10^{-5} ground motion, the difference in hazard between the two curves representing these two seismogenic thicknesses is less than 10% (Figures 9.3-19 through 9.3-22), indicating that mean hazards at Topeka and Houston are not significantly affected by having two alternative seismogenic thicknesses for the fault and area source. A thickness of 15 km (9.3 mi.) was selected as the seismogenic thickness that will represent this level of the logic tree because it is the more conservative value.

Level: Rupture Orientation

For the OKA area source, there is a range of rupture orientations outlined in the Meers RLME source model HID logic tree. Ruptures are oriented N60°W $\pm$ 15°, parallel with the long axis of the area source (modeled as N50°W, N60°W, and N70°W, with weights of 0.333, 0.334, and 0.333, respectively, for the sensitivity analysis at Houston). The results from the sensitivity analysis show that, at the 10^{-5} ground motion, the difference in hazard between the two curves (N60°W and N60°W $\pm$ 15°) representing these two orientations is less than 10% (Figures 9.3-23 and 9.3-24), indicating that mean hazard at Houston is not significantly affected by having two alternative rupture orientations for the OKA area source. An orientation of N60°W was selected as the value that will represent this level of the logic tree because it is the average value.

For the OKA area source, there is a range of fault dips outlined in the Meers RLME source model HID logic tree. The dips of the faults range from 40° to 90° (modeled as 40°, 50°, 60°, 65°, 70°, 80°, and 90°, with weights of 0.143 in the sensitivity analysis). The results from the sensitivity analysis show that, at the 10^{-5} ground motion, the difference in hazard between the seven curves representing the seven fault dips is less than 10% (Figures 9.3-25 through 9.3-28), indicating that mean hazards at Topeka and Houston are not significantly affected by having seven alternative fault dips for the OKA area source. The 65°SW dip was selected as the orientation that will represent this level of the logic tree because it is the average value.

For the Meers fault source, there are two rupture orientations outlined in the Meers RLME source model HID logic tree. The dip of the fault is either 90° (vertical) or 40°SW, both with weights of 0.5. The results from the sensitivity analysis show that, at the 10^{-5} ground motion, the difference in hazard between the two curves representing these two orientations is less than 10% (Figures 9.3-29 through 9.3-32), indicating that mean hazard at Topeka and Houston is not significantly affected by having two alternative rupture orientations for the fault source. The 90° dip was selected as the orientation that will represent this level of the logic tree because it is the simpler model.

9.3.1.9 New Madrid Fault System RLME

A sensitivity study was performed at the Jackson test site using Appendix H.

Level: Seismogenic Thickness

For all fault sources, there are three seismogenic thicknesses outlined in the NMFS RLME source model HID logic tree. The seismogenic thicknesses are 13, 15, and 17 km (8, 9.3, and 10.6 mi.), with weights of 0.2, 0.5, and 0.3, respectively. The results from the sensitivity analysis show that, at the 10^{-5} ground motion, the difference in hazard of the three curves representing these three seismogenic thicknesses is less than 10% (Figures 9.3-33 and 9.3-34), indicating that mean hazard at Jackson is not significantly affected by having three alternative seismogenic thicknesses for the fault sources. A thickness of 15 km (9.3 mi.) was selected as the seismogenic thickness that will represent this level of the logic tree because it is approximately the average of the three thicknesses.

9.3.1.10 Wabash Valley RLME

A sensitivity study was performed at the Central Illinois test site using Appendix H.

Level: Seismogenic Thickness

For the area source, there are two seismogenic thicknesses outlined in the Wabash Valley RLME source model HID logic tree. The seismogenic thicknesses are 17 and 22 km (10.6 and 13.7 mi.), with weights of 0.7 and 0.3, respectively. The results from the sensitivity analysis show that, at the 10^{-5} ground motion, the difference in hazard between the two curves representing these two seismogenic thicknesses is less than 10% (Figures 9.3-35 and 9.3-36), indicating that mean hazard at Central Illinois is not significantly affected by having two alternative seismogenic thicknesses for the area source. A thickness of 17 km (10.6 mi.) was selected as the seismogenic thickness that will represent this level of the logic tree because it has the highest weight and is the more conservative of the two thicknesses.

Level: Rupture Orientation

For the area source, there are multiple rupture orientations (outlined in e-mails from Kathryn Hanson on June 9 and 20, 2010) that replace the rupture orientations outlined in the Wabash Valley RLME source model HID logic tree. Ruptures in the area source are to be modeled in three ways: parallel to the long axis of the source zone (which is oriented N51°E); N50°W; and

N20°W, with weights of 0.8, 0.1, and 0.1, respectively. For the ruptures oriented parallel to the long axis, the dips of the faults are vertical or 40°NW to 60°NW (modeled as 40°NW, 50°NW, and 60°NW), with weights of 0.666, 0.111, 0.112, and 0.111, respectively. For ruptures oriented N50°W, the dips of the faults are vertical. For the ruptures oriented N20°W, the dips of the faults are oriented 40°SW to 60°SW (modeled as 40°SW, 50°SW, and 60°SW), with weights of 0.333, 0.334, and 0.333, respectively.

The results from the sensitivity analysis show that, at the 10^{-5} ground motion, the hazard at Central Illinois is sensitive to the three rupture orientations and, therefore, this level of the logic tree will not be collapsed. However, the results from the sensitivity analysis show that, at the 10^{-5} ground motion, the difference in hazard between dips for each fault orientation is less than 10% (Figures 9.3-37 and 9.3-38), indicating that mean hazard at Central Illinois is not significantly affected by having one dip for each of the fault orientations for the area source. Therefore, one dip can be selected for the two fault orientations that have multiple dips: ruptures oriented parallel to the long axis and ruptures oriented N20°W. For ruptures oriented parallel to the long axis, a dip of 90° was selected (vertical faults) because it was assigned the highest weight (0.666) and is the simpler model. For the ruptures oriented N20°W, a dip of 50°SW was selected because it is the average of the three dips.

9.3.1.11 Background Sources

A sensitivity study was performed at the Central Illinois test site using Midcontinent A as a background source. For this sensitivity study, the focus was on determining the influence of fault ruptures on seismic hazard vs. using point sources within background sources to represent earthquake energy release. For the fault rupture model, multiple fault orientations, dips, and seismogenic depths are used in each background source characterization. In the hazard calculations, ruptures are represented explicitly, and the appropriate distance to the rupture is calculated for the ground motion equations. For the point source model, earthquake occurrences are represented as point sources, and correction factors are used (as published in EPRI, 2004) to modify the distance from the point-source distance to an equivalent rupture distance, and to increase aleatory uncertainties in ground motion estimates to account for random rupture orientation.

Figures 9.3-39 and 9.3-40 compare seismic hazards at the Central Illinois test site for the two models. For ground motions with a frequency of exceedence greater than 10^{-5} per year, the difference is less than 10%. Given that background sources generally make up only a fraction of the total hazard, using the point source model for background sources is an acceptable approximation. The fault rupture model is fully documented and available if future ground motion equations require the fault rupture geometry to be specified explicitly.

9.3.2 Accessing the SSC Model and Components from the Website

A hazard input document (HID) was developed for the CEUS SSC Project that documents the SSC model, including logic trees, parameter distributions, and derived Mmax and recurrence parameters. The HID specifies the inputs provided by the SSC model to the hazard calculations, providing a clear and complete record of how the SSC model is translated into hazard calculations. The HID is presented in Appendix H of the CEUS SSC Report, which is available on the CEUS SSC website at www.ceus-ssc.com.

The HID provides sufficient documentation for users to implement the SSC model in PSHA calculations for future applications. Demonstration hazard calculations were made at seven test sites to illustrate the effects of seismic sources on calculated seismic hazard and to compare hazards calculated using other SSC models. The demonstration hazard calculations are provided in Chapter 8 of this report; these can be used to confirm the seismic hazard results calculated by other hazard analysts using their hazard calculation software.

9.3.3 Accessing Project Databases

The data for the CEUS SSC Project were managed and documented in accordance with a data management procedure developed specifically for the project; this procedure is discussed in Task 2 of the CEUS SSC Project Plan, *Develop a Database*, and is described in further detail in Appendix A of the CEUS SSC Report. The CEUS SSC Project Plan, the project databases, and the CEUS SSC Report are available on the CEUS SSC website, www.ceus-ssc.com.

The CEUS SSC Project databases were compiled to organize and store those data and resources that were carefully and thoroughly collected and described for the TI Team's use in characterizing potential seismic sources in the CEUS. Development of the project database began at the inception of the project, and continued throughout the project using new references and data collected by the TI Team and project subcontractors. These updates included information from several sources, including presentations at project workshops by resource experts and proponents and review documentation provided by the PPRP.

Listed below are the contents of the CEUS SSC website, all of which are accessible.

- CEUS SSC Report
- HID data necessary to implement the CEUS SSC model
- Project GIS database including magnetic, gravity and stress data compiled for the CEUS SSC Project
- Project paleoliquefaction database
- Complete CEUS SSC earthquake catalog
- Bibliography (master list of all references used during the project, also provided in Chapter 10 of the CEUS SSC report)
- New computer code used to smooth *a* and *b* values
- All stakeholder and non-PPRP reviewer comments and correspondence, including response tables (Note: PPRP comments and correspondence are in Appendix I of the CEUS SSC Report)
- CEUS SSC Project Plan dated June 2008
- Information from Workshops 1–3, including meeting agendas, lists of participants, summaries, presentations, and a photo album of participants

Note that the project GIS database is provided in a format that will allow other investigators to use the CEUS SSC database in subsequent CEUS seismic hazard assessments.

9.3.4 Use of SSC Model with Site-Specific Refinements

The seismic source characterization developed under this project is a regional characterization of seismic sources, useful as a starting point for site-specific calculations. Any site-specific application will need to be conducted according to the applicable regulatory guidance for the nuclear facility of interest (e.g., NRC Regulatory Guide 1.208, ANSI/ANS-2.27-2008). These guidance documents typically require the development of a site-specific database that might include local geologic, tectonic, geophysical, seismicity, and paleoseismic data indicative of local seismic sources that could affect the site.

9.4 Hazard Significance

A PSHA integrates a range of SSC and GMC input models and parameters, which, collectively, represent current knowledge and uncertainties. After a PSHA is completed, it is expected that new data, models, and methods will subsequently emerge within the technical community. Some of those data, models, and methods may have implications to the existing PSHA model and some will not. This section presents an approach to assessing the significance of new findings that result in new inputs to the PSHA. The approach looks at the quantitative precision in seismic hazard implied by prior studies, and derives *minimum* estimates of hazard uncertainty to use as a guide in assessing the significance of future changes to seismic hazard estimates.

9.4.1 Data Available to Evaluate the Precision of Seismic Hazard Estimates

The purpose of this section is to investigate what level of precision should be associated with seismic hazard estimates in the CEUS. In other words, how might the seismic hazard estimates change if the analysis were to be repeated with independent experts who have access to the same basic information (geology, tectonics, seismicity, ground motion equations, site characterization)? In effect, we are asking, how precise are the estimates of seismic hazard? If a data set or interpretation were to change, and that change were to cause a change in the assessed seismic hazard, how would we judge whether that change in hazard were significant or insignificant? So the question of significance is closely linked to the level of precision with which we can assess seismic hazard.

Three fundamental sets of information contribute to the precision of seismic hazard estimates:

1. Seismic sources and parameters, which may be derived by individuals or teams of experts.
2. Ground motion equations, which are generally derived by a single expert or team using available equations but are sometimes derived by multiple experts.
3. Site response estimates, which are generally derived by a single expert but are sometimes derived by multiple experts.

A realistic assumption can be made that, for seismic hazard analysis at a site, these information inputs are separate and independent. It is understood that ground motion equations are developed for a wide range of magnitudes and distances, and that site response estimates are developed for a wide range of input motions. Additionally, it is assumed that we are interested in the precision of the *mean* seismic hazard curves, rather than any particular fractile. The mean seismic hazard curve is used to make decisions regarding design levels for nuclear facilities.

Estimates of the precision in mean hazard associated with each of these inputs can be made by examining existing seismic hazard results from published studies. Table 9.4-1 indicates available studies that can be used for this purpose.

The underlying concept is that we can estimate the uncertainty in mean hazard from available studies by examining the variability in hazard caused by team-to-team variations or expert-to-expert variations in hazard. For example, if six teams are used to derive seismic sources for a hazard estimate, there will be a distribution of total hazard (i.e., annual frequency of exceedance) for a given ground-motion amplitude. This distribution will have a standard deviation σ_{TH} caused by team-to-team variability, and this standard deviation can be calculated using the conditional total hazard curves for each team. The uncertainty in *overall mean* hazard σ_{MH} caused by the different seismic source interpretations is $\sigma_{MH} = \sigma_{TH}/\sqrt{6}$, assuming the teams' hazard estimates are uncorrelated. We put aside questions of team-to-team correlation that result from common data sets, availability of published papers, and similar items, because this correlation is a condition under which we are evaluating the precision of hazard. Similar "independent" teams would have access to the same data sets and published papers.

As additional background, note that the term *mean hazard* has several meanings. The total hazard curve calculated for one team, or one ground-motion equation, or some other assumption, is a *conditional mean* hazard curve. This curve, along with others, is used to calculate σ_{TH}. The family of *conditional mean* hazard curves is used, with weights, to calculate an *overall mean* hazard curve. We are interested in the uncertainty σ_{MH} in this overall mean.

9.4.2 Observed Imprecision in Seismic Hazard Estimates

The imprecision inherent in seismic hazard calculations from past studies provides a guide as to what levels of precision we should associate with current or future studies. To this end, we use the coefficient of variation (COV) of the mean annual frequency of exceedance (the mean hazard) as the fundamental estimate of how precise or imprecise the estimates of mean hazard are. The COV is the calculated standard deviation (σ) of mean hazard divided by the mean hazard, and is a good measure of how precisely we can characterize the mean hazard. When used in this sense, the coefficient of variation is designated COV_{MH}.

9.4.2.1 Area Seismic Sources

Figures 9.4-1 and 9.4-2 show the calculated COV_{MH} as a function of ground motion amplitude and seismic hazard (i.e., annual frequency of exceedance), respectively, for study (1A) in Table 9.4-1. These COV_{MH} values were calculated at the seven test sites using only hazard from the six EPRI (1989) team interpretations of seismic sources, and do not include hazard from the New Madrid and Charleston RLME sources. At some sites (e.g., Manchester), RLME sources such as the Charlevoix zone are distant, and area sources dominate the hazard. At other sites (e.g., Savannah), the RLME hazard is dominant because the site lies very close to a seismic source zone (the Charleston seismic zone, in the case of Savannah) and the area sources contribute relatively less hazard. COV_{MH} tends to increase with decreasing annual frequency; between 10^{-4} and 10^{-6} (the mean hazard range of interest) it ranges from about 0.1 to 0.4.

Figure 9.4-3 shows COV_{MH} at four Swiss nuclear power plant sites (i.e., Beznau, Goesgen, Leibstadt, and Muehleberg) studied during the PEGASOS project (study 1B in Table 9.4-1). In that project, four experts developed seismic source interpretations. Based on these four interpretations, Figure 9.4-3 (top) plots COV_{MH}, calculated from the standard deviation of hazard σ_{MH} at each amplitude, as $\sigma_{MH} = \sigma_{TH}/\sqrt{4}$. Results from the PEGASOS project are available only for peak ground acceleration (PGA) and spectral acceleration at 1 Hz. For mean annual frequencies in the range of 10^{-4} to 10^{-6}, COV_{MH} ranges from about 0.13 to 0.3, with one set of results (PGA for Goesgen) falling as low as 0.05 (see the solid blue curve on Figure 9.4-3 top and bottom).

Regarding imprecision in seismic hazard estimates for area seismic sources, the conclusion from Figures 9.4-1 through 9.4-3 is that typical COV_{MH} values will range from perhaps 0.15 to 0.3 at a mean annual frequency of 10^{-4} to perhaps 0.2 to 0.4 at a mean annual frequency of 10^{-6}, with a wide variation in that range. A typical minimum COV_{MH} is 0.1, with one result (i.e., Goesgen PGA on Figure 9.4-3b) falling below that minimum.

9.4.2.2 RLME Seismic Sources

For seismic hazard calculations in the CEUS, two sources of RLME are the Charleston seismic zone and the New Madrid seismic zone. Nuclear plant seismic hazard studies have relied on two interpretations for these RLME sources: the WLA model (Southern Nuclear, 2008) for the Charleston seismic zone and the Geomatrix model (Exelon, 2003) for the New Madrid seismic zone. A general representation of the logic tree representing uncertainties in the Charleston seismic zone model is given in Table 9.4-2. For many sites in the southeastern United States, seismic hazard will be dominated by this source, rather than by area sources represented by multiple interpretations. COV_{MH} values for area sources were described in the previous section, but for sites dominated by RLMEs, it is reasonable that there is some uncertainty in the mean hazard coming from the RLME, even though only one interpretation is currently used (e.g., Table 9.4-2).

It is notable that weights on alternatives are generally given to one-decimal-place precision, and that while these weights indicate quantitative preferences on alternatives, an independent evaluation by another investigator might assign somewhat different weights (both because the weights themselves are imprecise and because a different investigator might assign substantially different weights). Because alternative weights would change the mean hazard at a site, there is imprecision in the current estimates of mean hazard from the base-case model.

To determine the potential effect of alternative weights, an adaptation of the statistical bootstrap technique (e.g., Efron, 1982) was used. This application has the underlying assumption that the weights given to alternative interpretations (e.g., in Table 9.4-2) are variables with distributions. It is reasonable that, to estimate a *minimum* variation on the weights given in Table 9.4-2, we should pick a COV_{WT} for the weights that correspond to a change of 0.1 in the highest weight among the alternatives for each interpretation, because this is the precision with which weights were assigned. Designating this coefficient of variation COV_{WT}, we calculate the following values:

Source geometry	COV_{WT} = 0.1/0.7 = 0.143
Maximum magnitudes	COV_{WT} = 0.1/0.3 = 0.333
Paleoseismic record length	COV_{WT} = 0.1/0.8 = 0.125
Activity rate given record	COV_{WT} = 0.1/0.4 = 0.25

The statistical bootstrap method consisted of generating random weights for the alternative interpretations given in Table 9.4-2, using the listed values as mean values and using the COV_{WT} given above to calculate standard deviations for the weights. A normal distribution for weights was assumed, truncated at 0 and 1. For each interpretation, the random weight for the alternative with the highest mean weight was generated first, and weights for the other alternatives followed. The values of these other weights are not independent, but instead depend on previously generated weights. In particular, they must sum to unity.

The paleoseismic record length is an easy example to explain because it has only two alternatives. The weight for the preferred alternative, W_1, is generated from a normal distribution with a mean of 0.8 and a standard deviation of 0.1. The weight for the other alternative, W_2, is simply 1-W_1. For 100 samples these assumptions result in the following statistics:

	W_1	W_2
Mean	~0.8	~0.2
Standard deviation	~0.1	~0.1
COV_{WT}	~0.125	~0.5

Since mean seismic hazard is linearly proportional to the weights given to alternative interpretations, the effect on COV_{MH} for W_1 and W_2 will depend on the relative contributions of the alternative interpretations to mean hazard. (As one example of a trivial case, if the mean hazard for each alternative paleoseismic record length is the same, then uncertainty in W_1 and W_2 will result in zero uncertainty in mean hazard.)

For the interpretations in Table 9.4-2 with four or five alternatives, the bootstrap application generates a random weight for the preferred alternative first, followed by the next -preferred alternative, and so on. Any symmetry in the weights (e.g., in the maximum magnitude distribution) is maintained, so that the overall mean is maintained. The mean weight of the second -preferred alternative is adjusted downward if the random weight of the preferred alternative exceeds its mean, by the ratio (1-W_1)/(1-mean[W_1]). This has the effect of maintaining a near-normal (truncated) distribution shape for the less-preferred alternatives. The last weight is set equal to one minus the sum of previous weights, so that the weights sum to unity.

The total mean hazard (annual frequency of exceedance) is the sum of weighted hazards from the available alternatives. For example, for the alternative geometries with four alternatives,

$$\text{mean}(H) = W_1 H_1 + W_2 H_2 + W_3 H_3 + W_4 H_4 \qquad (9\text{-}1)$$

where the H_i's are the mean hazard conditional on geometry i. In the current context, the H_i's are constant and the W_i's are random variables, so that

$$\text{mean (H)} = \Sigma_i \, E[W_i]H_i \tag{9-2}$$

(where *E[.]* indicates expectation) and

$$\sigma_k^2 \text{ (H)} = \Sigma \, \sigma_i^2 \, H_i^2 + 2 \, \Sigma_i \, \Sigma_{j>i} \, H_i \, H_j \, cov(W_i, W_j) \tag{9-3}$$

where σ is standard deviation, *cov* is covariance, *k* indicates a specific interpretation from Table 9.4-2, and the σ_i's, H_i's, and W_i's are with respect to alternatives for that interpretation. The W_i's are correlated because, for example, a higher-than-mean value of W_1 will generally be associated with lower-than-mean values of the other W_i's, since they must sum to unity. The covariance of the W_i's can be estimated from samples generated using the bootstrap technique.

To calculate the total variance of the mean hazard (designated here as σ_{MH}^2), we assume that the contributions from the four alternatives in Table 9.4-2 are independent. This is an explicit assumption in the logic tree summarized in Table 9.4-2 (e.g., the maximum magnitude alternatives and weights apply to all geometries). We also assume that effects of uncertainties in parameters are multiplicative on hazard. For example, if a variation of weights on alternative rates reduces the hazard by 20%, and a variation of weights on alternative geometrics increases the hazard by 10%, the total effect on hazard would be 0.8 × 1.1 = 0.88.

Because hazard values of interest vary over several orders of magnitude, it is convenient to present uncertainties as COV_{MH}, which for total hazard H_T is defined as follows:

$$COV_{MH} = \sigma_{MH} / E[H_T] \tag{9-4}$$

Under the independence assumption, COV_{MH} can be estimated as follows:

$$COV_{MH}^2 \simeq COV_{GEOM}^2 + COV_{Mmax}^2 + COV_{SEIS}^2 + COV_{RATE}^2 \tag{9-5}$$

where Equation 9-5 neglects cross-product terms involving the COVs that are small.

Figures 9.4-4 through 9.4-6 present COV_K (where K represents GEOM, Mmax, etc.) and COV_{MH} for PGA, 10 Hz, and 1 Hz spectral accelerations, respectively, for the Charleston model developed by WLA (Southern Nuclear, 2008). These plots were calculated using hazard results at a generic site located in Columbia, South Carolina, from only the Charleston source. From these figures it is evident that the alternative Mmax distribution dominates the uncertainty in mean hazard, except at low amplitudes (i.e., at high annual frequencies of exceedance).

From Figures 9.4-4 through 9.4-6, the COV_{MH} for annual frequencies in the range of 10^{-4} to 10^{-6} is 0.25 to 0.45, with a minimum of 0.25.

Figure 9.4-7 shows a similar comparison of hazard sensitivity at the Jackson site to New Madrid alternatives, which include Mmax, seismicity rate, and alternative geometries for the three faults in the New Madrid region (designated "RFgeom" for the Reelfoot fault, "NNgeom" for the New Madrid North fault, and "NSgeom" for for the New Madrid South fault). A cluster model (Exelon, 2003) is used to calculate hazard.

Unlike the results for Charleston, the results for the New Madrid model indicate that uncertainty in the rate of seismicity is the dominant contributor to uncertainty in hazard. The sensitivity to Mmax is low because, when one fault produces a high characteristic magnitude, other faults may produce a low characteristic magnitude during the cluster of earthquakes. COV_{MH} is about 0.25 for all amplitudes, and this result will be consistent across spectral frequencies because seismicity rate affects hazard equally across spectral frequencies.

9.4.2.3 Ground Motion Equations

As indicated in Table 9.4-1, direct estimates of the uncertainty in seismic hazard caused by different interpretations of ground motion equations are available using three studies (labeled 2A, 2B, and 2C in Table 9.4-1): EPRI (2004), PEGASOS (NAGRA, 2004), and USGS (Petersen et al., 2008). These studies are described below.

EPRI Equations. Hazards calculated with the the EPRI (2004) ground motion equations were analyzed in a fashion similar to the Charleston seismic source, i.e., using an application of the statistical bootstrap technique. Weights given in EPRI (2004) for the various ground-motion equations depend on whether ground motions from a general source or an RLME source are being modeled, as shown in Table 9.4-3.

The ground motion models for general sources and RLME sources are used in hazard calculations in specific combinations; they are not independent.

We applied the statistical bootstrap procedure to generate random weights using the following principles:

1. The mean weights are the weights given in Table 9.4-3.
2. Weights are assigned a normal distribution.
3. Uncertainties in the randomly generated weights were controlled using standard deviations that are 0.3, 0.5, and 0.7 times the mean weight (these choices are designated "COV_{WT}" below).
4. Equations with equal weights (e.g., C1 and C3) kept this characteristic.
5. Weights for the last pair of equally weighted equations (e.g., for C7 and C9 of the general source equations) were chosen so that the sum of all weights was unity.

Under principle 3 above, the COV_{WT} values were chosen using the following reasoning. A typical weight on the higher-weighted equations in Table 9.4-3 is 0.2, and it seems reasonable that an alternative study of ground motions would assign weights for these preferred equations in the range of 0.1 to 0.3, about two-thirds of the time. Stated another way, given today's knowledge, if several equations had weights of 0.2, and those equations were re-weighted by another study, it is unlikely that the revised weights would be less than 0.1 or greater than 0.3; these cases might occur for one-third of the equations, but the other two-thirds would have results within $\pm$0.1 of the original weight of 0.2. This supports the COV_{WT} of 0.5; the alternative values of 0.3 and 0.7 are calculated to show sensitivity to this choice.

Results are presented separately for sites dominated by general sources and RLME sources, to better understand any differences caused by these two cases. The variance of mean hazard σ_{MH}^2 that results from these random weights is calculated using Equation 9-3 above, and COV_{MH} is calculated (at each ground-motion amplitude) by dividing σ_{MH} by the mean hazard at that amplitude.

General Sources. As an example of hazard results affected by general sources, Figure 9.4-8 shows PGA seismic hazard curves for the Manchester test site, for each of the nine general-source ground-motion equations. Curves are also shown for the mean hazard, for "sigma," which is the standard deviation of total hazard σ_{TH}, and for "classical mean sigma," the classical standard deviation of the mean, an estimate of the standard deviation of mean hazard as if the hazards from each ground-motion equation were independent. While this assumption does not hold, it is a useful comparative curve. It is calculated as $\sigma_{MH} \times \sqrt{\Sigma W_i^2}$, where W_i are the weights given in Table 9.4-3. (This is equivalent to calculating the standard deviation of the mean of a group of equally weighted observations using $\sigma/\sqrt{n}$.) This estimate is designated as σ_{CL} here.

Figure 9.4-9 shows the COV_{MH} from ground motion equations plotted vs. PGA level for the Manchester site, for the two methods of calculating COV_{MH} (the classical mean sigma divided by the mean, designated as COV_{CL}, and the bootstrap procedure, designated by the values of COV_{WT}). At PGA amplitudes above 0.2 g, all measures of COV_{MH} increase. This is consistent with the hazard plot on Figure 9.4-8, which shows that the relative range of hazard increases for those amplitudes, and the sigma estimates increase relative to the mean hazard.

Figure 9.4-10 plots COV_{MH} of PGA hazard vs. mean hazard for the Manchester site. Typically, the range of hazards from 10^{-4} to 10^{-6} are of most interest in seismic hazard studies for nuclear plants, and in this range, even the lowest assumption on COV_{WT} (COV_{WT} = 0.3) indicates that COV_{MH} is between 0.1 and 0.4. The assumption of COV_{WT} = 0.5 indicates results similar to COV_{CL}, but this is not a universal result, as will be demonstrated below.

Figures 9.4-11 and 9.4-12 show plots of COV_{MH} at Manchester for 10 Hz and 1 Hz, respectively. The 10 Hz COV_{MH} is similar to that for PGA, but the 1 Hz COV_{MH} (Figure 9.4-12) shows markedly higher COV_{MH} values. The reason is that the 1 Hz hazard curves (Figure 9.2-13) show a larger range and both a larger σ_{MH} and a larger σ_{CL} than do the PGA hazard curves (for PGA on Figure 9.4-8, the "sigma" curve generally lies below the mean hazard, but for 1 Hz on Figure 9.4-13, the "sigma" curve generally lies above the mean hazard). Figure 9.4-13 also shows that the "cl. mean sigma" curve peaks, relative to the mean hazard curve, at an amplitude of about 0.1 g. At higher ground motions (lower annual frequencies), the "cl. mean sigma" decreases relative to the mean hazard. This leads to decreasing COV_{CL} and COV_{WT} curves on Figure 9.4-12 for hazards in the range of 10^{-5} to 10^{-7}.

As another example of the effect of ground motion equations for general sources, Figures 9.4-14 through 9.4-16 show plots of COV_{MH} from ground motion equations for the Chattanooga test site. This site is dominated by local sources, with small contributions to hazard coming from the distant Charleston and New Madrid sources. The COV_{MH} plots are similar to those for Manchester, with PGA and 10 Hz showing COV_{MH} in the range of 0.15 to 0.25 for hazards in the range of 10^{-4} to 10^{-6}, and 1 Hz showing higher COV_{MH} (for the same reason discussed for the Manchester site).

RLME Sources. In the EPRI (2004) study there were 12 equations recommended for sources that can generate large-magnitude earthquakes, as indicated in Table 9.4-3. As an example, Figure 9.4-17 shows seismic PGA hazard curves for these 12 equations for the Savannah test site, along with mean, σ_{MH}, and σ_{CL} curves. This site is located quite close to the Charleston seismic zone, and hazard at the site is dominated by that source.

Figures 9.4-18 through 9.4-20 show the COV_{MH} resulting from ground motion equations for PGA, 10 Hz, and 1 Hz respectively. At the close distance from the Savannah site to the Charleston seismic zone, the hazard curves span a small range (for hazard curves), e.g., for PGA amplitudes corresponding to mean hazards of 10^{-4} and 10^{-5}, the range of hazard among the 12 ground motion equations on Figure 9.4-17 is about a factor of 20 to 30 in annual frequency. As a result, Figure 9.4-18 shows COV_{MH} around 0.1 for COV_{WT} = 0.3, and higher COV_{MH} for higher values of COV_{WT}.

For the central case of COV_{WT} = 0.5, for 10 Hz spectral accelerations, COV_{MH} is around 0.1 for mean hazards in the range of 10^{-4} to 10^{-6}, and for 1 Hz spectral acceleration, COV_{MH} ranges from about 0.12 to 0.15.

The relative agreement among PGA hazard curves at the Savannah site results from the proximity of this site to the Charleston seismic zone. To illustrate this, seismic hazard was calculated at Columbia, South Carolina, from the Charleston seismic zone. Columbia lies roughly 150 km (93 mi.) from the center of the Charleston seismic zone. Figure 9.4-21 plots the PGA hazard curves for Columbia for the 12 ground motion equations, and plots the mean hazard, σ_{TH}, and σ_{CL}. For PGA corresponding to mean hazards of 10^{-4} and 10^{-5}, the range in hazards from the 12 ground motion equations spans two to three orders of magnitude, which is much greater than the range illustrated on Figure 9.4-17 for Savannah. As a result, the COV_{HAZ} at Columbia is larger, as illustrated on Figures 9.4-22 through 9.4-24 for PGA, 10 Hz, and 1 Hz, respectively, particularly for mean hazard values that are less than 10^{-4}.

To provide further perspective, Figures 9.4-25 through 9.4-27 plot COV_{MH} vs. mean hazard at the Chattanooga site, but only for the hazard caused by earthquakes in the New Madrid seismic zone (NMSZ). Chattanooga is about 400 km (250 mi.) from the NMSZ, and ground motion equations show a wider range of hazard at these long distances, as reflected on Figures 9.4-25 through 9.4-27, wherein the COV_{WT} = 0.5 curves indicate that COV_{MH} is between 0.2 and 0.4 for mean hazards between 10^{-4} and 10^{-6}. This confirms the trend seen with the Savannah and Columbia results that COV_{MH} increases with increasing distance from an RLME source.

Another trend that appears in the COV_{MH} plots for Savannah, Columbia, and Chattanooga is that COV_{CL} is much higher than COV_{MH} estimated by bootstrap techniques. The reason is related to the dominance of one RLME ground-motion equation, F9 in Table 9.4-3, in the mean hazard calculations (see Figures 9.4-17 and 9.4-21). The classical mean estimate of hazard uncertainty assumes that all estimates are independent, whereas the bootstrap technique maintains the symmetry in weights between RLME ground-motion equations F7 and F9 (the former gives estimates lower than equation F8, the latter gives estimates greater than F8, by a consistent multiplicative factor). This symmetry results in a lower estimate of COV_{MH} from the bootstrap technique and is important in the case of RLME sources when equation F9 results in a hazard curve that greatly exceeds the curves from other equations.

<u>PEGASOS Study</u>. In the PEGASOS project (NAGRA, 2004), five ground-motion experts provided recommendations on sets of ground motion equations with weights, and hazard results are available at four Swiss nuclear power plant sites for PGA and 1 Hz SA conditional on each ground-motion expert. The standard deviation of hazard σ_{MH} can be calculated for this set of

conditional hazards, and COV_{MH} is taken as $\sigma_{MH}/\sqrt{5}$ divided by the overall mean hazard. Figures 9.4-28 and 9.4-29 show COV_{MH} at the four sites, plotted vs. ground motion amplitude and vs. annual frequency of exceedance, respectively. For PGA the COV_{MH} exceeds 0.2, and for 1 Hz SA the COV_{MH} exceeds 0.3, for mean hazards in the range of 10^{-4} to 10^{-6}.

USGS Study. The USGS (Petersen et al., 2008) calculation of seismic hazard for the national seismic hazard maps uses multiple weighted ground-motion equations. These allow an estimate of the COV_{MH} to be derived. Equations and weights used in the USGS study for the CEUS are shown in Table 9.4-4.

Different weights are used for background sources and for RLME sources in the USGS application. The way hazards from alternative ground-motion-prediction equations (GMPEs) are combined when the total hazard is calculated from background and RLME sources does not affect the mean hazard and is not specified in the USGS study. But the combination of hazards does affect the uncertainty in total hazard. In order to avoid the arbitrariness of adopting any specific combination rule, and with the goal of calculating the *minimum* estimate of hazard uncertainty, we assume that the GMPEs in Table 9.4-3 combine independently, and adopt the *classical standard deviation* designated σ_{CL} above. Accounting for correlations of estimates (e.g., that equation *i* for background seismicity would be associated with equation *i* for RLMEs) would increase the estimates of the uncertainty in mean hazard from the classical estimate.

Figures 9.4-30 and 9.4-31 show COV_{MH} for Chattanooga and Central Illinois, respectively, for the USGS 2008 hazards at seven spectral frequencies. Total hazard at the Chattanooga site is dominated by background seismicity, and at the Central Ilinois site is a combination of hazard from background and RLMEs, and this combination depends on spectral frequency. For both sites, COV_{MH} ranges from 0.15 to 0.25 for total mean hazard between 10^{-4} and 10^{-6}, with a minimum COV_{MH} of about 0.15.

Note that additional epistemic uncertainties are not used in the USGS GMPEs, as they are in the EPRI (2004) GMPEs. Rather, the USGS GMPEs adopts the best estimate of what each author believes are appropriate ground-motion amplitudes in the CEUS, along with aleatory uncertainties. Some of the authors, in their original publications, discuss how to extend their models to estimate epistemic uncertainties, but these extensions have not been used in the USGS model. This, along with the assumption of independence between area source and RLME estimates discussed above, contributes to the USGS COV_{MH} estimates in some cases appearing to be low relative to other estimates.

Overall, uncertainties in hazard caused by uncertainty in ground motion equations shown for the PEGASOS project (Figures 9.4-28 and 9.4-29) and from the USGS (Figures 9.4-30 and 9.4-31) are consistent with the results shown for the results in the CEUS (Figures 9.4-8 through 9.4-27). That is, hazard uncertainties are lower for high frequencies than for 1 Hz spectral amplitudes, and hazard uncertainties increase with ground motion amplitude. Focusing on COV_{MH} estimated using $COV_{WT} = 0.5$, a typical range of COV is from 0.1 to 0.45 across all spectral frequencies and amplitudes of interest, with some specific results falling outside of this range.

9.4.2.4 Site Response

Most sites in the CEUS are not classified as hard rock sites, and at these sites, uncertainty in site response plays a role in the uncertainty in site hazard calculations. Results from the PEGASOS project allow a direct estimate of the hazard uncertainty caused by uncertainty in site response calculations, because four site response experts provided recommendations on site response models, and hazard results are available at the four Swiss plant sites conditional on these four experts. The standard deviation of mean hazard σ_{MH} can be calculated for this set of conditional hazards, and COV_{MH} is taken as $\sigma_{MH}/\sqrt{4}$ divided by the overall mean hazard. Figure 9.4-32 shows COV_{MH} at the four sites for PGA and 1 Hz spectral acceleration (which are the only results available in this format), plotted vs. ground motion amplitude. COV_{MH} is relatively small for PGA, generally below 0.1. For 1 Hz spectral acceleration, COV_{MH} is small at low amplitudes and increases with amplitude. Figure 9.4-33 shows COV_{MH} plotted vs. mean hazard, where for the hazard range of 10^{-4} to 10^{-6}, and depending on spectral frequency, COV_{MH} values range from 0.03 to 0.4. Results differ among the four sites, which should be expected.

In the CEUS, an estimate is available of the uncertainty in hazard caused by alternative soil amplification models. This comes from the results of two EPRI-funded projects (EPRI, 2005a, 2005b, 2008) that calculated seismic hazard (including site response) at a group of nuclear power plants in the CEUS. Multiple models of site profiles and site characteristics were developed using available public information on the sites, and these multiple models were weighted to obtain the total site hazard. For the purposes of the current study, at each site the individual mean hazard curves for each soil model were obtained, and standard deviation of mean hazard σ_{MH} was calculated using these individual curves and weights. The classical standard deviation of the mean was then calculated as $\sigma_{CL} = \sigma_{TH} \times \sqrt{\Sigma\, W_i^2}$, where W_i are the weights for the various soil models. This calculation assumes that the estimates of hazard are independent.

Figure 9.4-34 shows COV_{MH} resulting from the alternative site response models, vs. mean hazard, for four sites with alternative site response models. COV_{MH} varies over a wide range, as might be expected for different sites, but results generally show that COV_{MH} exceeds 0.05, with one site (Site 4 for 10 Hz) showing lower COVs.

9.4.3 Conclusions on the Precision in Seismic Hazard Estimates

Results presented above are summarized in Table 9.4-5, which represents minimum COV_{MH} values observed in these sensitivity results. For reasons given above, COV_{MH} from the Savannah site and from the USGS ground-motion results are not used. Also, the COV_{MH} values from the PEGASOS study are downweighted, because only mean hazard curves conditional on each ground-motion expert are available, and these do not include within-expert variability. COV_{MH} values are summarized by spectral frequency and annual frequency of exceedance, and results are given separately for area sources and RLME sources. The last two columns represent the total COV_{MH}, calculated as the square root of the sum of squares of the individual COVs for sites affected primarily by area sources and by RLME sources. Table 9.4-5 presents COV_{MH} results for annual frequencies of exceedance of 10^{-4}, 10^{-5}, and 10^{-6}. This is a common hazard range for the seismic design of critical facilities, but note that investigations of seismic hazard for such facilities often require a wider range (e.g., 10^{-3} to 10^{-7}).

Table 9.4-5 shows that in general, minimum hazard uncertainties resulting from area source characteristics are smaller than minimum hazard uncertainties resulting from RLME source characteristics. But the reverse is true of uncertainties resulting from ground motion models, where minimum hazard uncertainties from area-source ground-motion models are larger than from RLME ground-motion models. These two effects compensate somewhat, so that total minimum uncertainties in hazard are comparable for the two types of sources. Uncertainty in site response contributes relatively little, at least for the example sites presented here from two major studies. As an overall conclusion, the minimum COV representing uncertainty in mean hazard over all spectral frequencies, and for annual mean hazards in the range of 10^{-4} to 10^{-6}, can be taken to be about 0.25 for 10^{-4}, 0.3 for 10^{-5}, and 0.35 for 10^{-6}. Because the contribution of site response uncertainty is a small part of this total, this conclusion applies to both rock and soil sites.

For decisions regarding the significance of changes in seismic hazard, the above results should be interpreted as follows. If an alternative assumption or parameter is used in a seismic hazard study, and it potentially changes the calculated mean hazard (mean annual frequency of exceedance) by less than $\pm$25% for ground motions corresponding to 10^{-4} annual frequency of exceedance, and it potentially changes the calculated hazard by less than $\pm$35% for ground motions corresponding to 10^{-6} annual frequency of exceedance, then that potential change is less than the best (highest) level of precision with which we can calculate mean seismic hazard. Under these circumstances, the potential change could be deemed not significant. For many sites we cannot be this precise, and the uncertainty in mean hazard will be higher than this, but the above interpretation gives a reasonable lower-bound guideline with which to evaluate the significance of potential changes in mean hazard. Note that regulators addressing the impacts of potential changes in seismic hazard on seismic design motions or on seismic risk-related decisions may (appropriately) require action even if potential changes are less than the guidelines given above.

Table 9.4-1
Available Information for Determining the Precision of Mean Hazard

Input	Subset of Application	Available Studies
(1) Seismic sources and parameters	Area sources	(1A) EPRI (1989) project (6 teams at 7 sites) (1B) PEGASOS project (NAGRA, 2004)
	RLME sources (Charleston, New Madrid)	(1C) Charleston (Southern Nuclear, 2008) (1D) New Madrid (Exelon, 2003)
(2) Ground motion equations	All	(2A) EPRI (2004) equations applied to 7 sites (2B) USGS equations (Petersen et al., 2008) applied to 7 sites (2C) PEGASOS study (NAGRA 2004) (5 experts applied to 4 sites)
(3) Site response	All (non-rock) sites	(3A) EPRI study (2005a, b, 2008) (1 expert applied to 45 sites) (3B) PEGASOS study (NAGRA, 2004) (4 experts applied to 4 sites)

Table 9.4-2
Summary of an Example Logic Tree Representing Uncertainties for the Charleston Seismic Zone

Interpretation	Alternatives	Weights on Alternatives	Designation[1]
Geometry of source	4 geometries	0.7, 0.1, 0.1, 0.1	GEOM
Maximum magnitude	5 values	0.1, 0.25, 0.3, 0.25, 0.1	Mmax
Paleoseismic record length	2 periods	0.8, 0.2	SEIS
Activity rate given record	5 rates	0.1, 0.2, 0.4, 0.2, 0.1	RATE

[1] Designation of curves in Figures 9.4-4 through 9.4-6

Table 9.4-3
Basic Weights Given in EPRI (2004) for Ground Motion Equations

General Source			RLME Source		
Equation	**Weight**	**Comment**	**Equation**	**Weight**	**Comment**
C1	0.065	—	F1	0.0509	—
C2	0.221	—	F2	0.173	—
C3	0.065	wt. equal to C1	F3	0.0509	wt. equal to F1
C4	0.0737	—	F4	0.0577	—
C5	0.251	—	F5	0.197	—
C6	0.0737	wt. equal to C4	F6	0.0577	wt. equal to F4
C7	0.0463	—	F7	0.0363	—
C8	0.158	—	F8	0.124	—
C9	0.0463	wt. equal to C7	F9	0.0363	wt. equal to F7
—	(not used)	—	F0	0.0401	—
—	(not used)	—	FA	0.137	—
—	(not used)	—	FB	0.0401	wt. equal to F0

Table 9.4-4
Ground Motion Equations and Weights Used in USGS 2008 National Hazard Map for CEUS

Reference	Weight for Background Seismicity	Weight for RLME Sources
Atkinson and Boore (2006; 140 bars)	0.125	0.1
Atkinson and Boore (2006; 200 bars)	0.125	0.1
Campbell (2003)	0.125	0.1
Frankel et al. (1996)	0.125	0.1
Tavakoli and Pezeshk (2005)	0.125	0.1
Silva et al. (2002)	0.125	0.1
Toro et al. (1997)	0.25	0.2
Somerville et al. (2001)	—	0.2

Table 9.4-5
Minimum COV_{MH} Values Observed in Seismic Hazard

Case	Area Sources	RLME Sources	Ground Motion (Area Sources[1])	Ground Motion (RLME Sources[1,2])	Site Response	Total COV_{MH}, General Site	Total COV_{MH}, RLME Site
PGA, 1E-4	0.15	0.27	0.20	0.15	0.05	~0.25	~0.31
PGA, 1E-5	0.18	0.31	0.25	0.22	0.05	~0.31	~0.38
PGA, 1E-6	0.20	0.40	0.30	0.28	0.05	~0.36	~0.49
10 Hz, 1E-4	0.15	0.27	0.17	0.10	0.05	~0.23	~0.29
10 Hz, 1E-5	0.18	0.31	0.25	0.13	0.05	~0.31	~0.34
10 Hz, 1E-6	0.21	0.4	0.37	0.16	0.05	~0.43	~0.43
1 Hz, 1E-4	0.10	0.25	0.30	0.12	0.05	~0.32	~0.28
1 Hz, 1E-5	0.10	0.30	0.40	0.18	0.05	~0.42	~0.35
1 Hz, 1E-6	0.10	0.35	0.50	0.23	0.05	~0.51	~0.42

[1] Excluding Savannah site
[2] Excluding USGS results

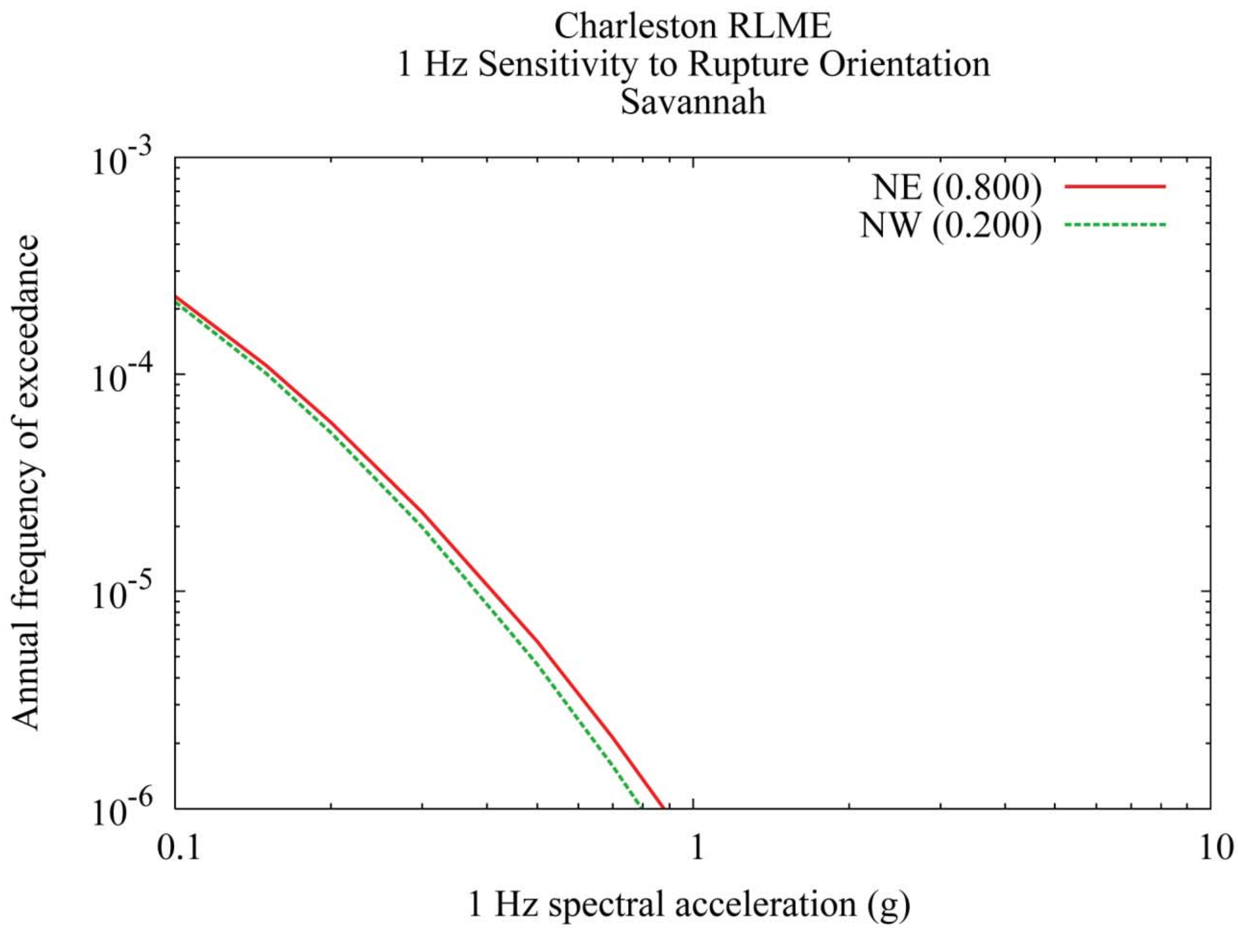

Figure 9.3-1
1 Hz sensitivity to rupture orientation at Savannah for the Charleston regional source

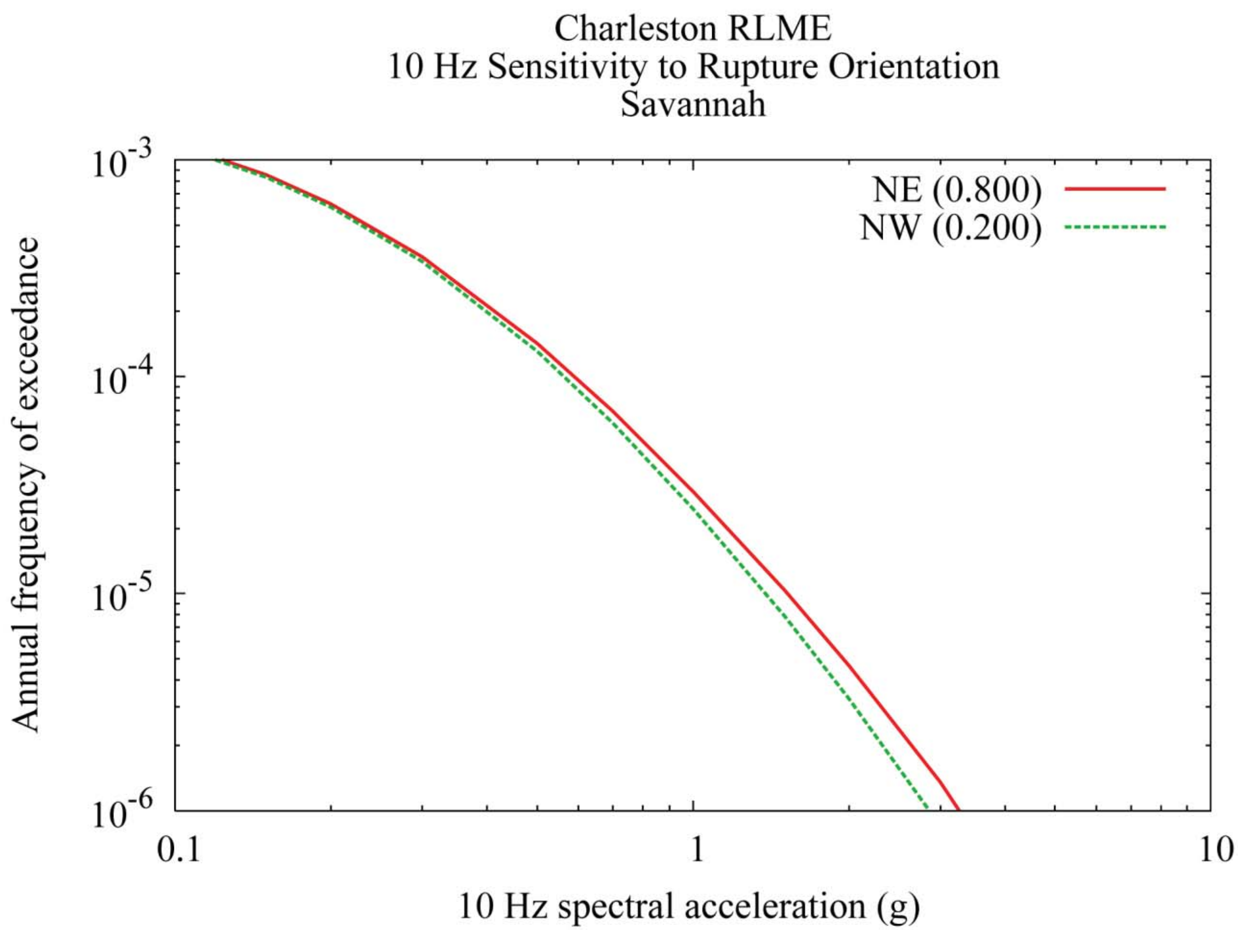

Figure 9.3-2
10 Hz sensitivity to rupture orientation at Savannah for the Charleston regional source

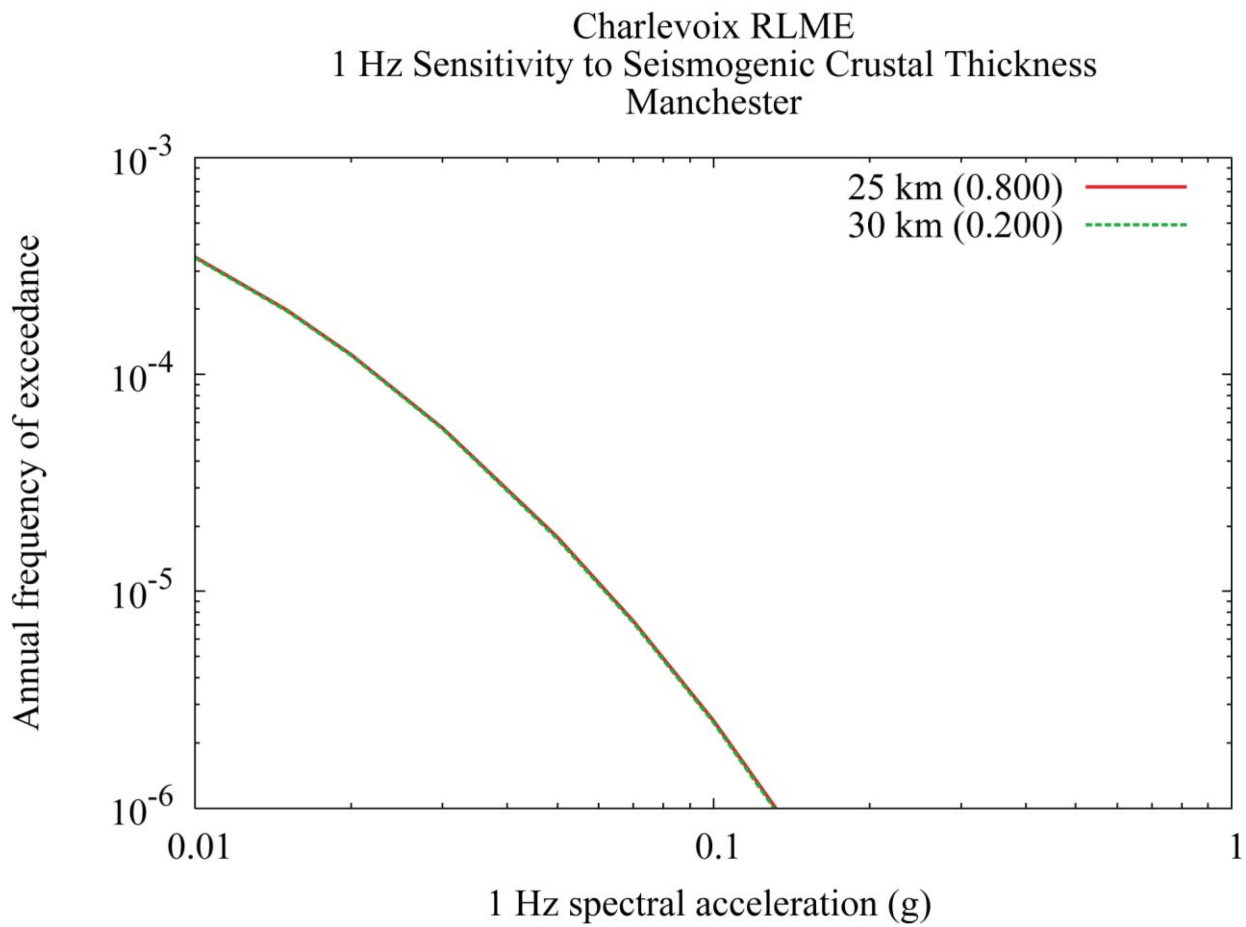

Figure 9.3-3
1 Hz sensitivity to seismogenic thickness at Manchester for the Charlevoix area source

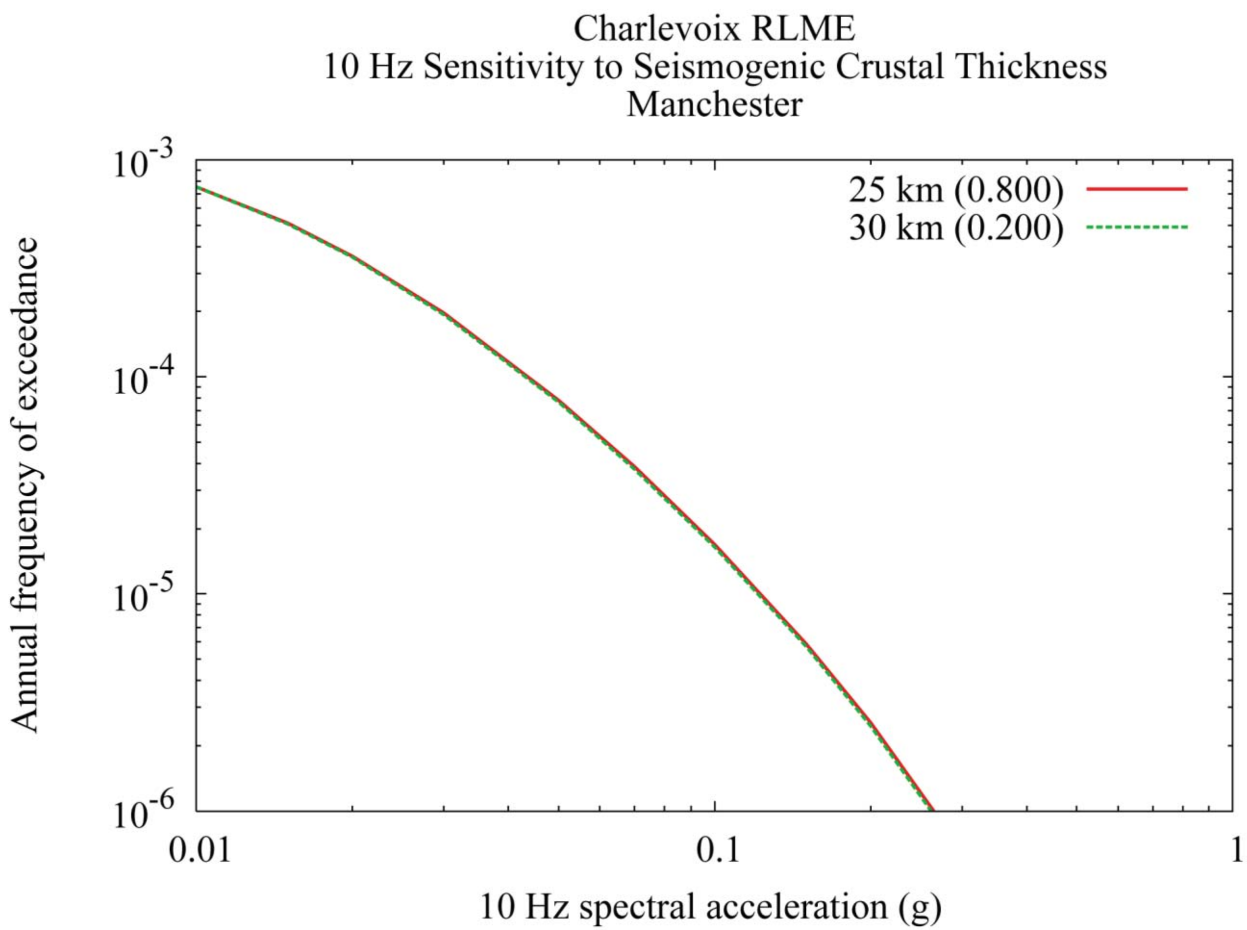

Figure 9.3-4
10 Hz sensitivity to seismogenic thickness at Manchester for the Charlevoix area source

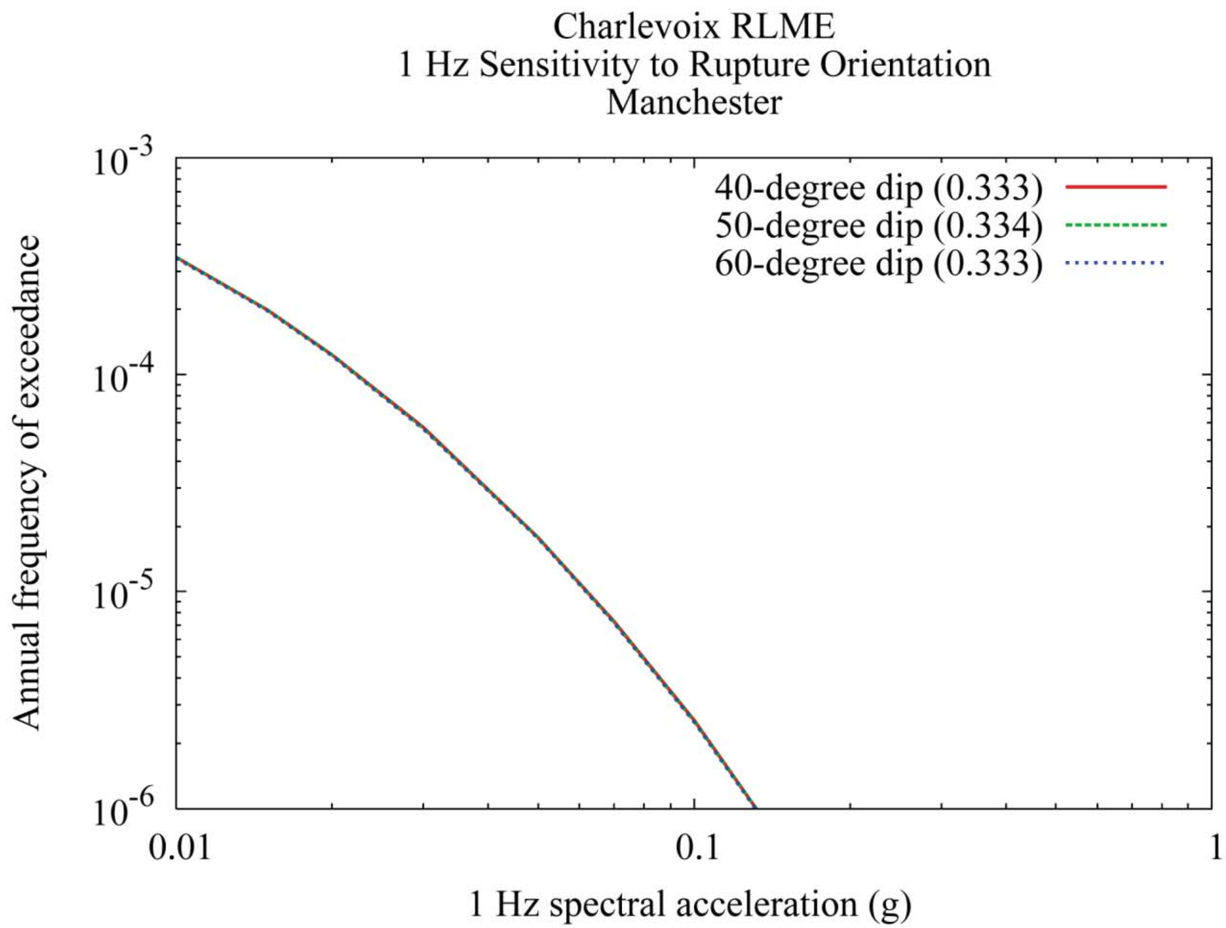

Figure 9.3-5
1 Hz sensitivity to rupture orientation (dip) at Manchester for the Charlevoix area source

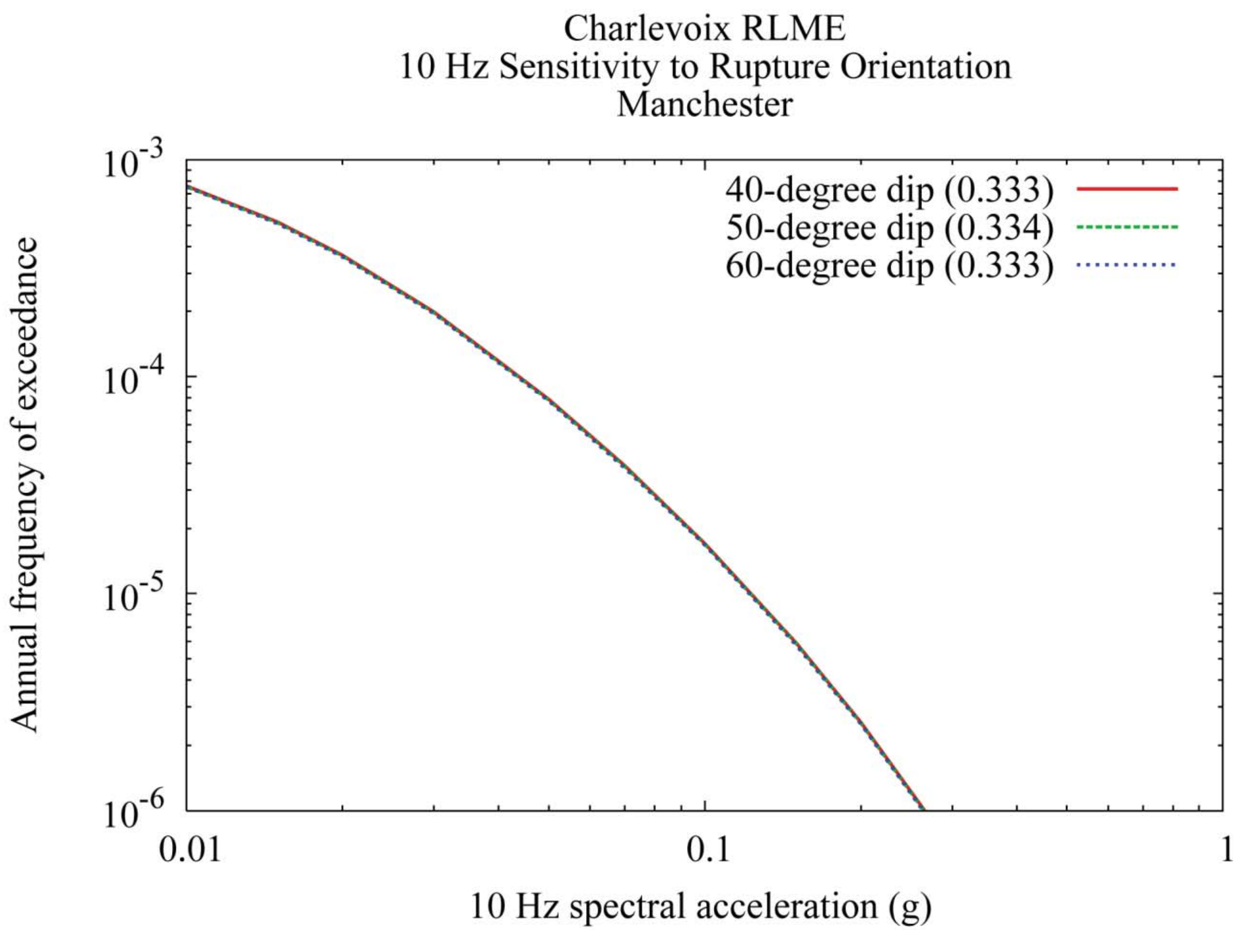

Figure 9.3-6
10 Hz sensitivity to rupture orientation (dip) at Manchester for the Charlevoix area source

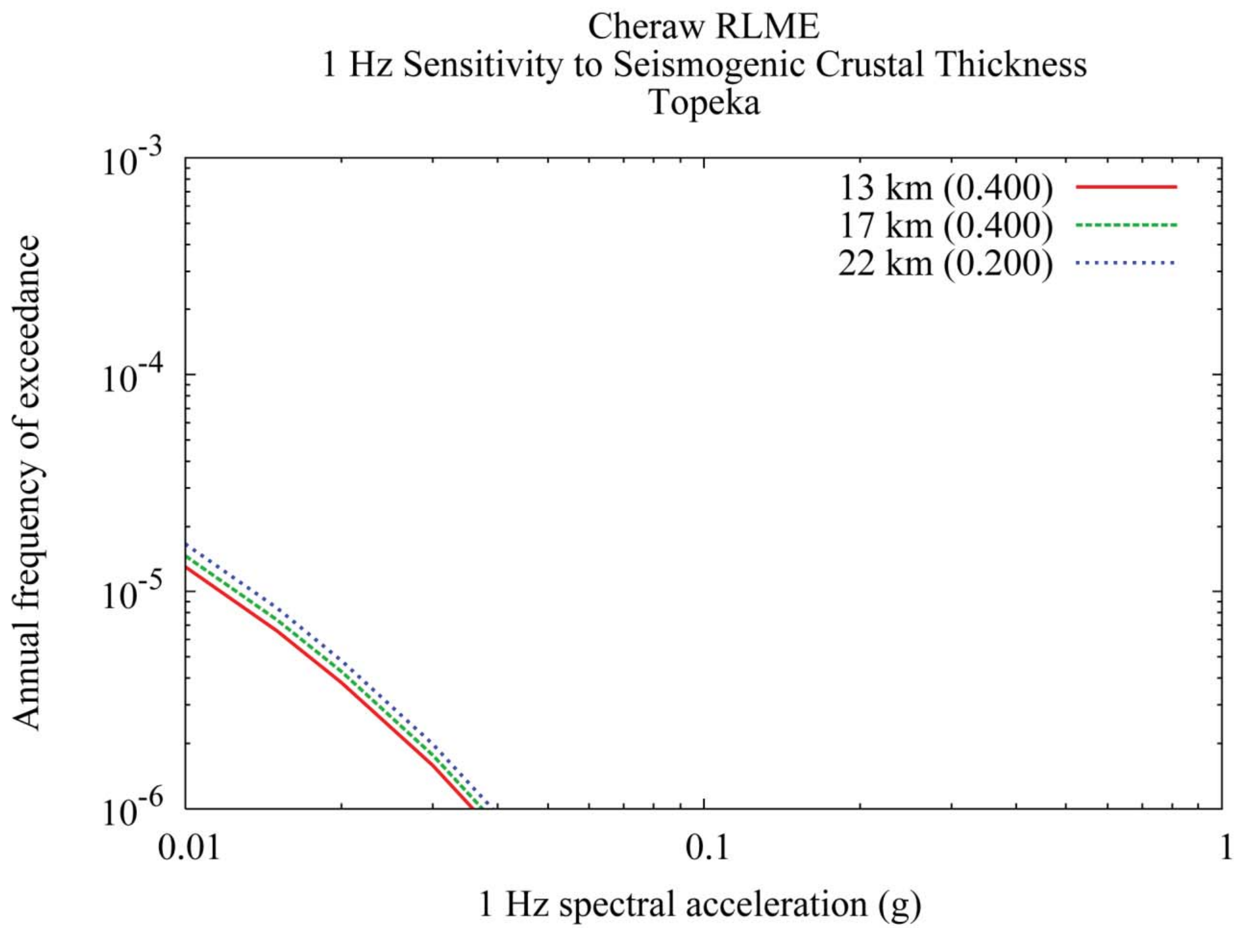

Figure 9.3-7
1 Hz sensitivity to seismogenic thickness at Topeka for the Cheraw fault source

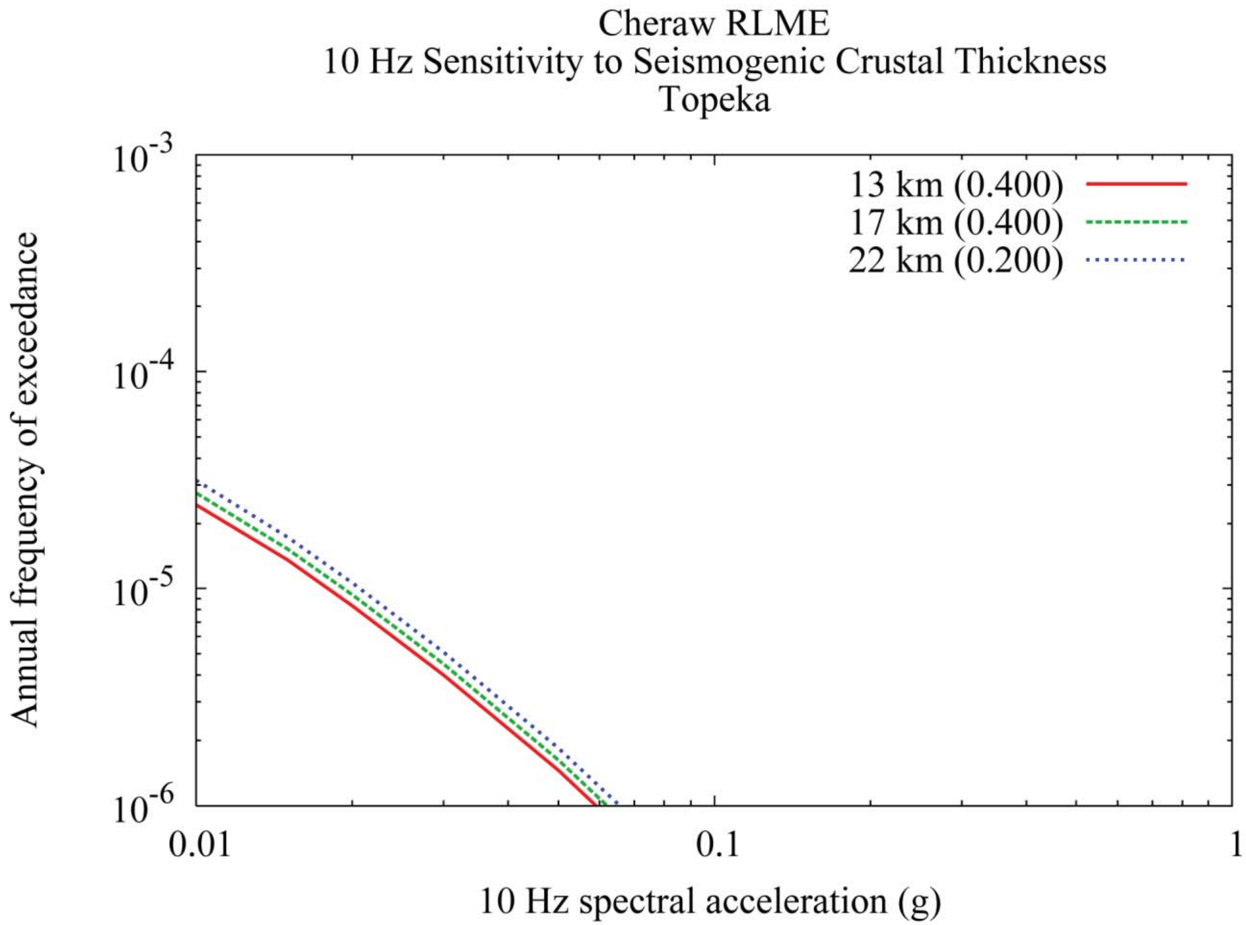

Figure 9.3-8
10 Hz sensitivity to seismogenic thickness at Topeka for the Cheraw fault source

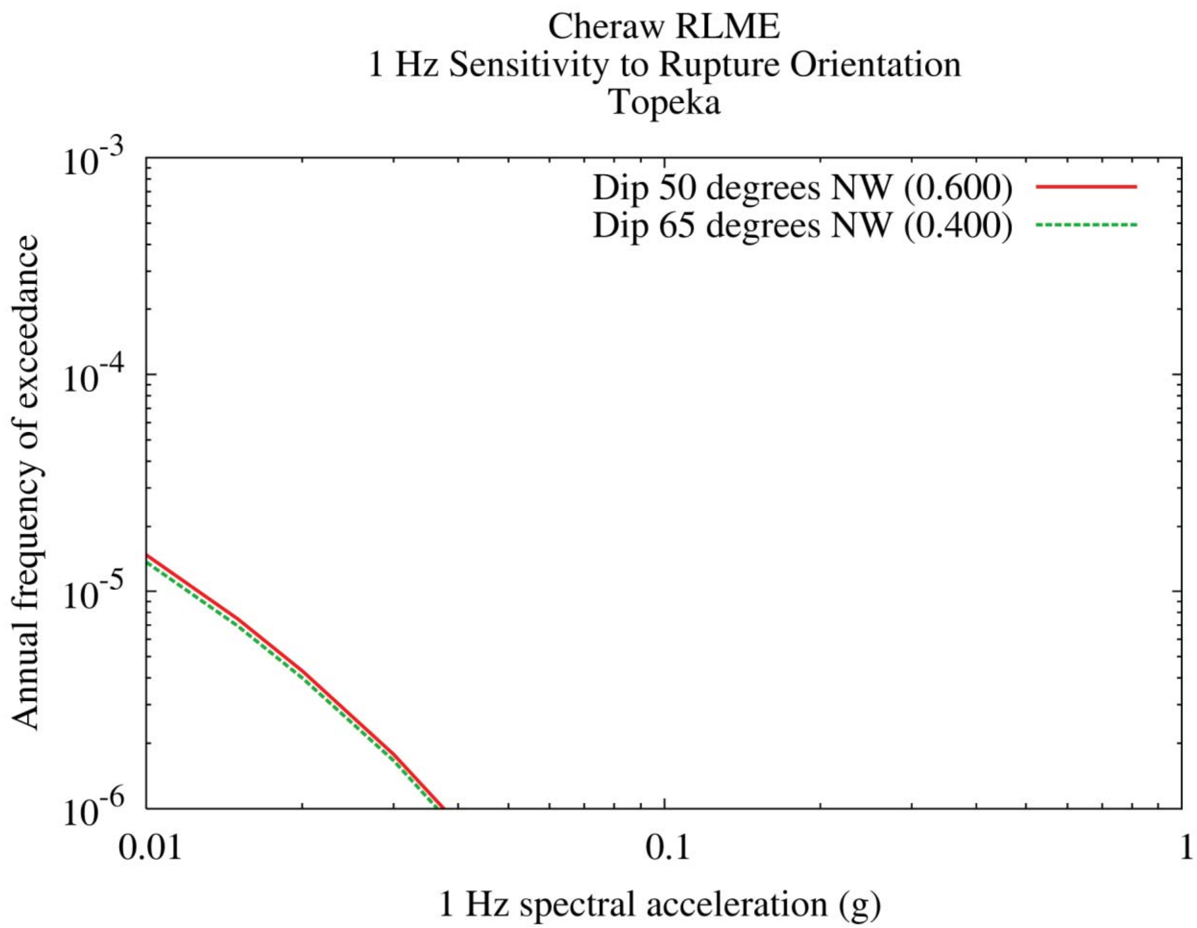

Figure 9.3-9
1 Hz sensitivity to rupture orientation (dip) at Topeka for the Cheraw fault source

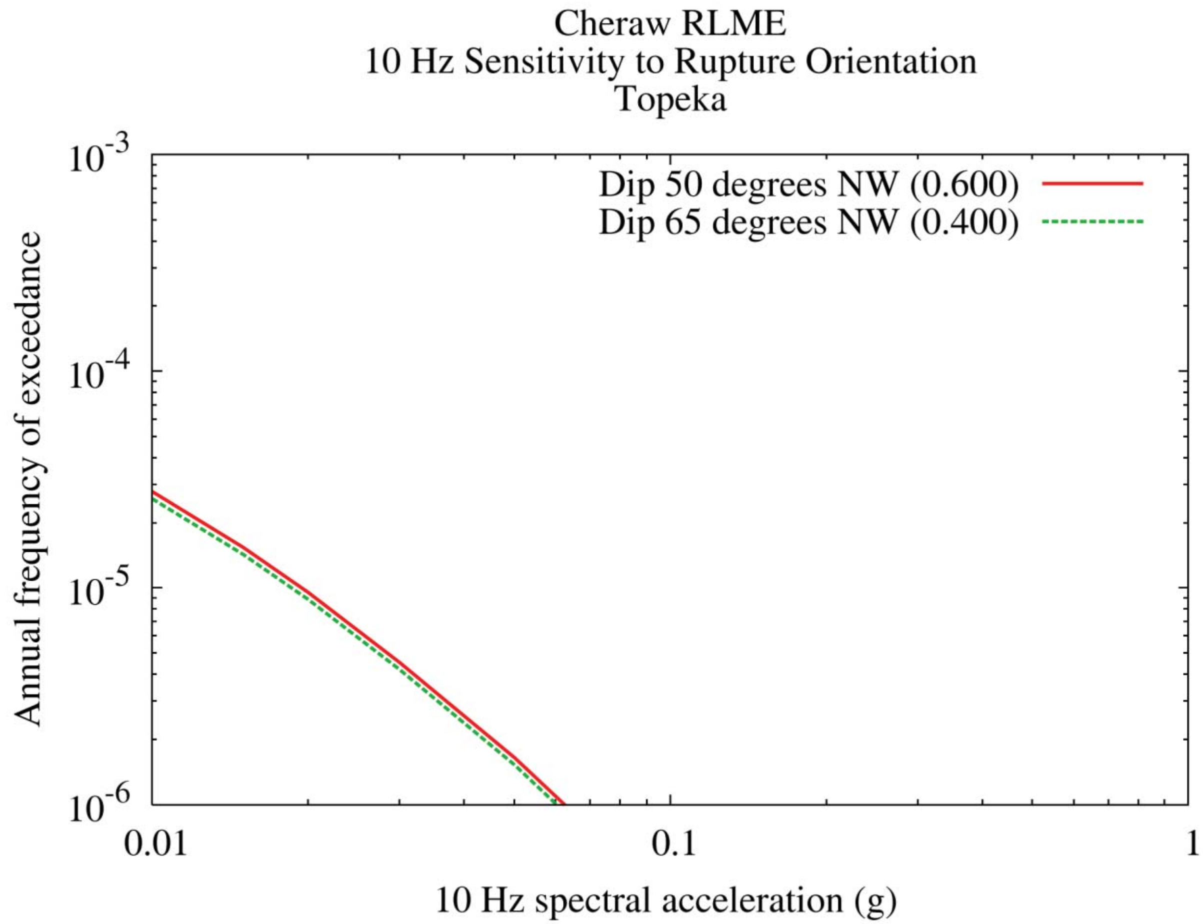

Figure 9.3-10
10 Hz sensitivity to rupture orientation at Topeka for the Cheraw fault source

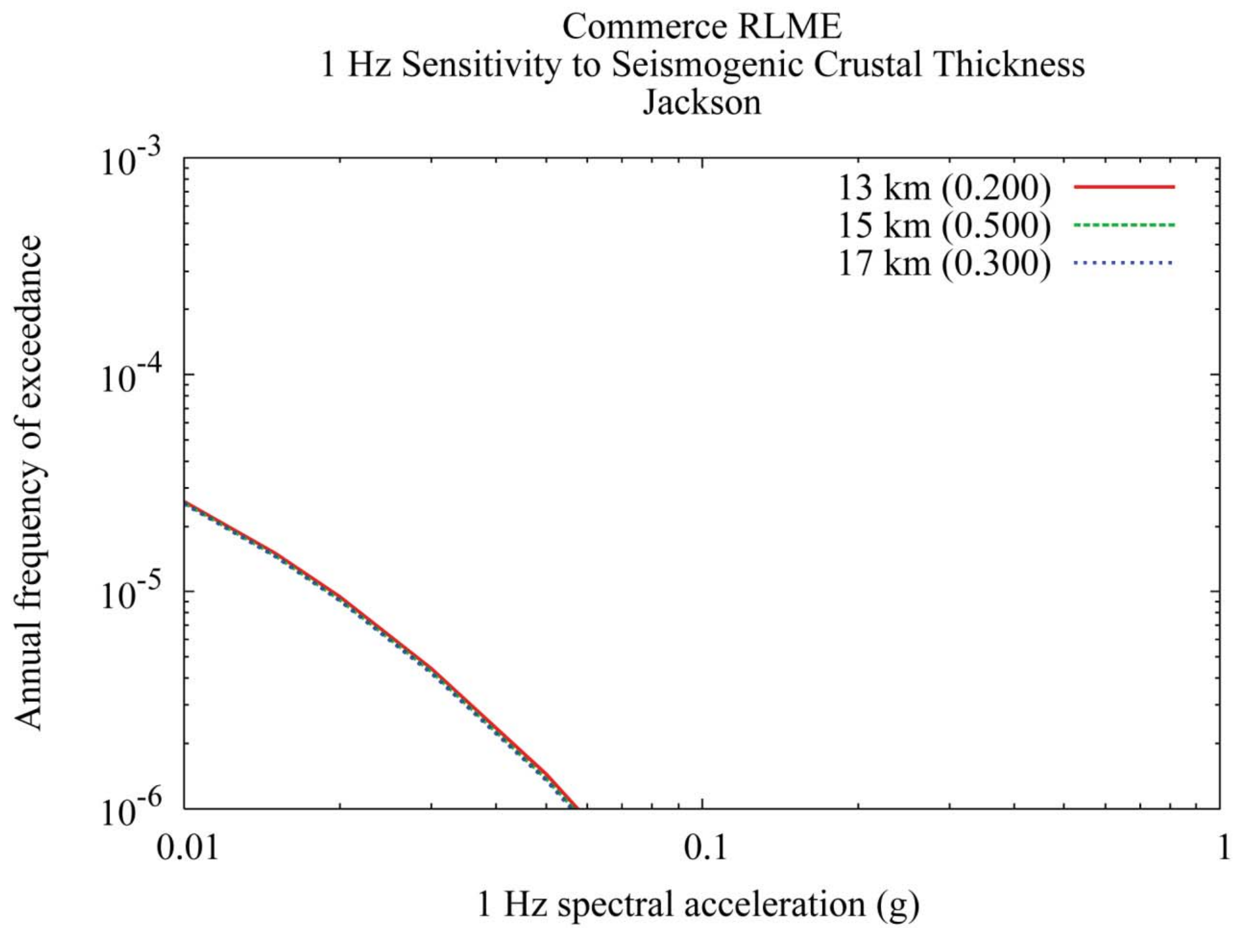

Figure 9.3-11
1 Hz sensitivity to seismogenic thickness at Jackson for the Commerce area source

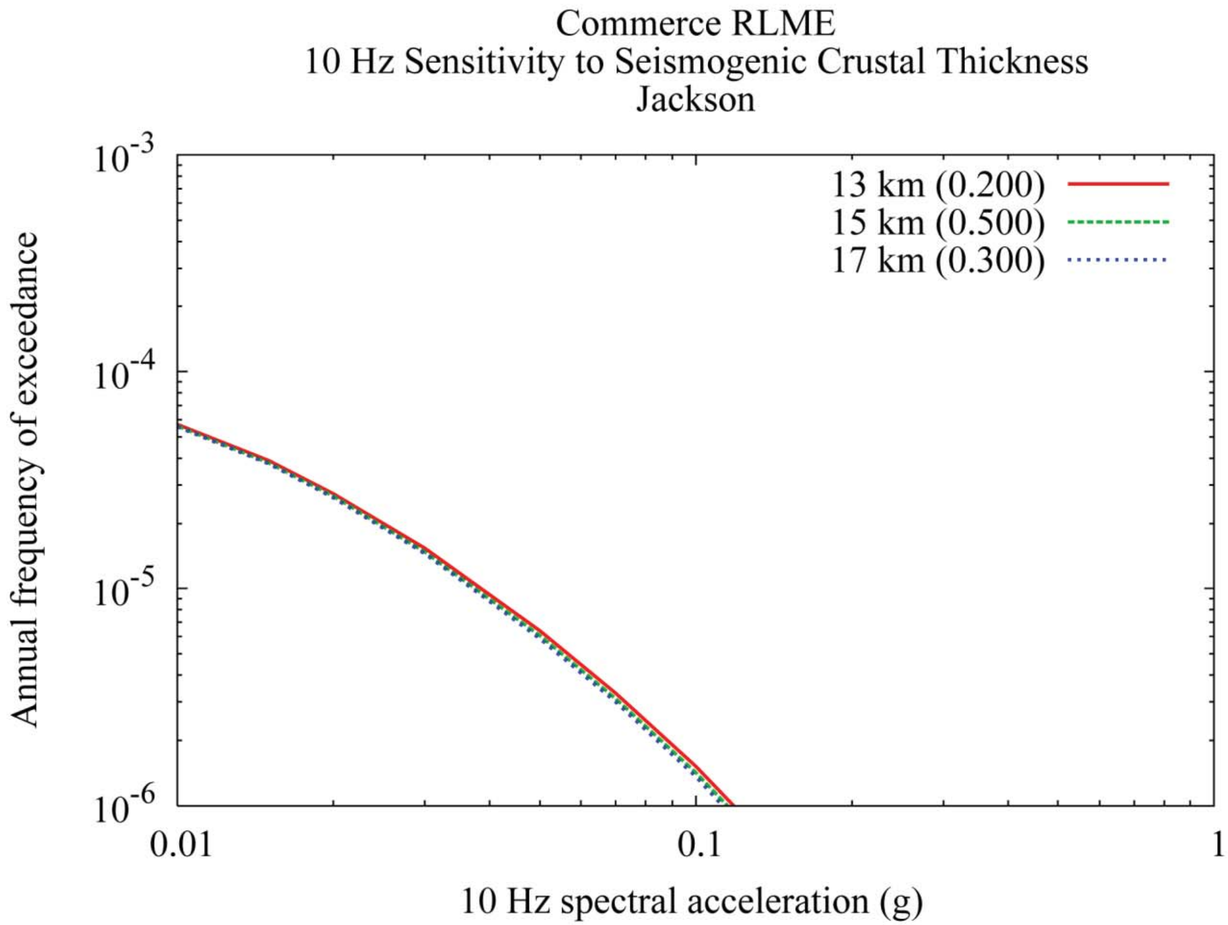

Figure 9.3-12
10 Hz sensitivity to seismogenic thickness at Jackson for the Commerce area source

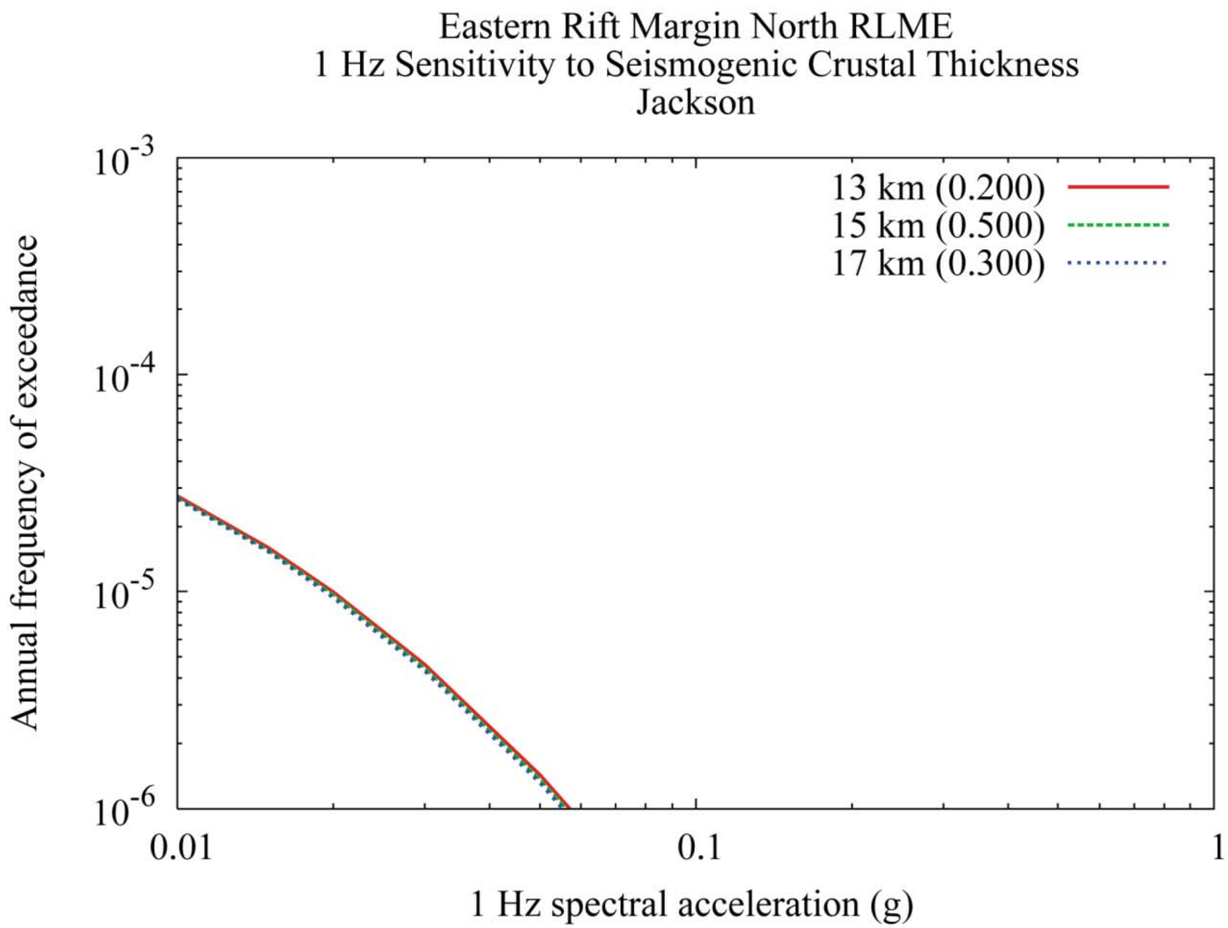

Figure 9.3-13
1 Hz sensitivity to seismogenic thickness at Jackson for the ERM-N area source

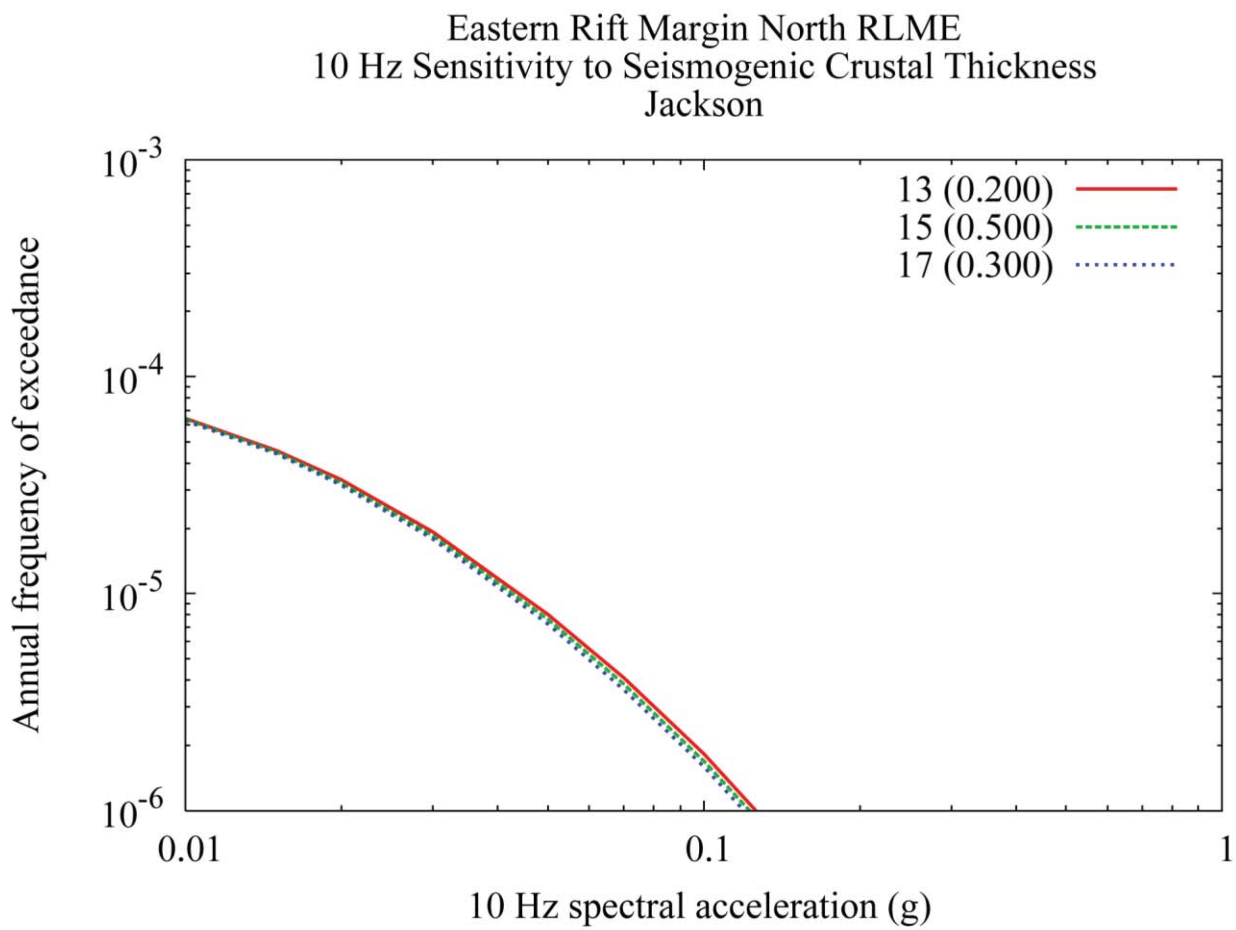

Figure 9.3-14
10 Hz sensitivity to seismogenic thickness at Jackson for the ERM-N area source

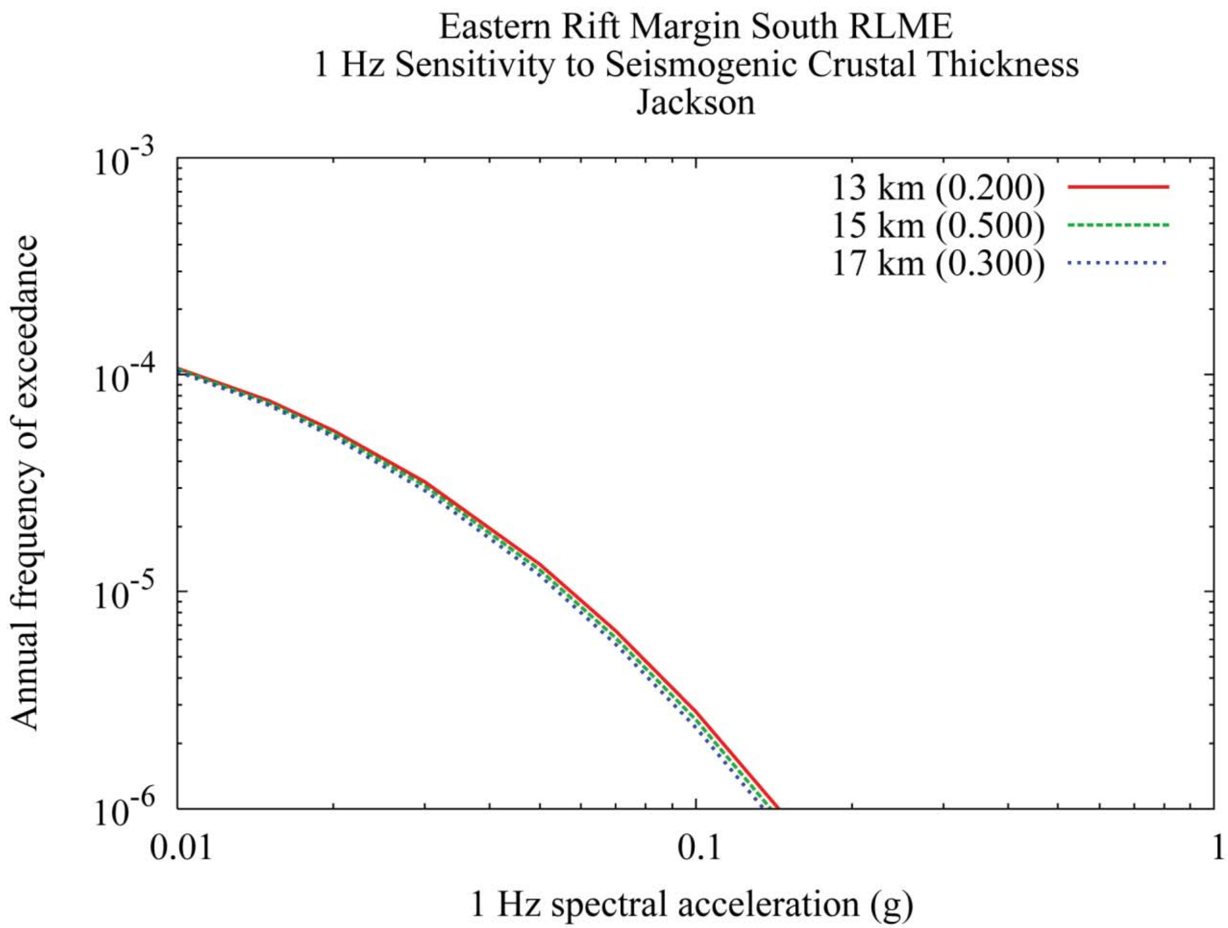

Figure 9.3-15
1 Hz sensitivity to seismogenic thickness at Jackson for the ERM-S area source

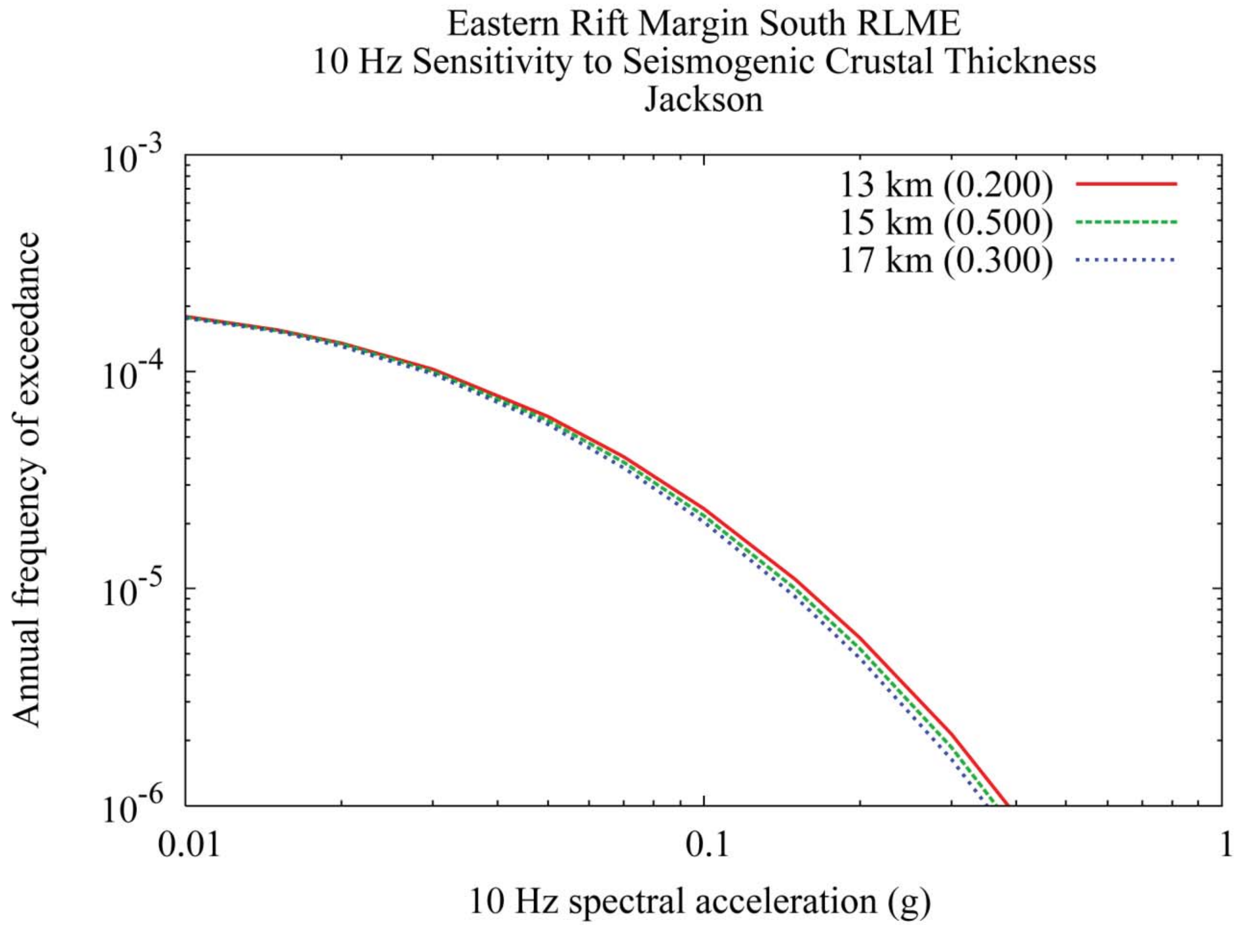

Figure 9.3-16
10 Hz sensitivity to seismogenic thickness at Jackson for the ERM-S area source

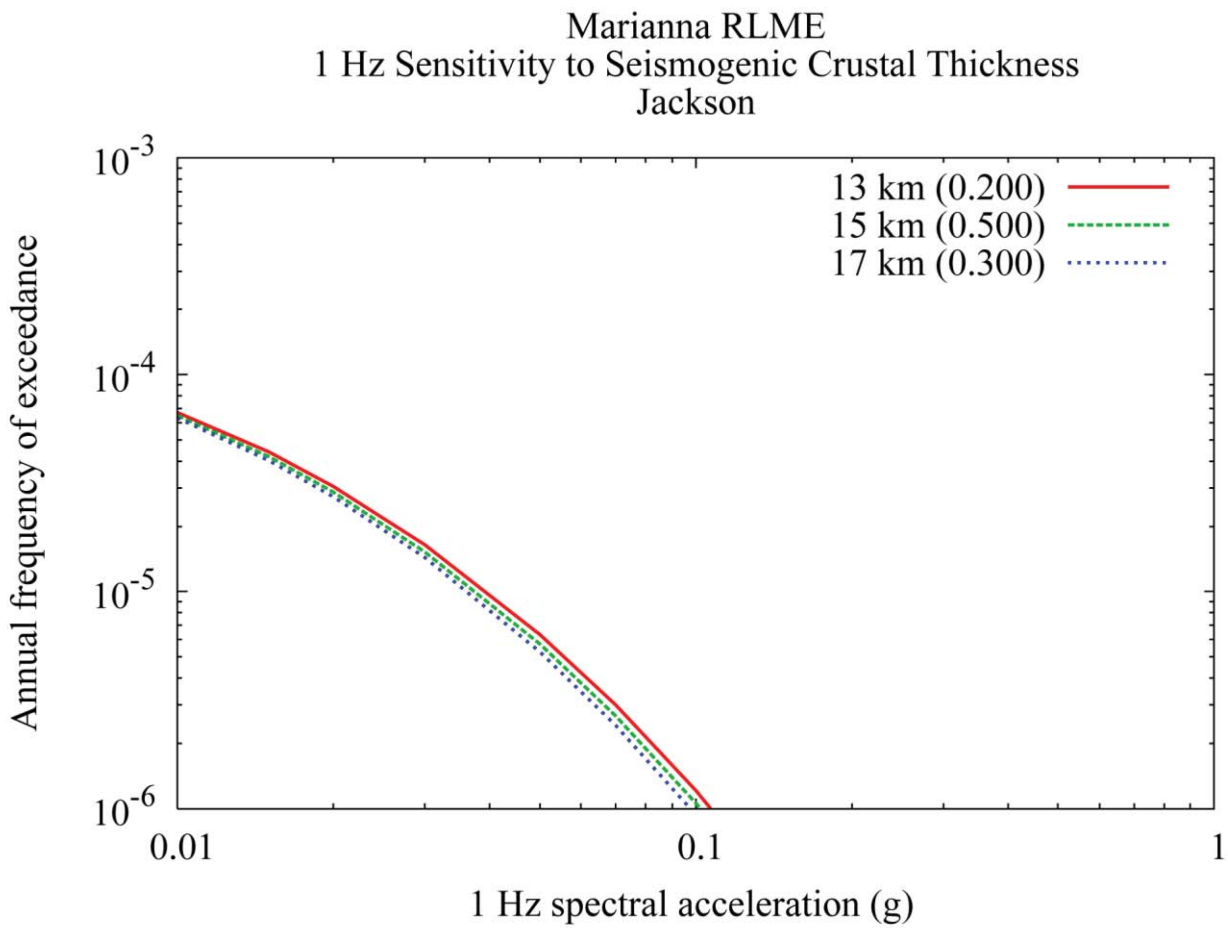

Figure 9.3-17
1 Hz sensitivity to seismogenic thickness at Jackson for the Marianna area source

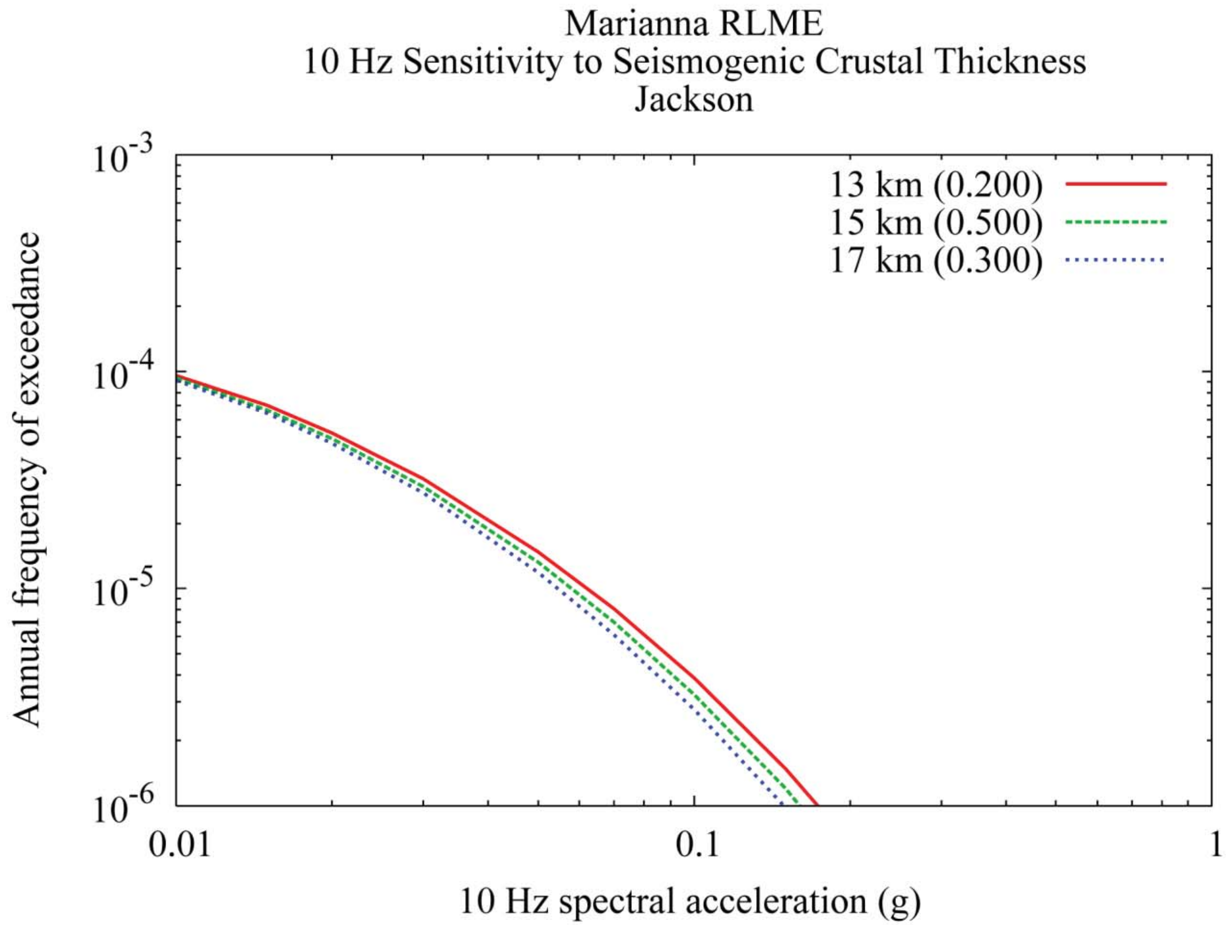

Figure 9.3-18
10 Hz sensitivity to seismogenic thickness at Jackson for the Marianna area source

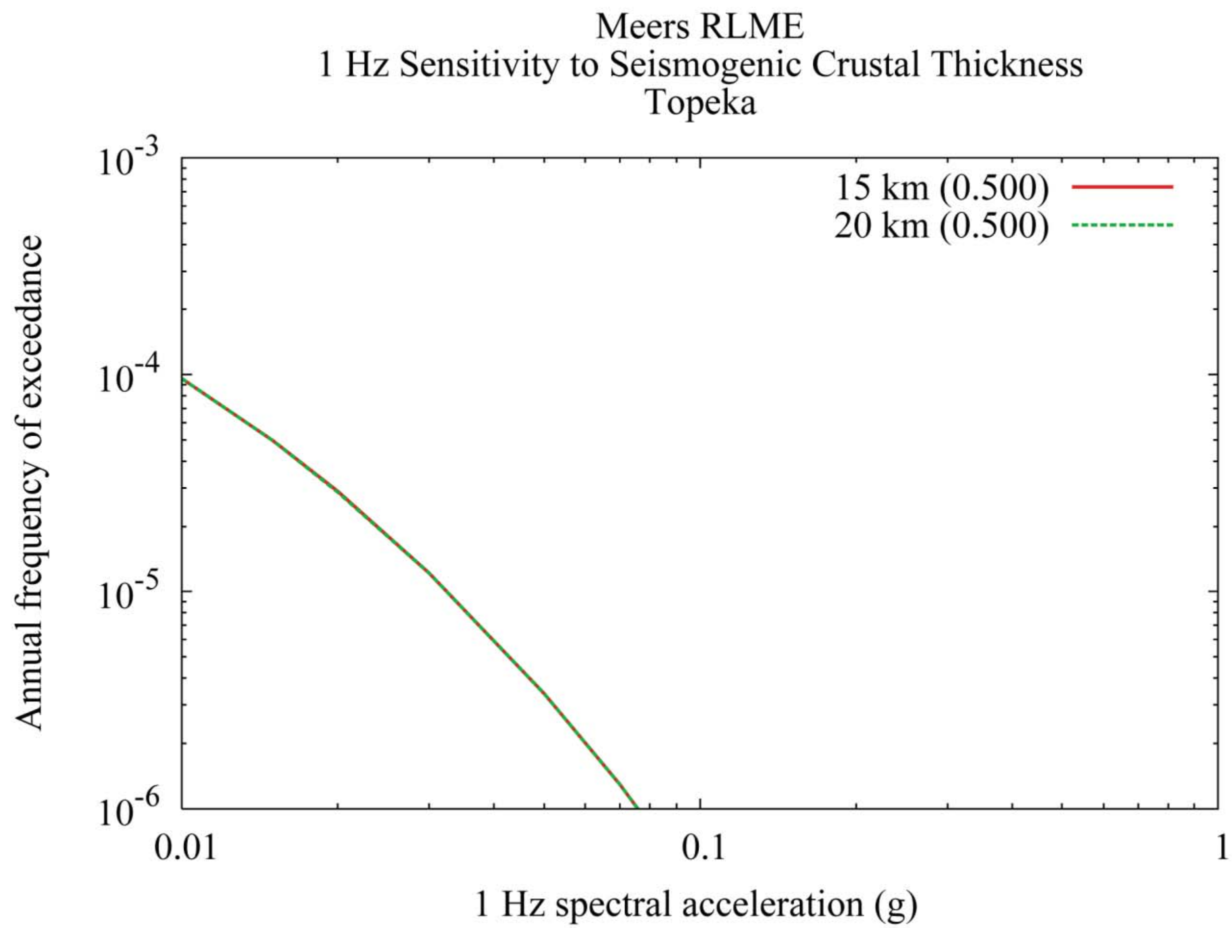

Figure 9.3-19
1 Hz sensitivity to seismogenic thickness at Topeka for the Meers fault and OKA area sources

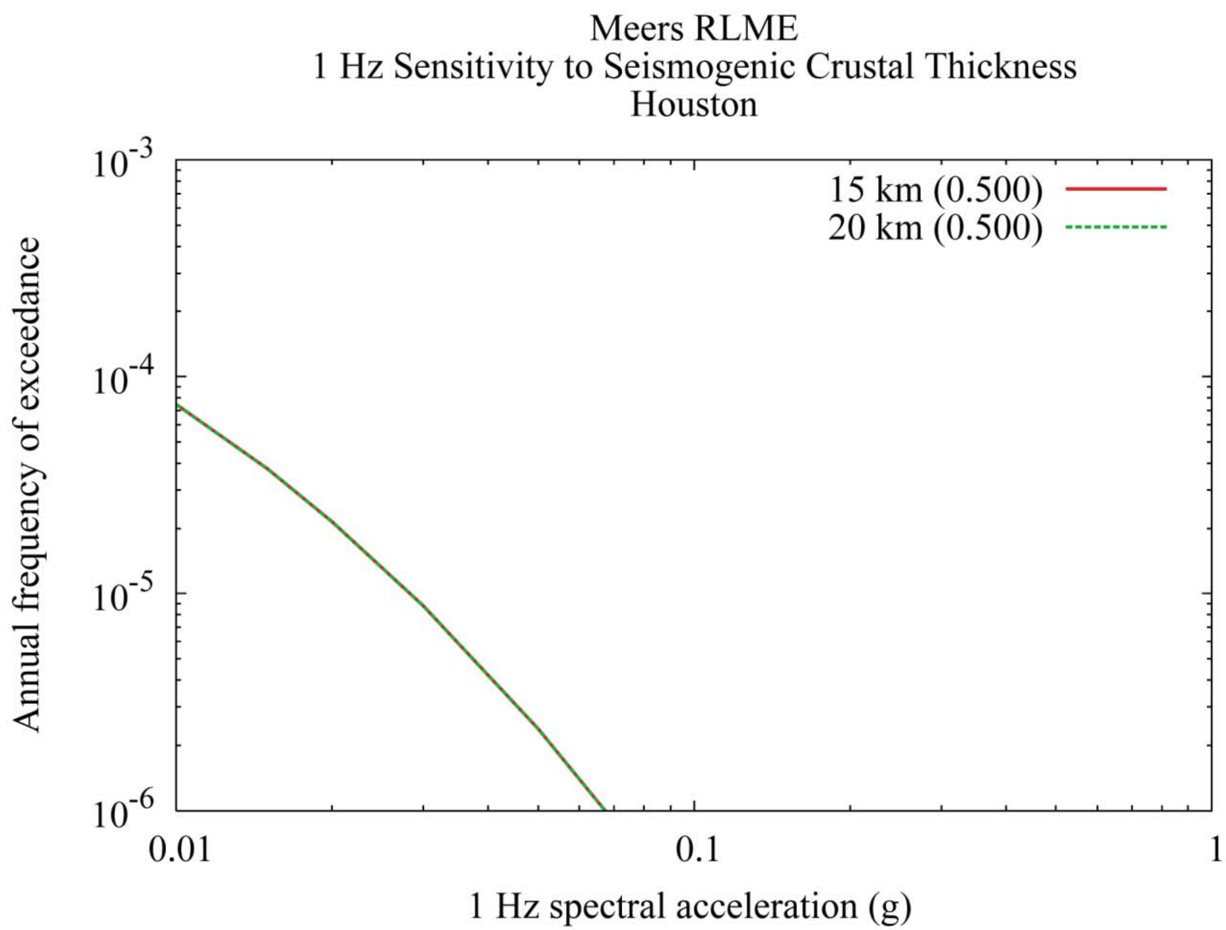

Figure 9.3-20
1 Hz sensitivity to seismogenic thickness at Houston for the Meers fault and OKA area sources

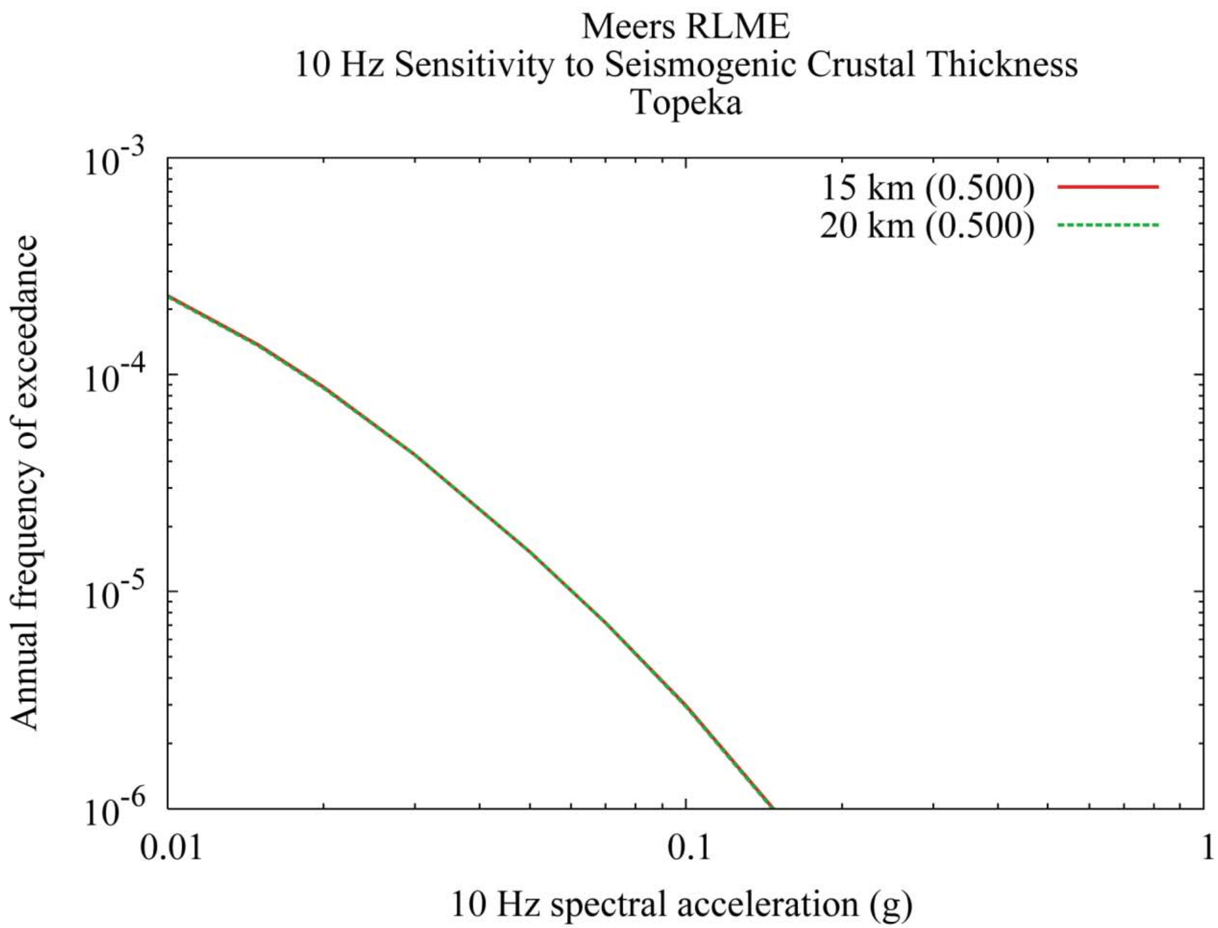

Figure 9.3-21
10 Hz sensitivity to seismogenic thickness at Topeka for the Meers fault and OKA area sources

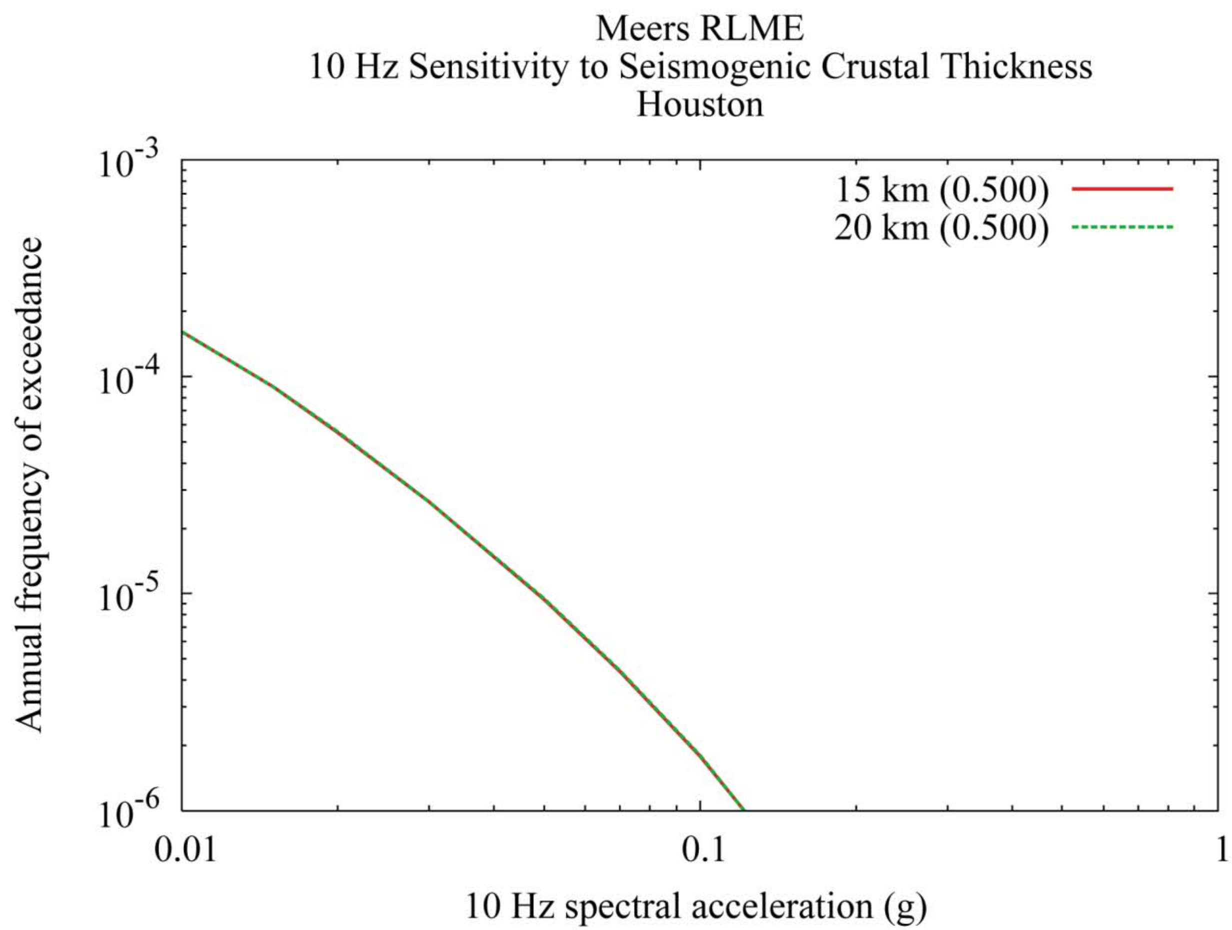

Figure 9.3-22
10 Hz sensitivity to seismogenic thickness at Houston for the Meers fault and OKA area sources

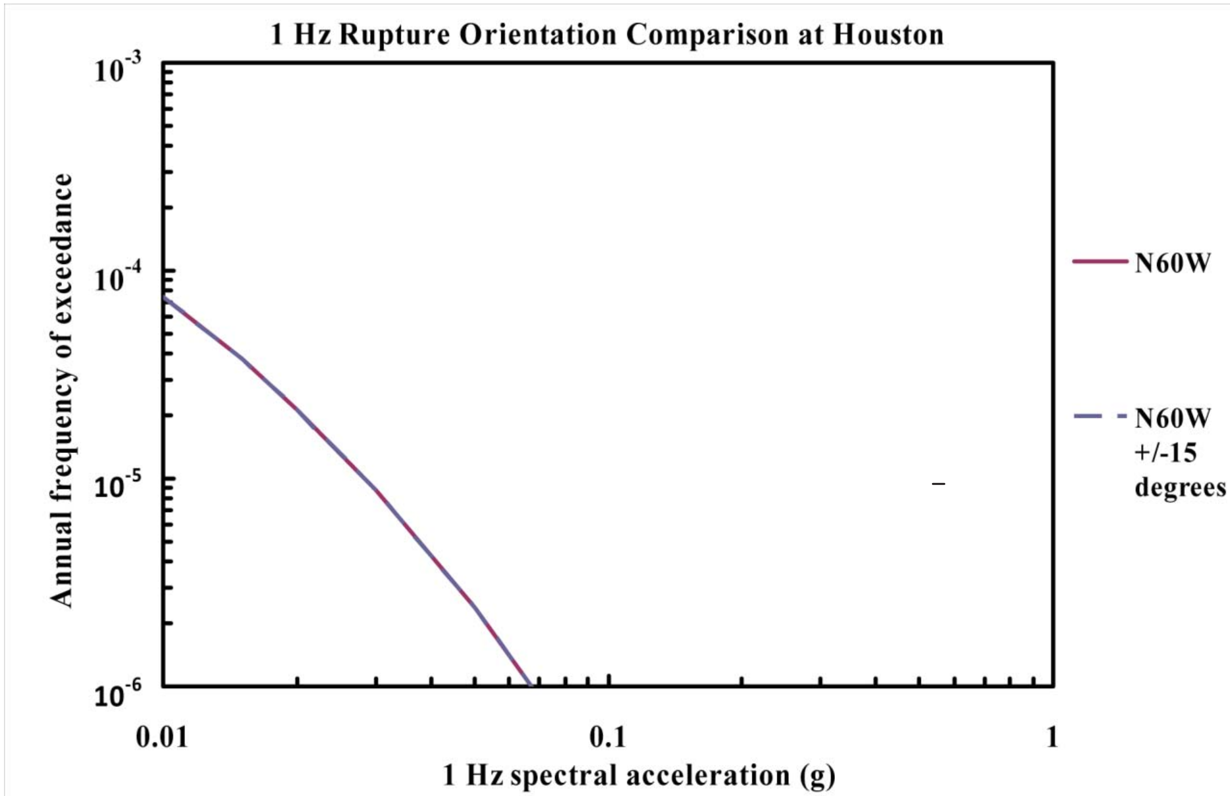

Figure 9.3-23
1 Hz sensitivity to rupture orientation at Houston for the OKA area source

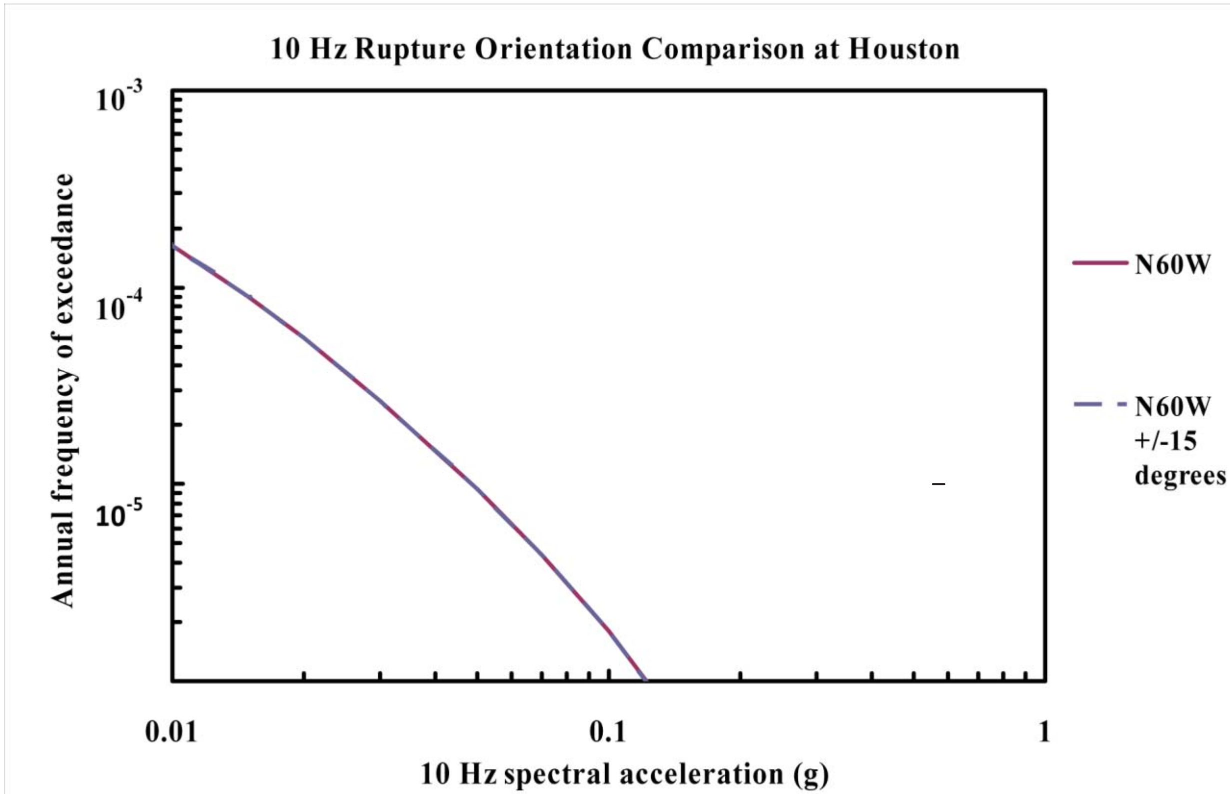

Figure 9.3-24
10 Hz sensitivity to rupture orientation at Houston for the OKA area source

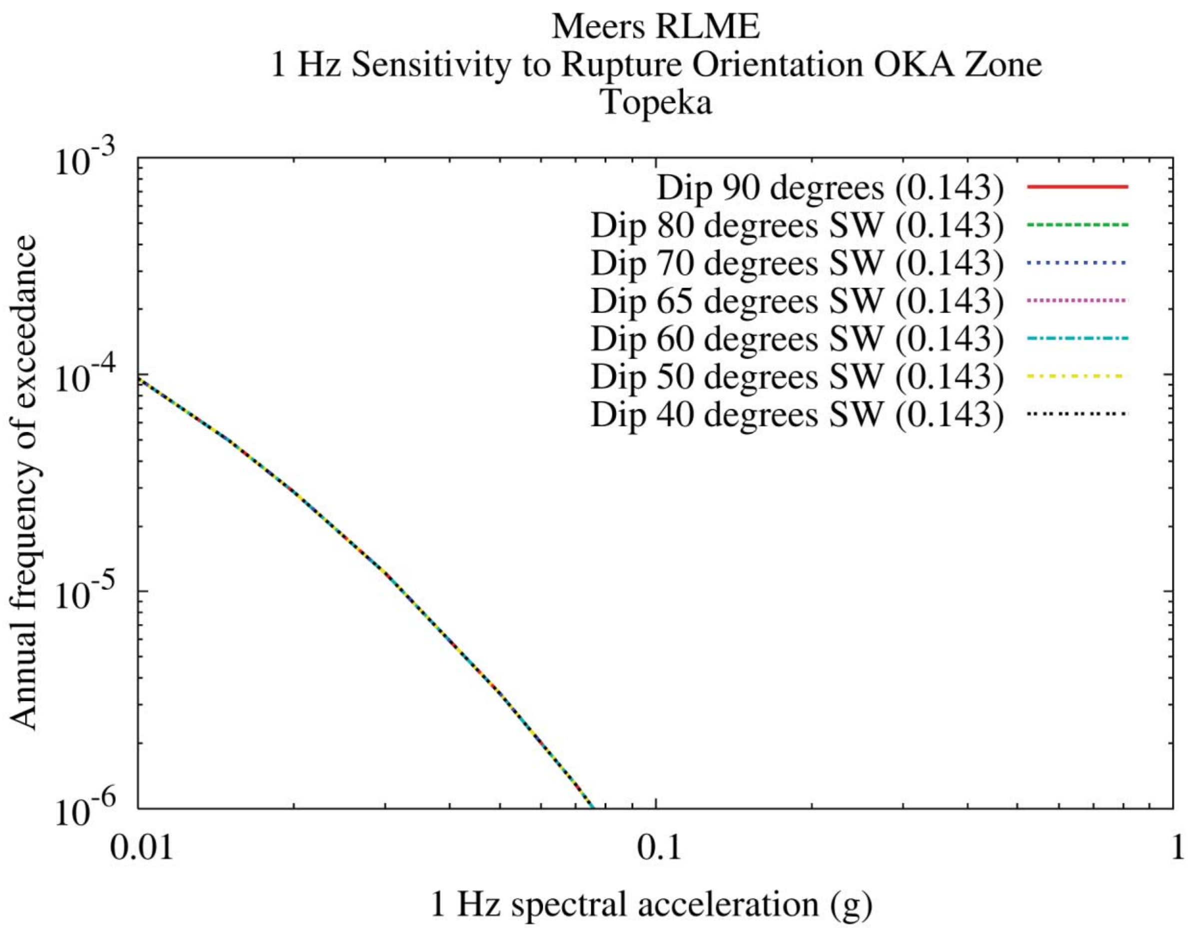

Figure 9.3-25
1 Hz sensitivity to rupture orientation (dip) at Topeka for the OKA area source

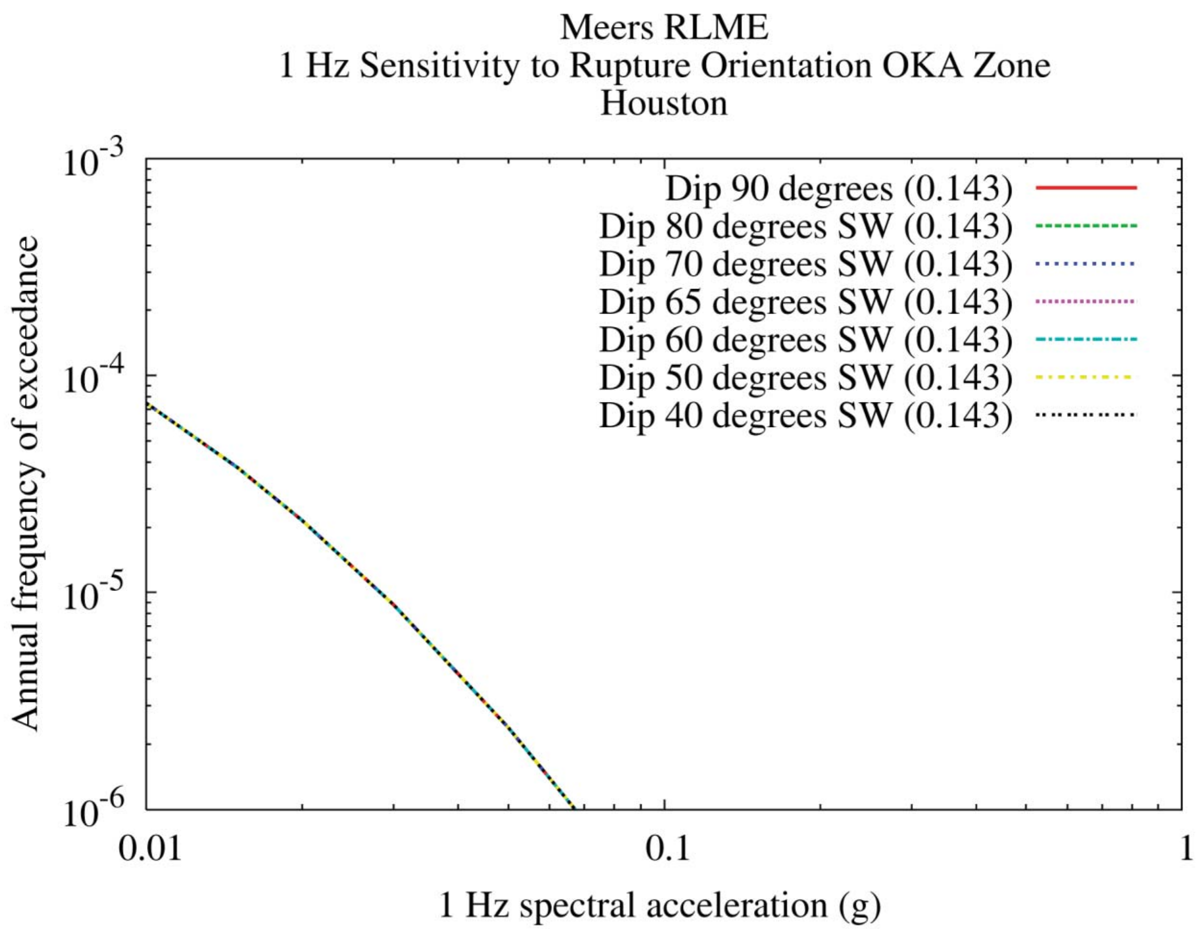

Figure 9.3-26
1 Hz sensitivity to rupture orientation (dip) at Houston for the OKA area source

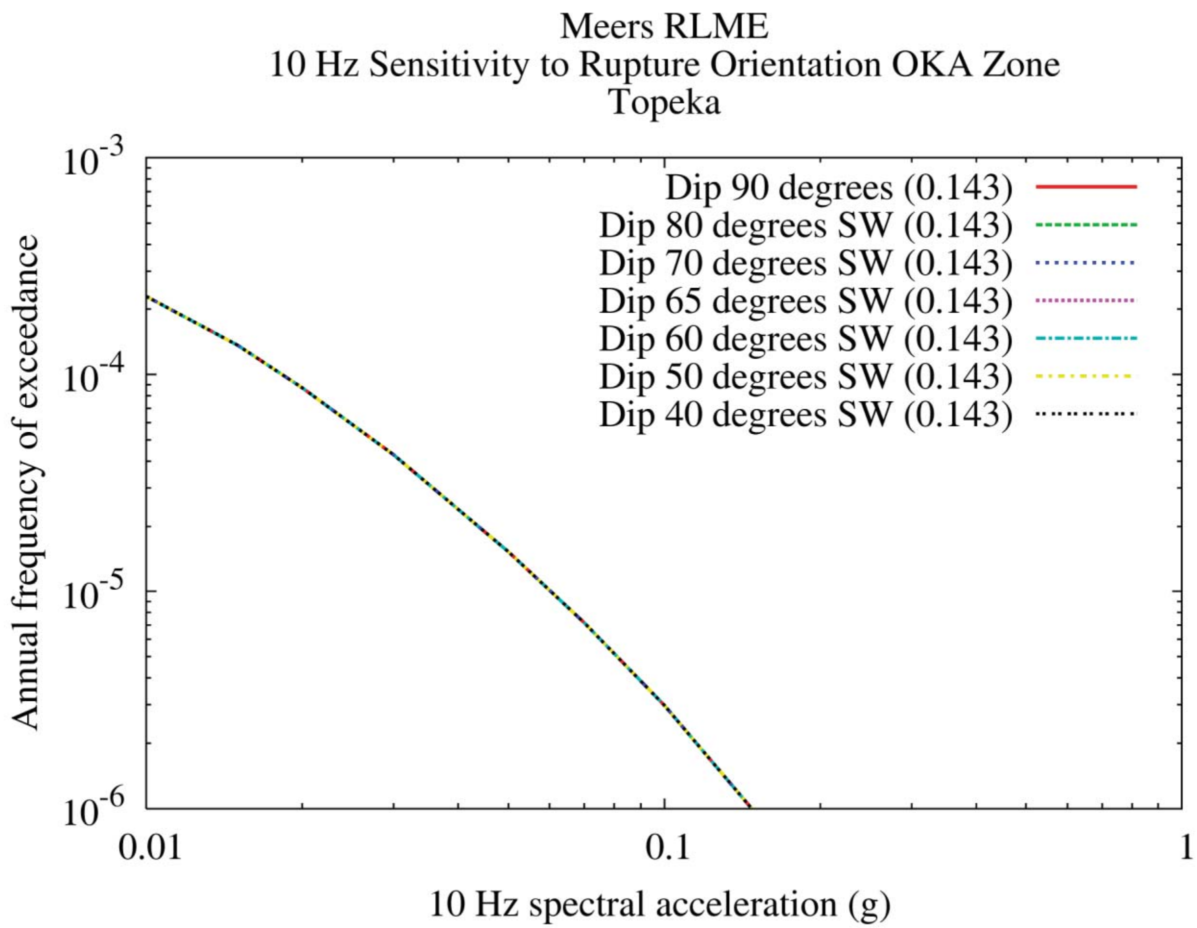

Figure 9.3-27
10 Hz sensitivity to rupture orientation (dip) at Topeka for the OKA area source

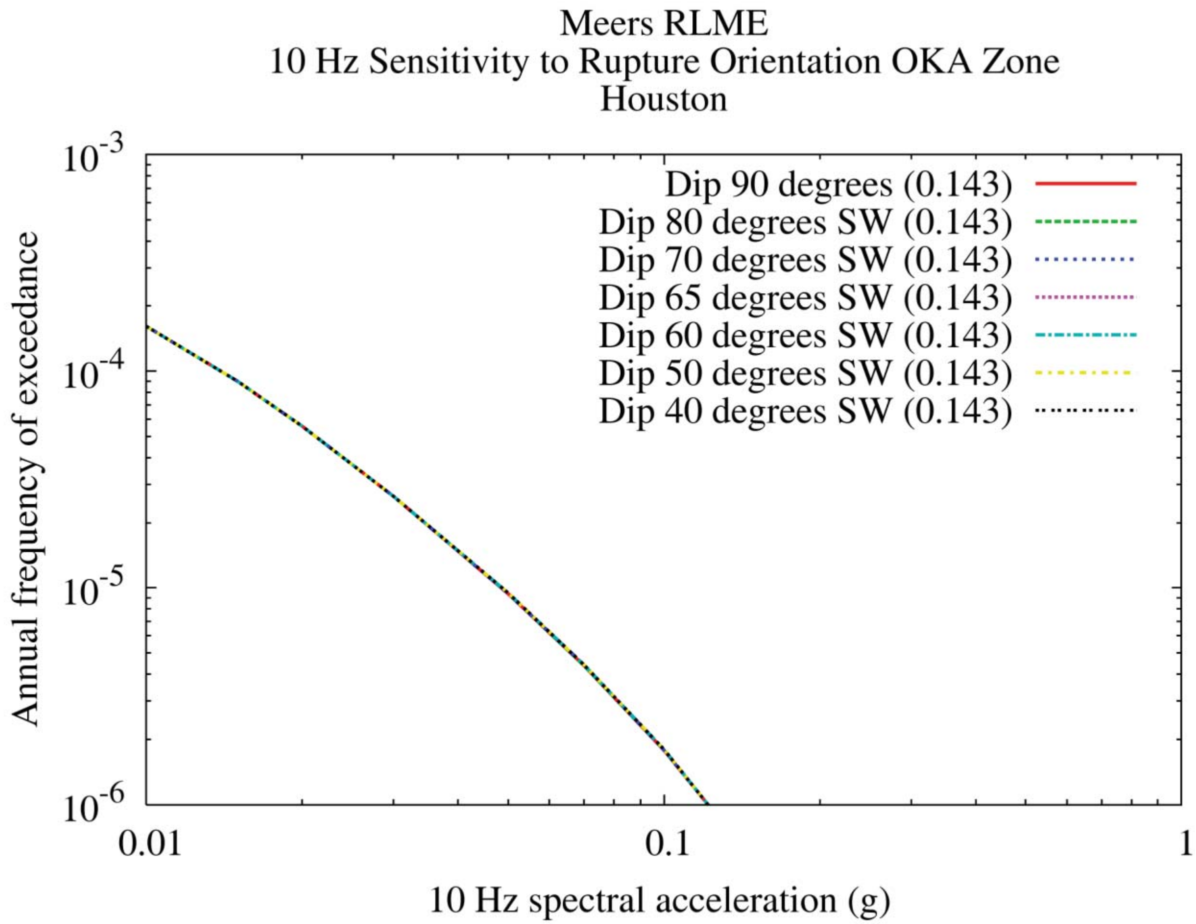

Figure 9.3-28
10 Hz sensitivity to rupture orientation (dip) at Houston for the OKA area source

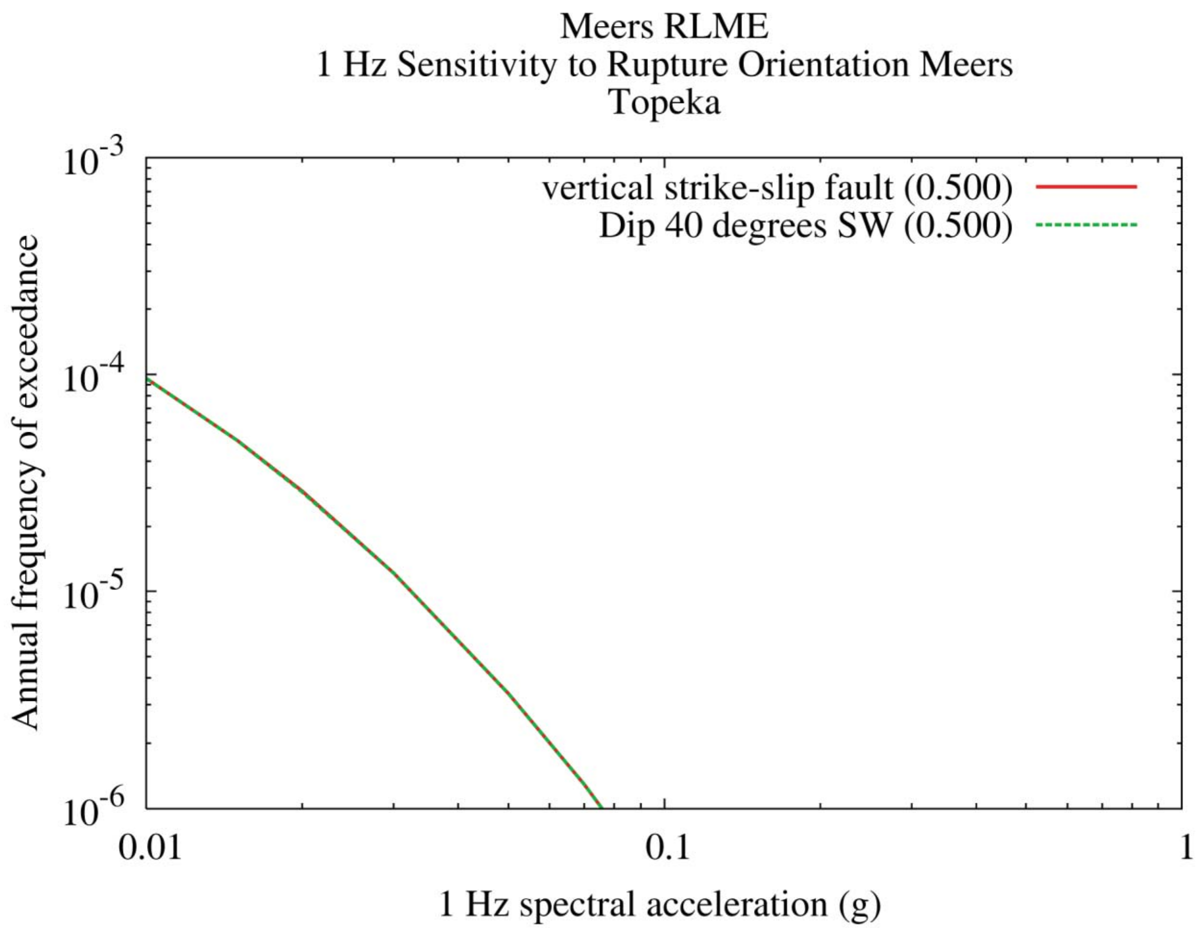

Figure 9.3-29
1 Hz sensitivity to rupture orientation (dip) at Topeka for the Meers fault source

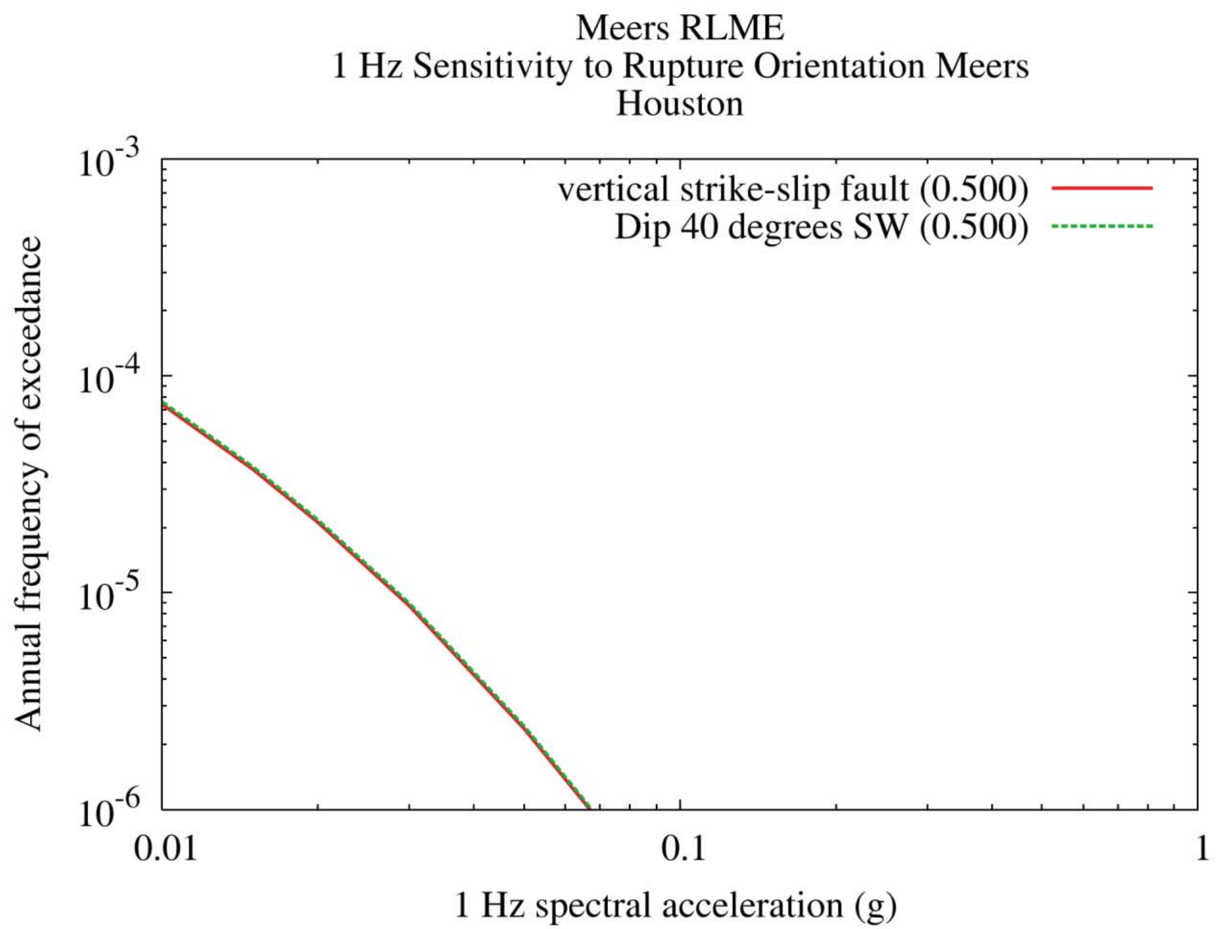

Figure 9.3-30
1 Hz sensitivity to rupture orientation (dip) at Houston for the Meers fault source

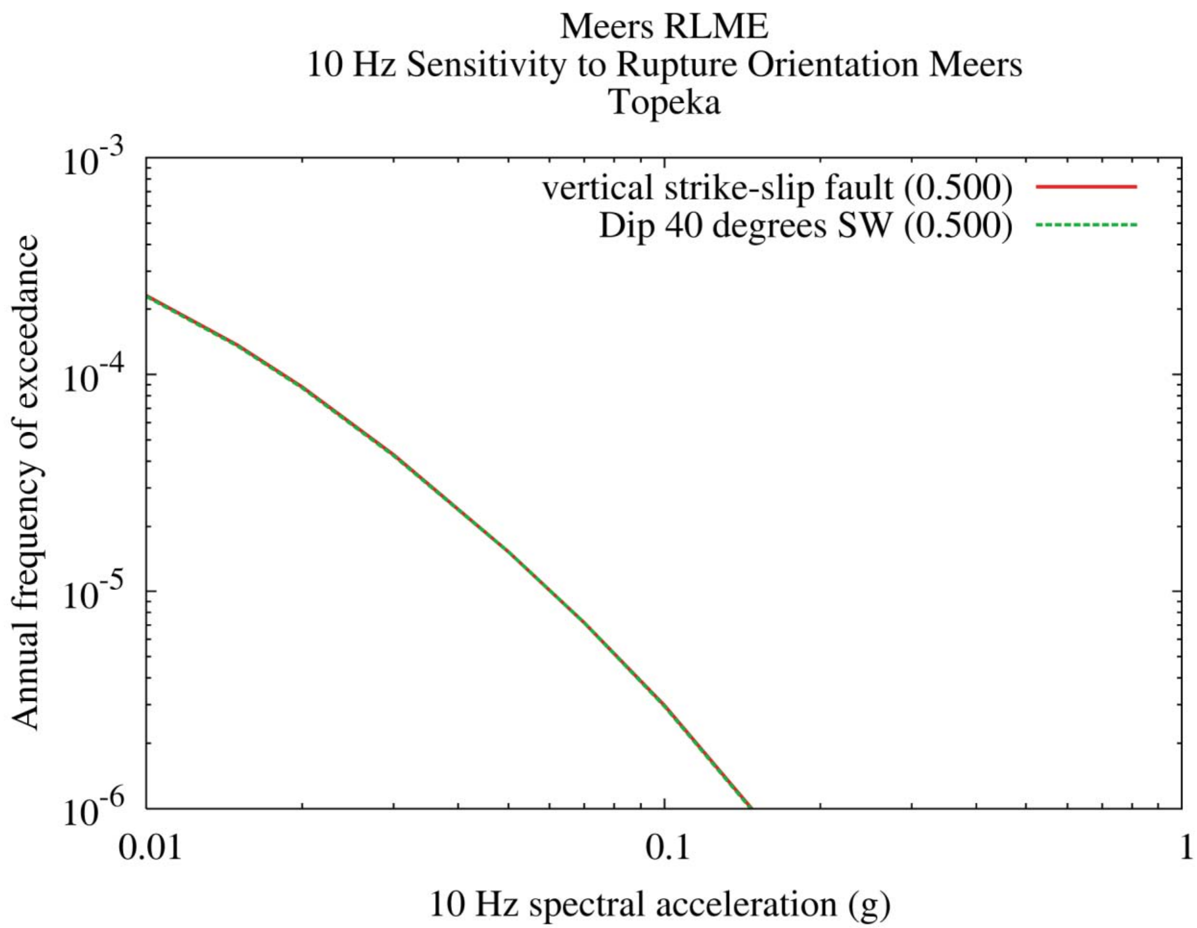

Figure 9.3-31
10 Hz sensitivity to rupture orientation (dip) at Topeka for the Meers fault source

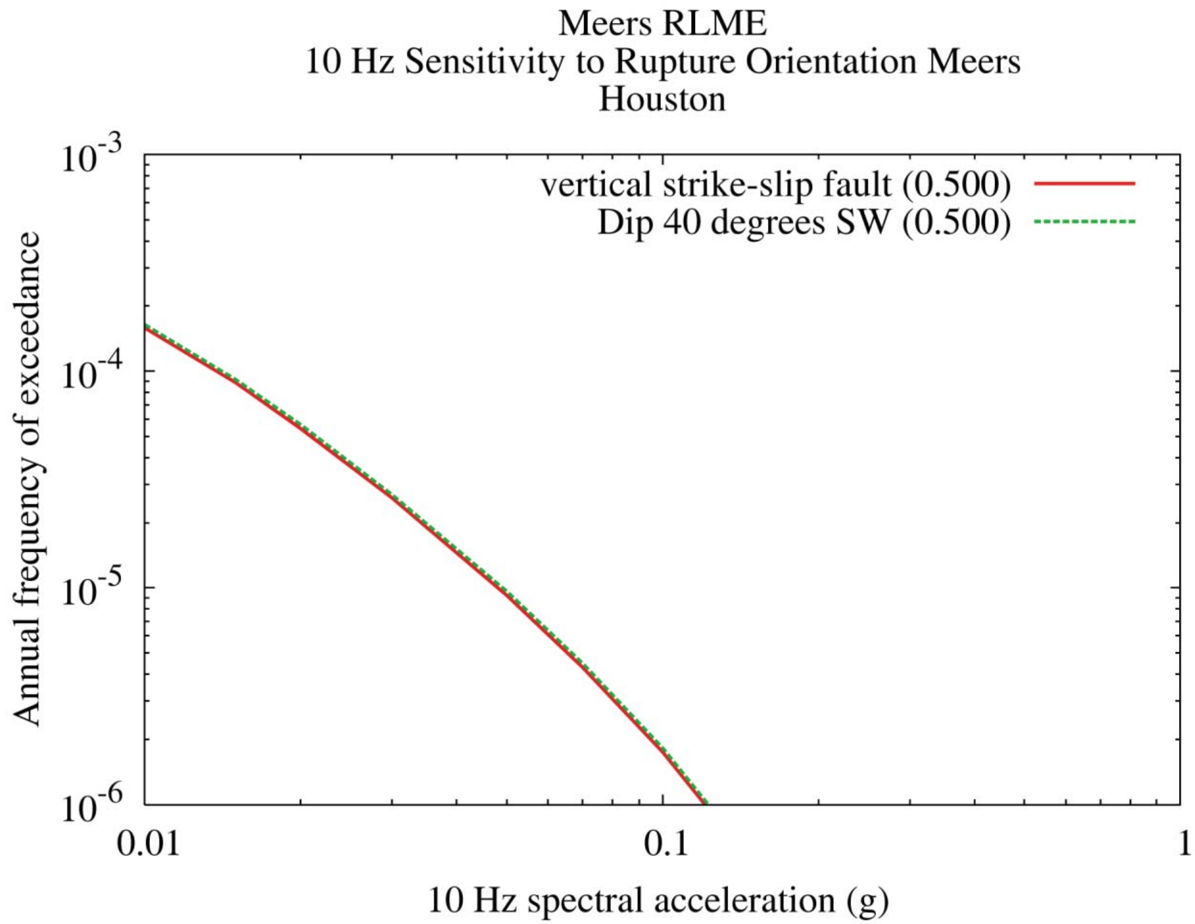

Figure 9.3-32
10 Hz sensitivity to rupture orientation (dip) at Houston for the Meers fault source

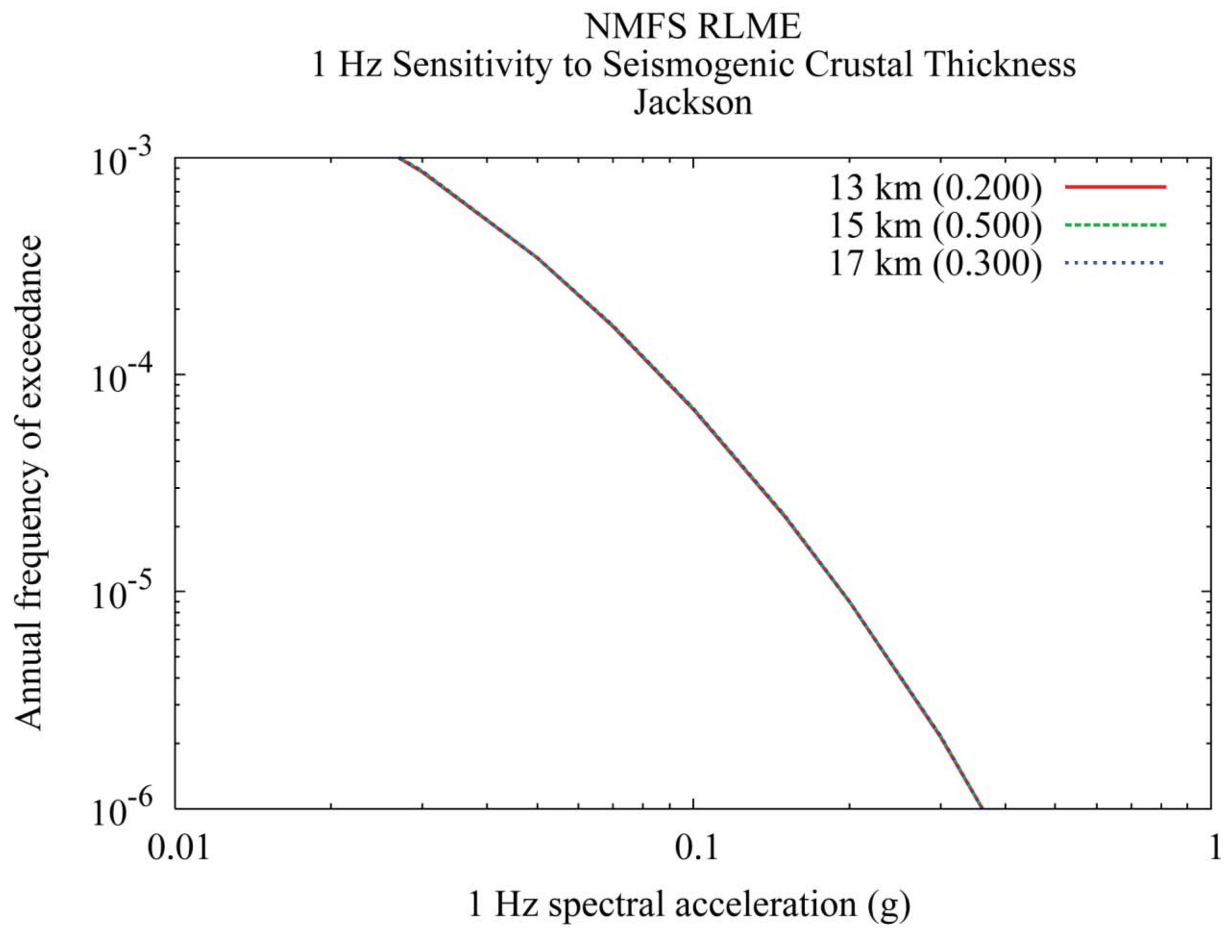

Figure 9.3-33
1 Hz sensitivity to seismogenic thickness at Jackson for the NMFS fault sources

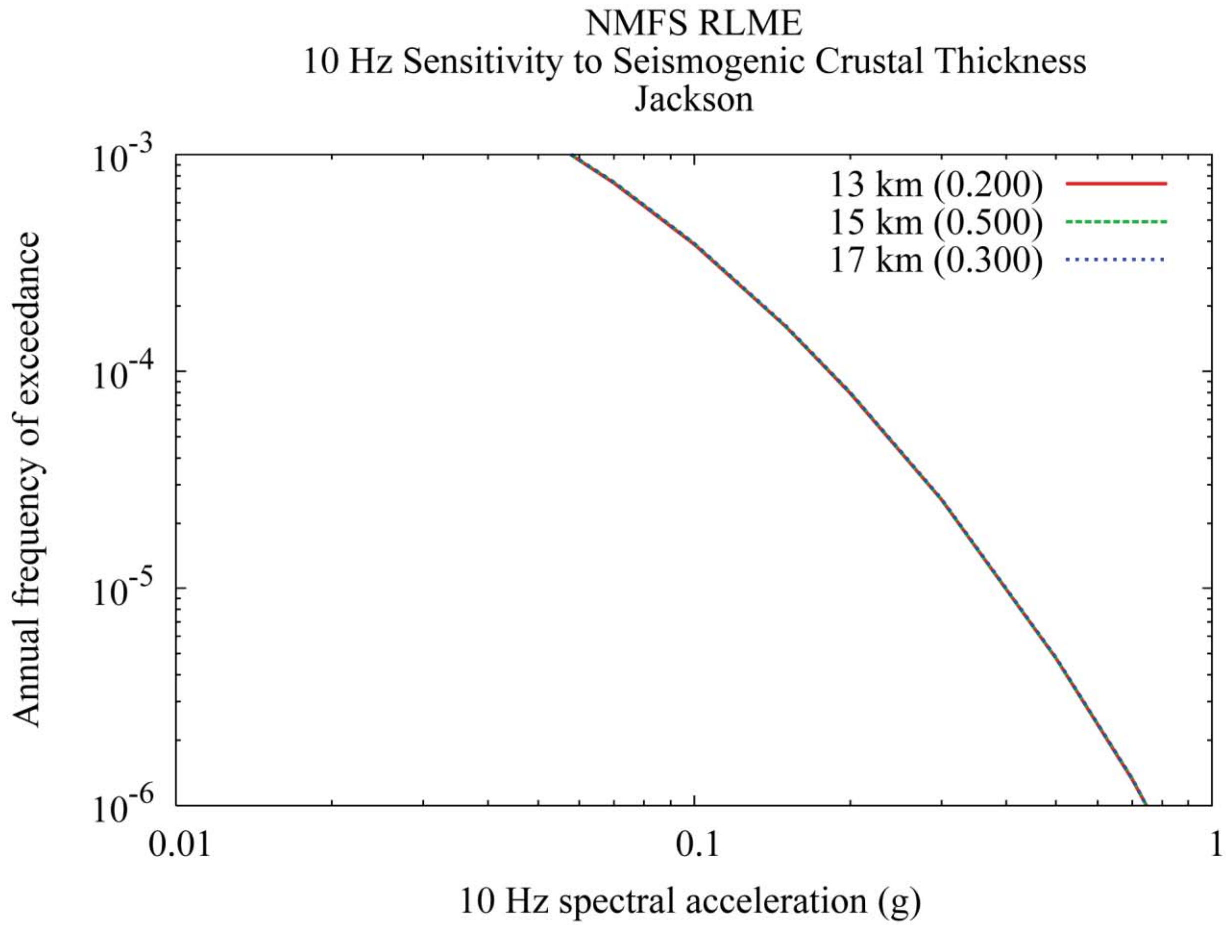

Figure 9.3-34
10 Hz sensitivity to seismogenic thickness at Jackson for the NMFS fault sources

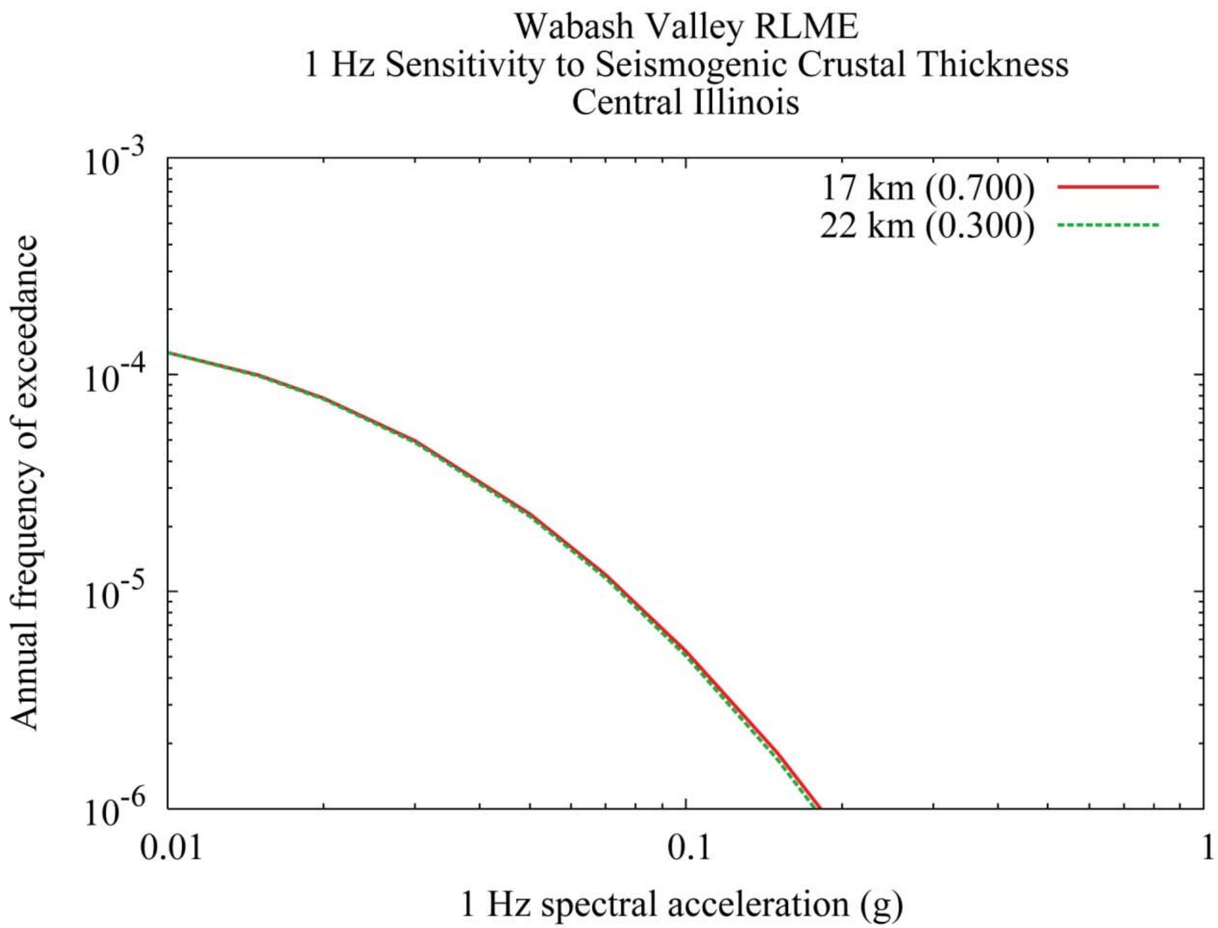

Figure 9.3-35
1 Hz sensitivity to seismogenic thickness at Central Illinois for the Wabash Valley area source

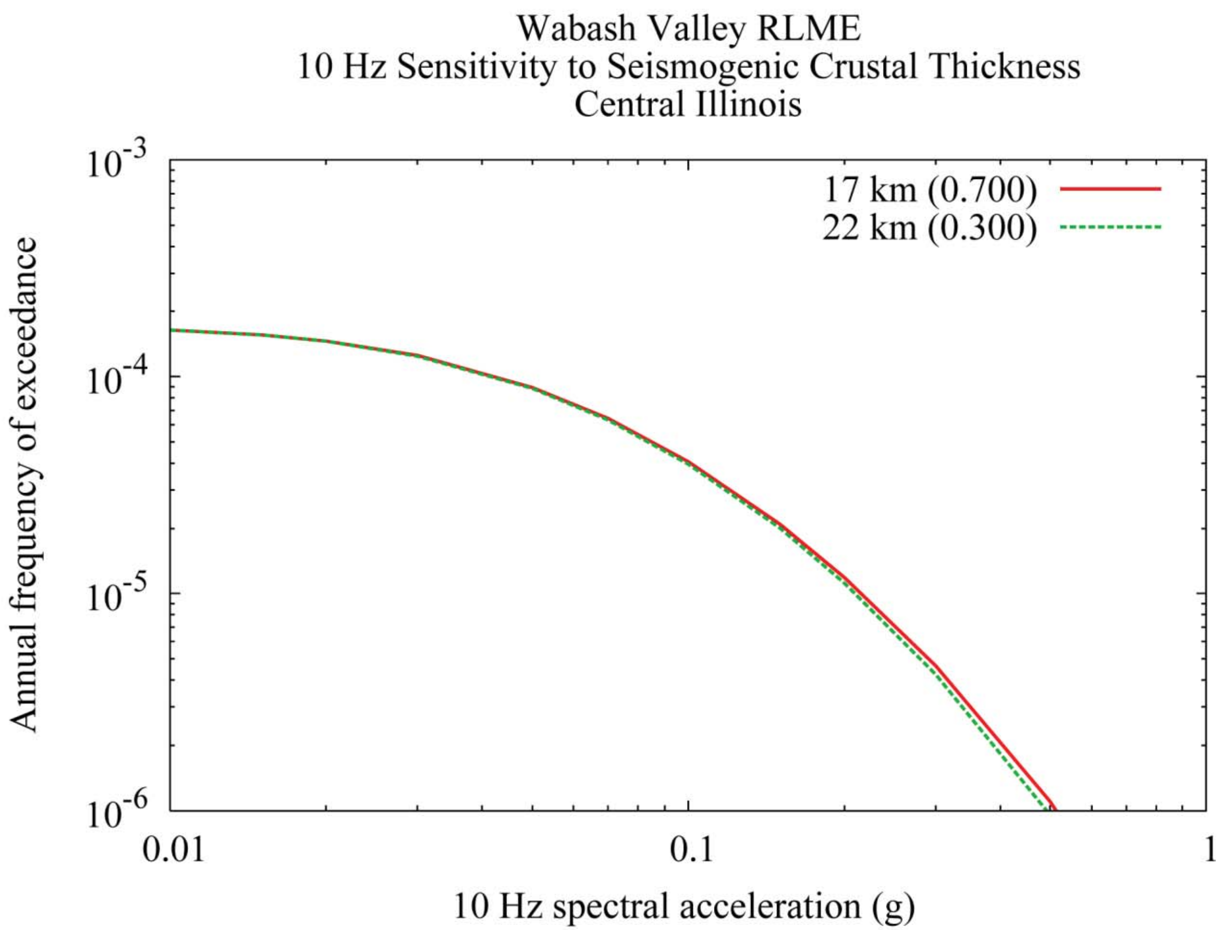

Figure 9.3-36
10 Hz sensitivity to seismogenic thickness at Central Illinois for the Wabash Valley area source

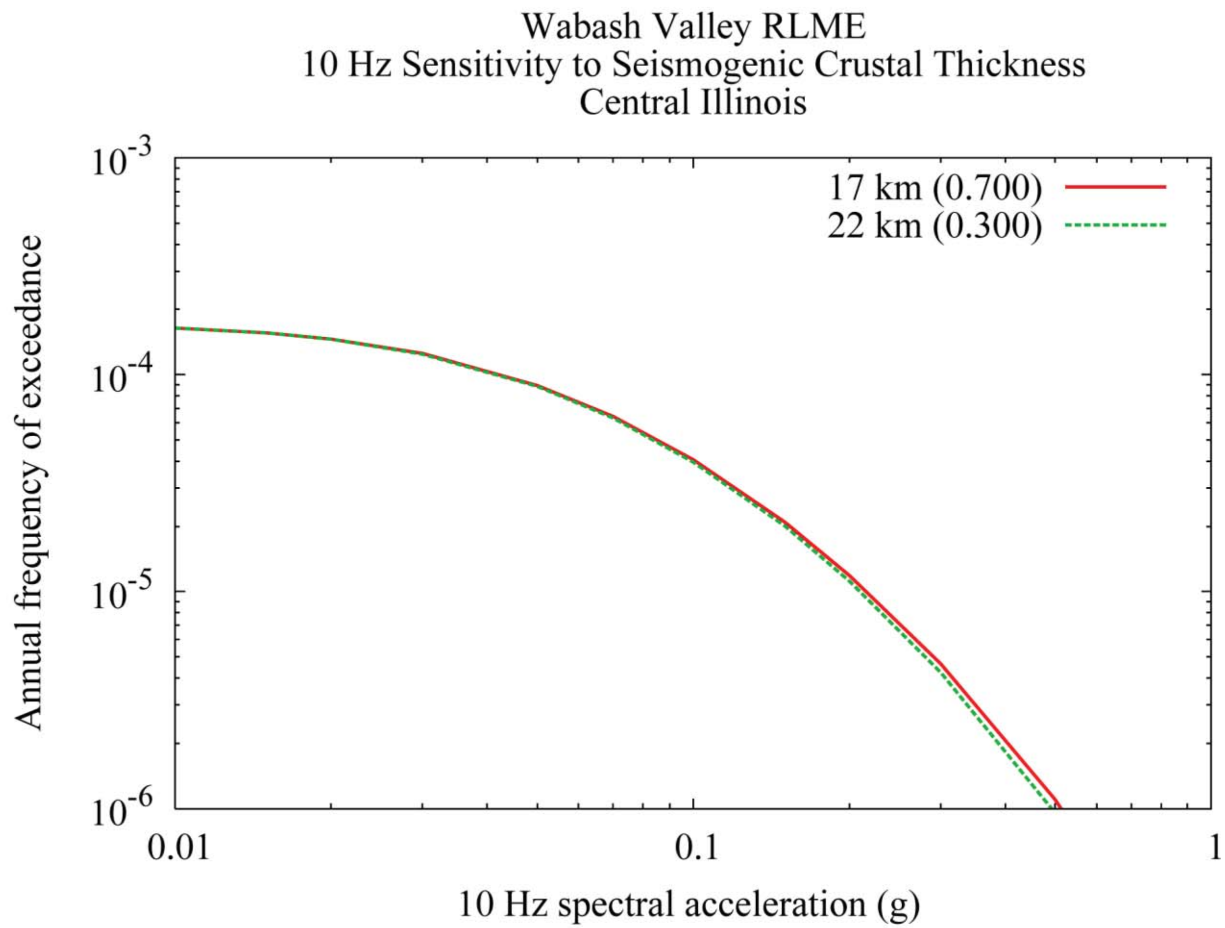

Figure 9.3-37
1 Hz sensitivity to rupture orientation (dip) at Central Illinois for the Wabash Valley area source

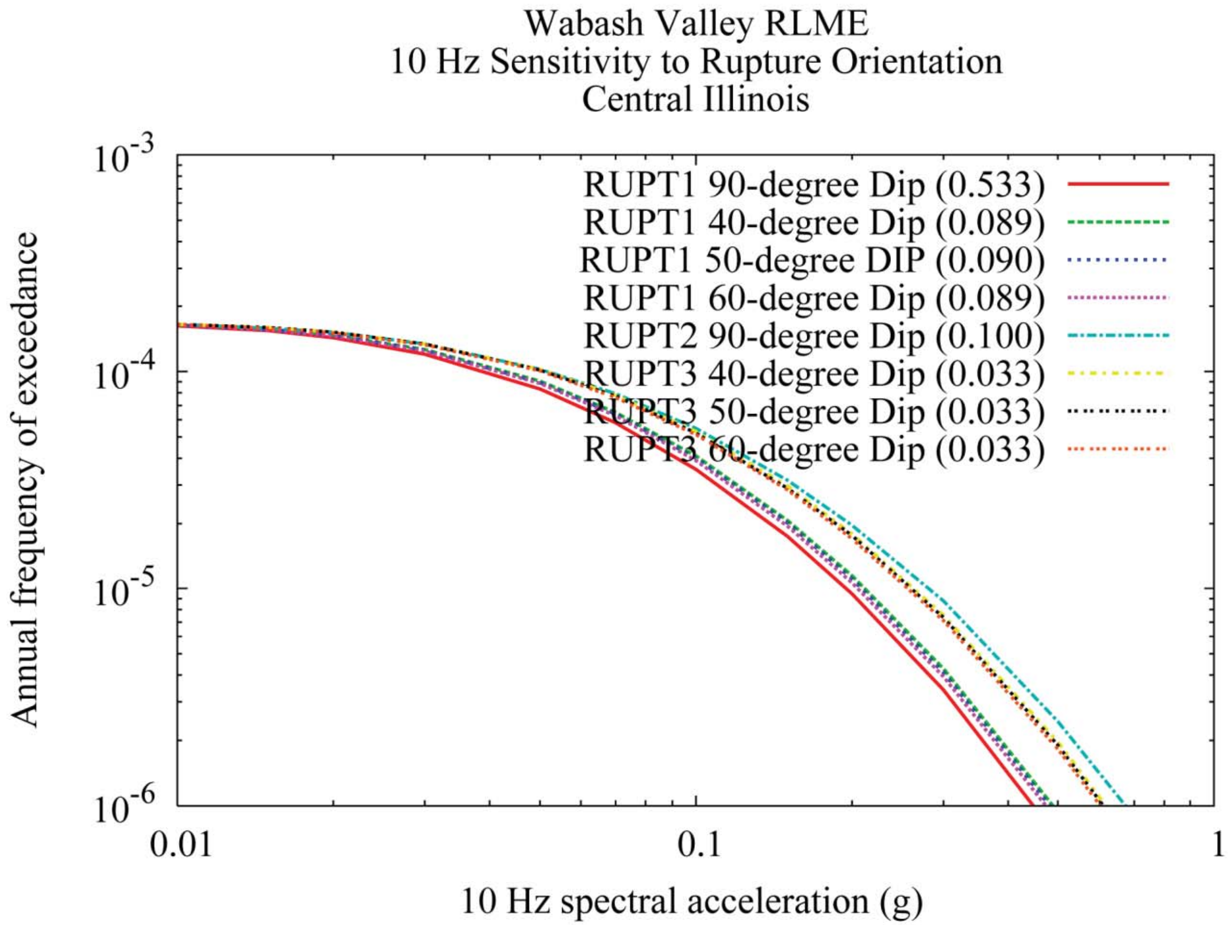

Figure 9.3-38
10 Hz sensitivity to rupture orientation (dip) at Central Illinois for the Wabash Valley area source

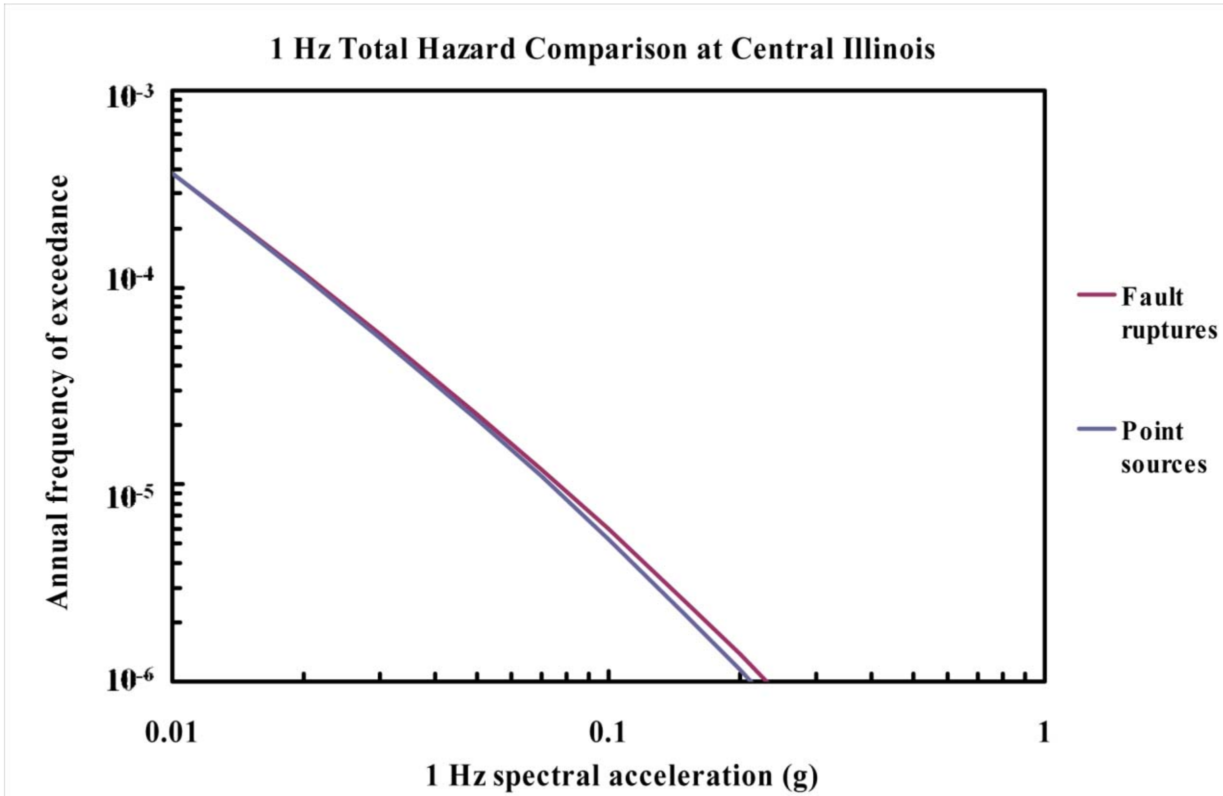

Figure 9.3-39
1 Hz sensitivity to fault ruptures vs. point source for the Central Illinois site from the Mid-C–A background source

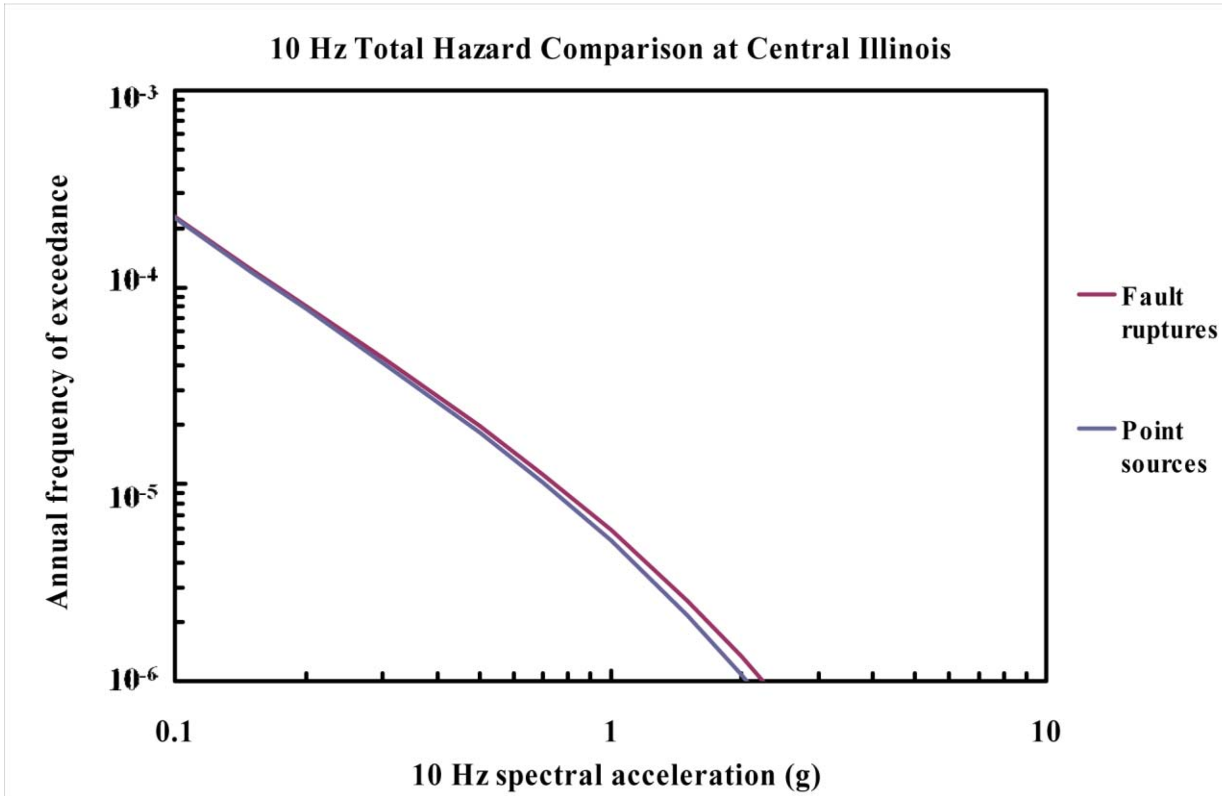

Figure 9.3-40
10 Hz sensitivity to fault ruptures vs. point source for the Central Illinois site from the Mid-C–A background source

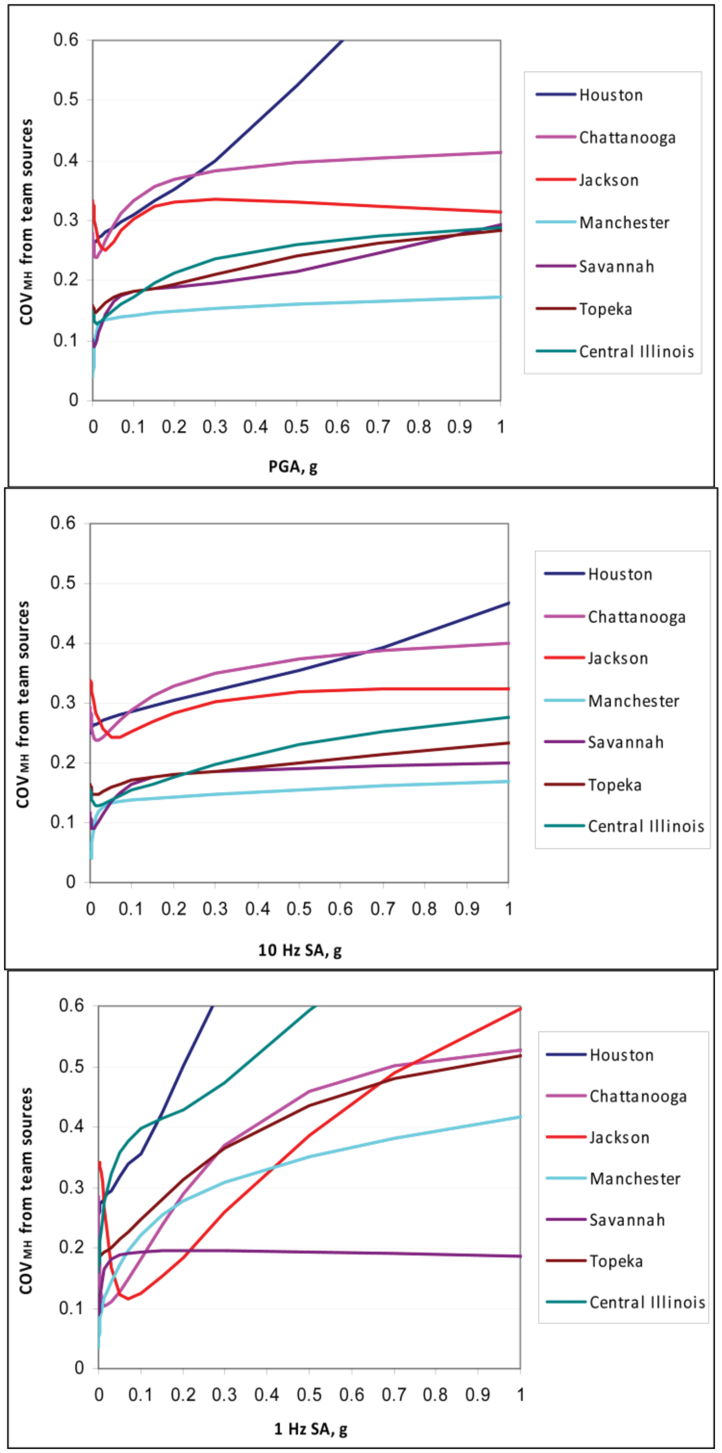

Figure 9.4-1
COV_{MH} from EPRI (1989) team sources vs. ground motion amplitude for seven test sites: PGA (top), 10 Hz SA (middle), and 1 Hz SA (bottom)

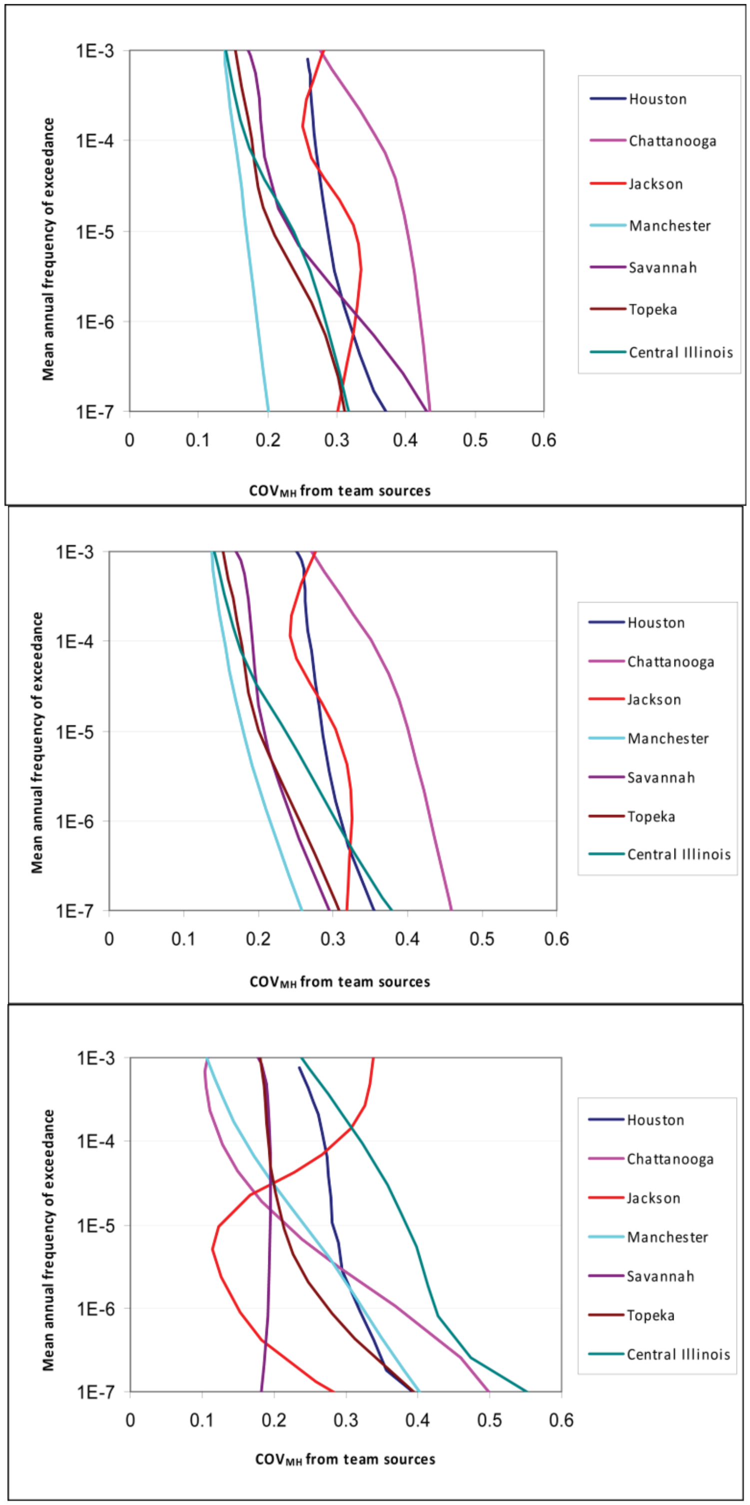

Figure 9.4-2
COV_{MH} from EPRI (1989) team sources vs. seismic hazard (i.e., annual frequency of exceedance) for seven test sites: PGA (top), 10 Hz SA (middle), and 1 Hz SA (bottom)

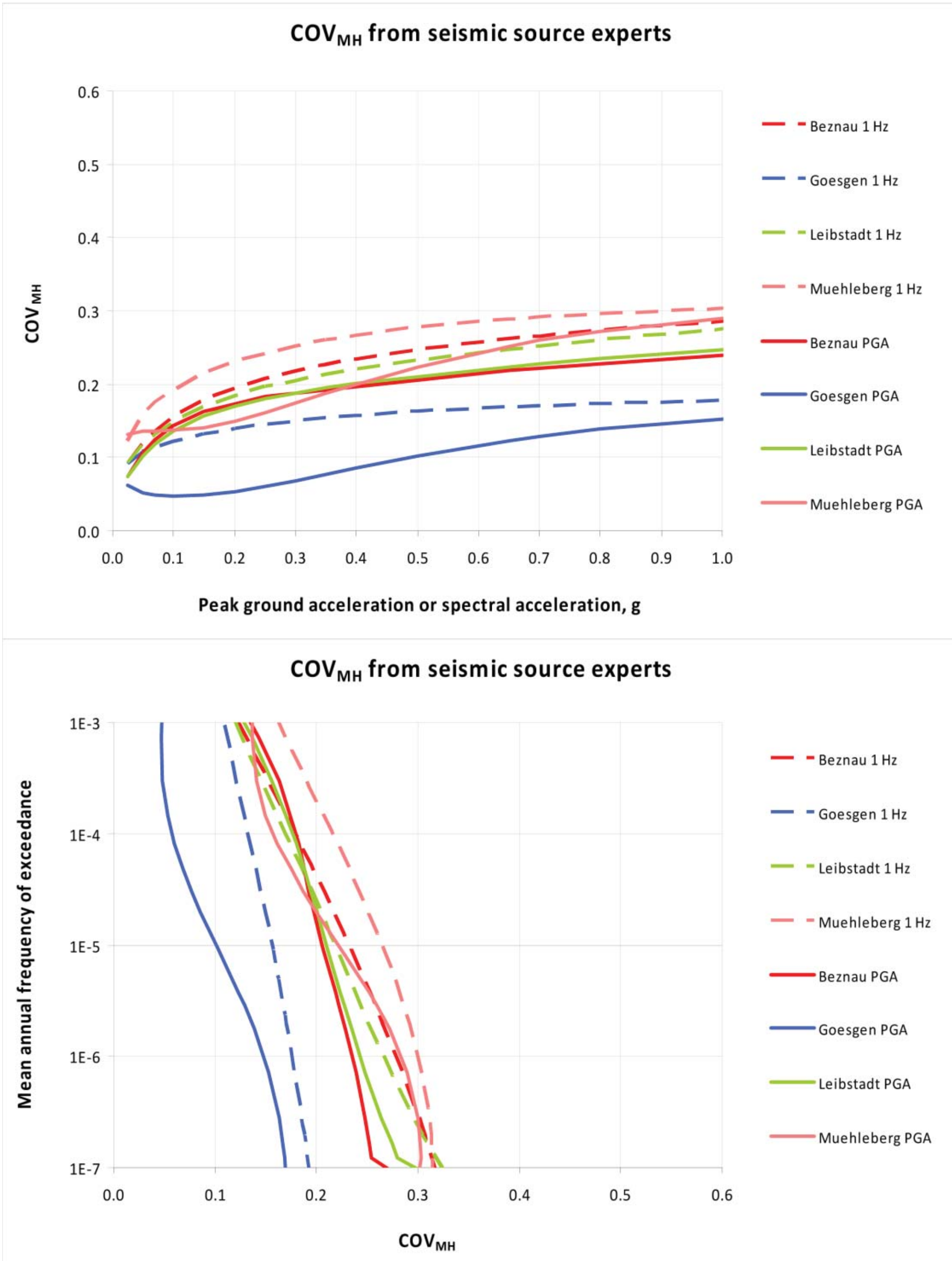

Figure 9.4-3
COV$_{MH}$ from seismic source experts (PEGASOS project) vs. amplitude (top) and annual frequency (bottom)

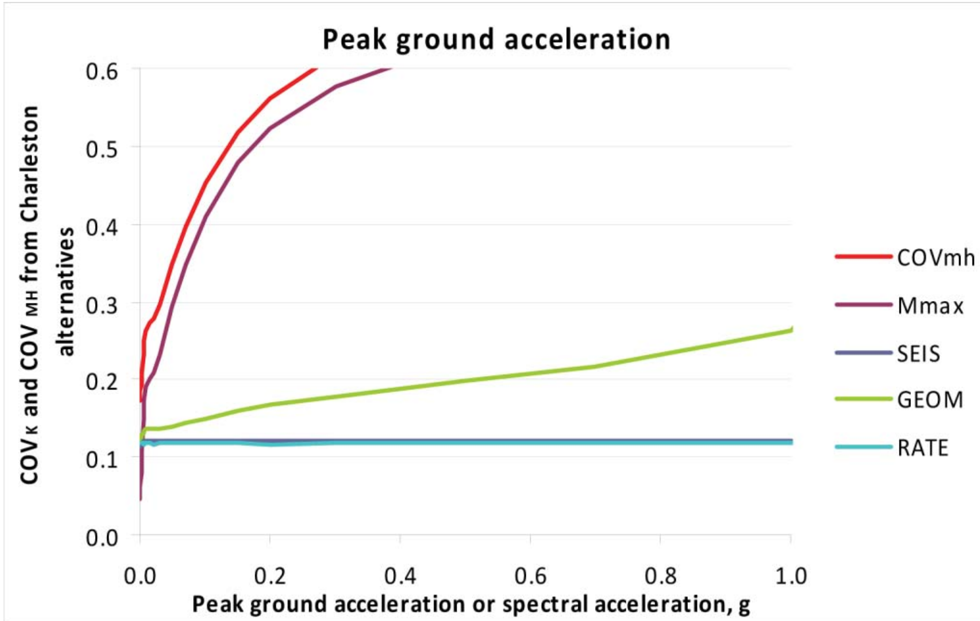

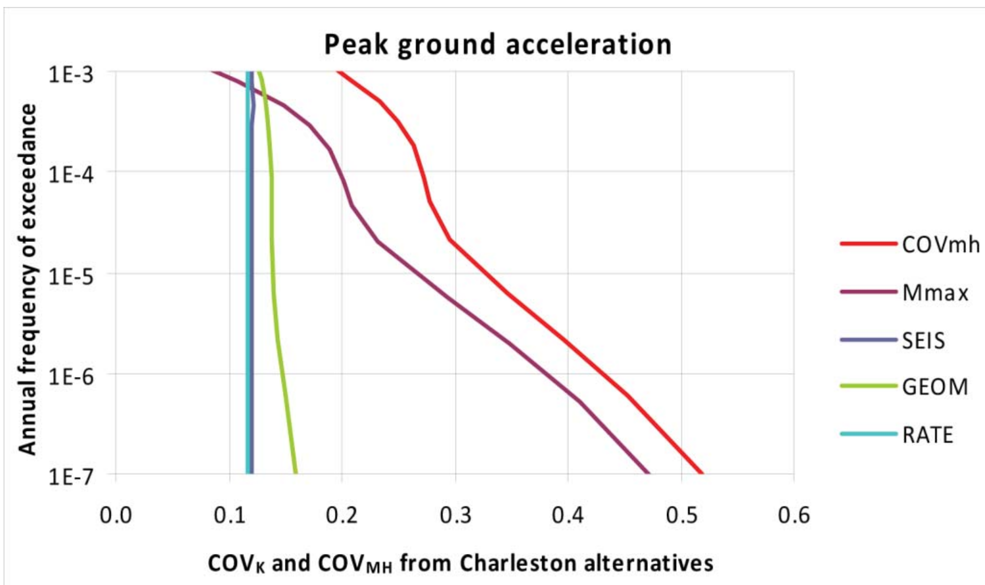

Figure 9.4-4
COV_K and COV_{MH} from Charleston alternatives for PGA, plotted vs. PGA amplitude (top) and hazard (bottom). COV_{MH} is the total COV of mean hazard; see Table 9.4-2 for other labels for curves.

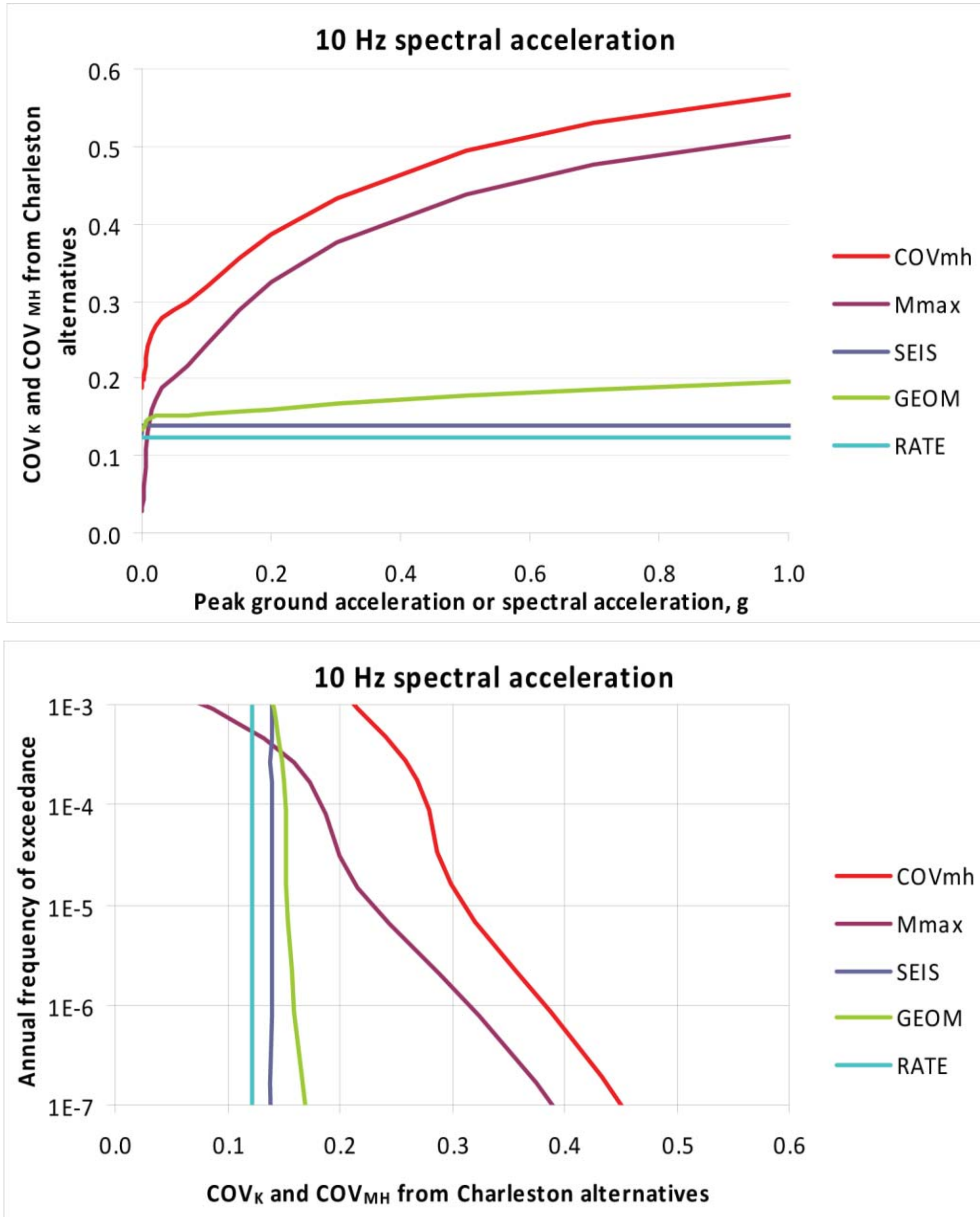

Figure 9.4-5
COV_K and COV_{MH} from Charleston alternatives for 10 Hz, plotted vs. 10 Hz amplitude (top) and hazard (bottom). COV_{MH} is the total COV of mean hazard; see Table 9.4-2 for other labels for curves.

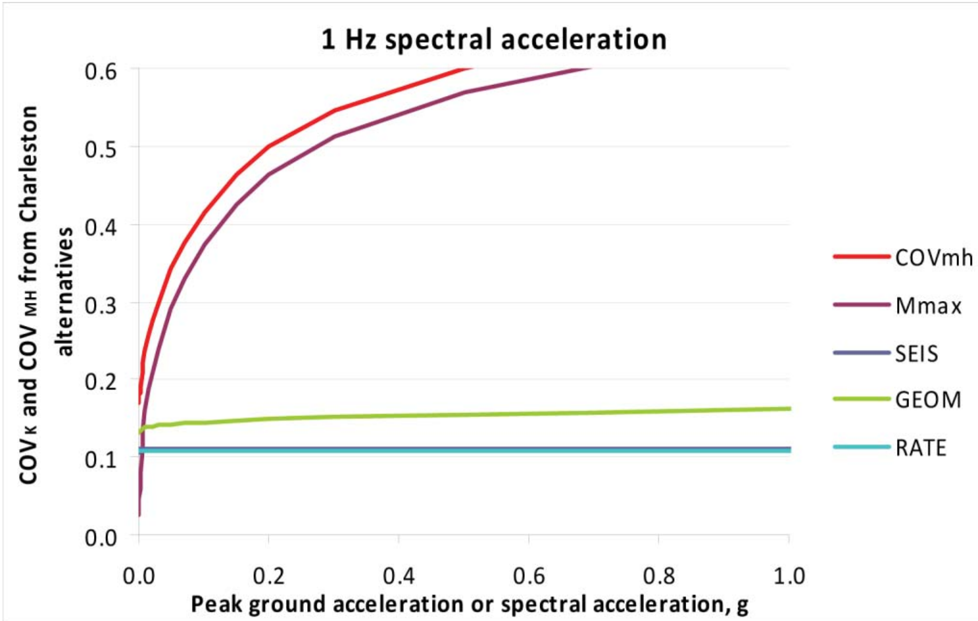

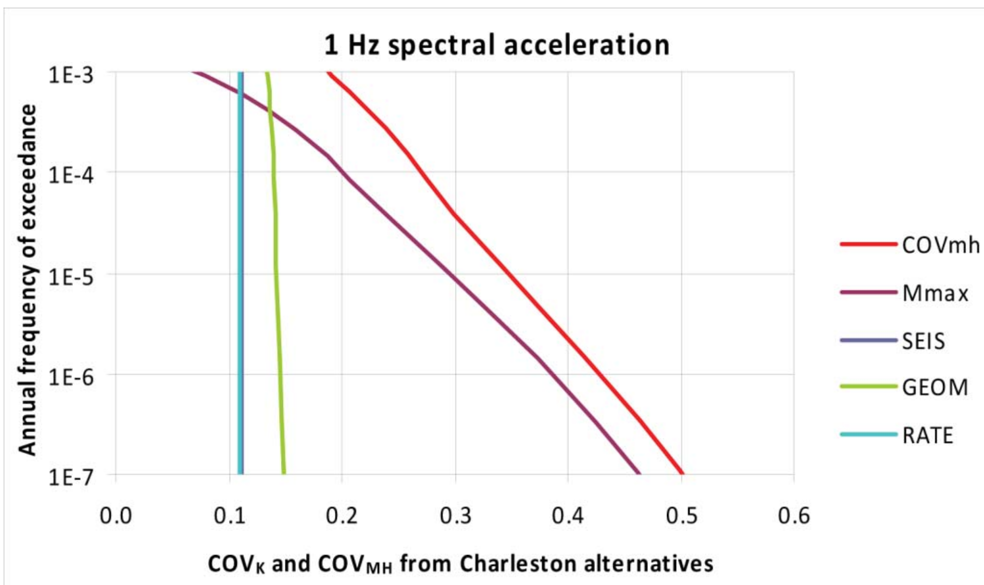

Figure 9.4-6
COV_K and COV_{MH} from Charleston alternatives for 1 Hz, plotted vs. 1 Hz amplitude (top) and hazard (bottom). COV_{MH} is the total COV of mean hazard; see Table 9.4-2 for other labels for curves..

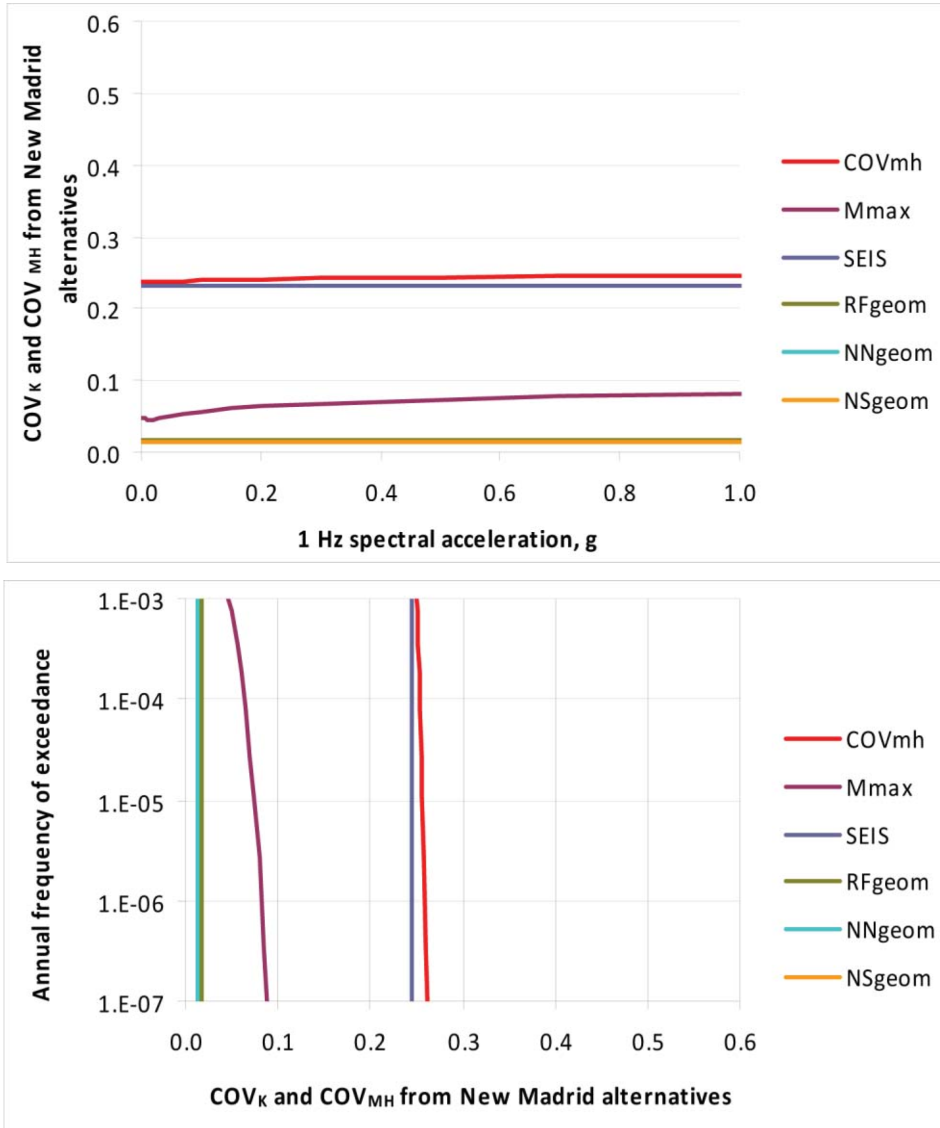

Figure 9.4-7
COV_K and COV_{MH} of total hazard from New Madrid for 1 Hz, plotted vs. 1 Hz amplitude (top) and hazard (bottom). COV_{MH} is the total COV; see the text for other labels for curves.

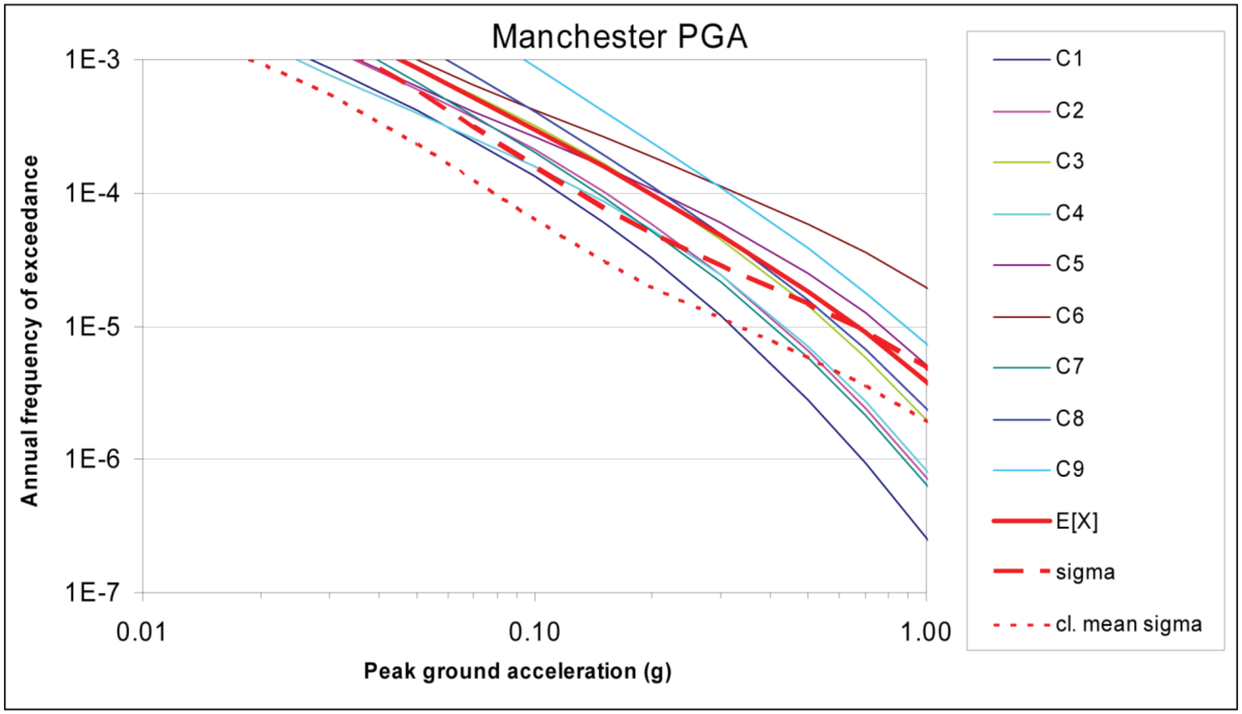

Figure 9.4-8
PGA hazard curves for Manchester test site

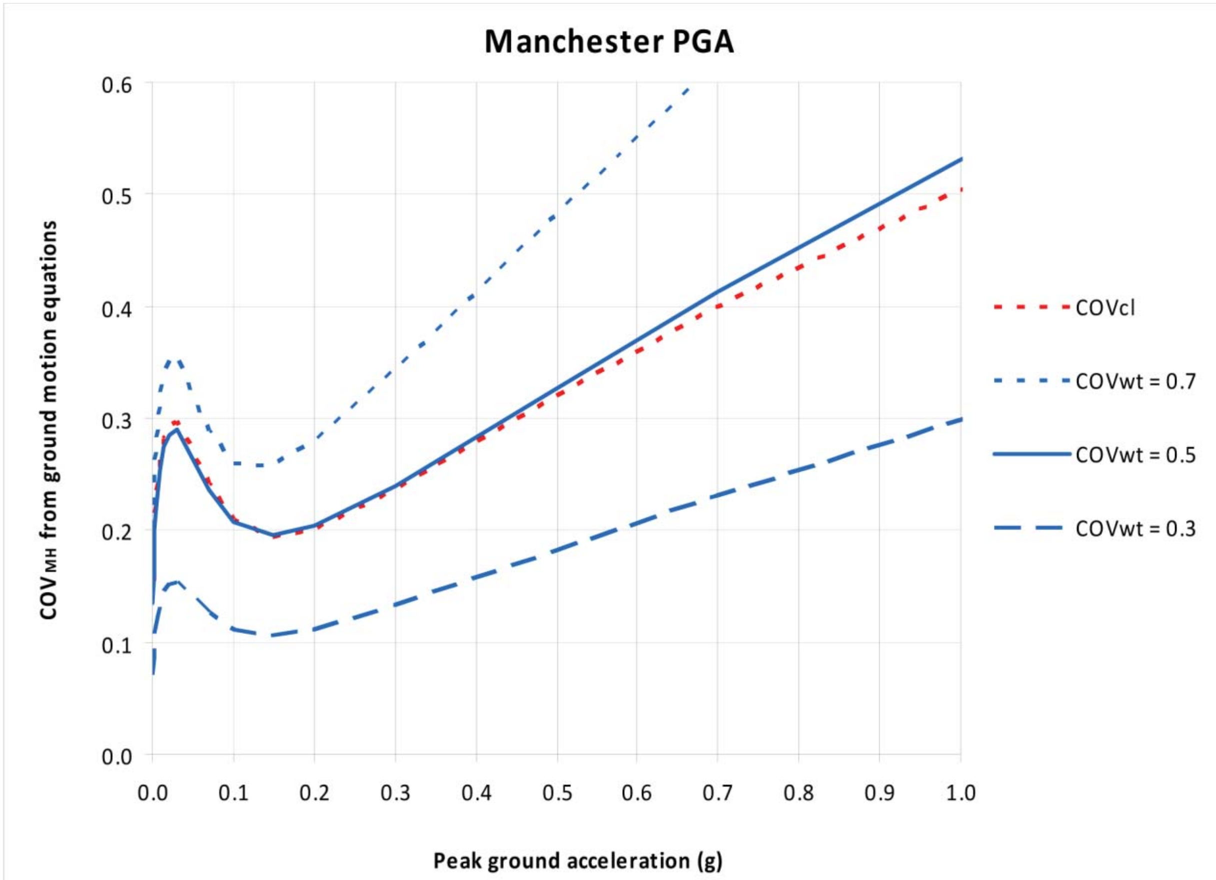

Figure 9.4-9
COV_{MH} of PGA hazard at Manchester site from ground motion equation vs. PGA

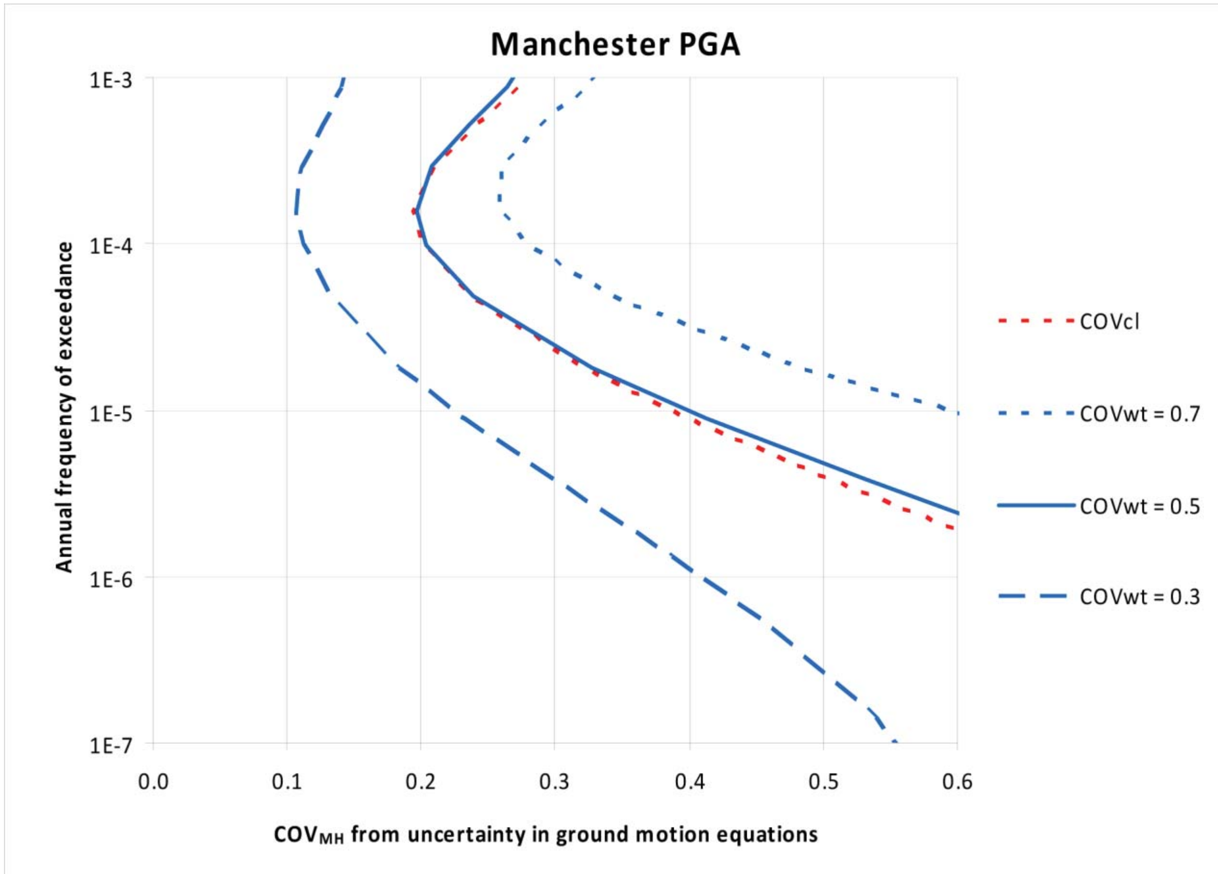

Figure 9.4-10
COV of PGA hazard at Manchester site from ground motion equation vs. hazard

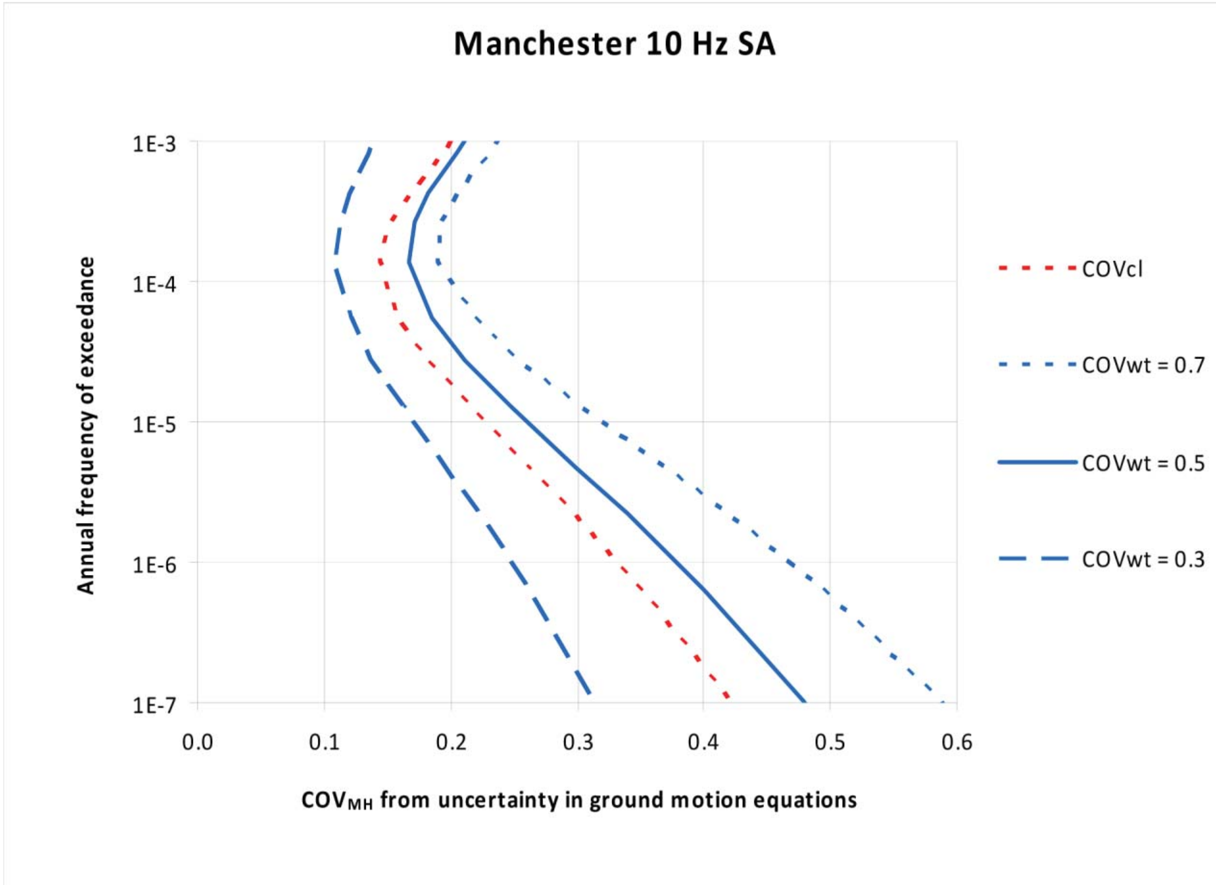

Figure 9.4-11
COV of 10 Hz hazard at Manchester site from ground motion equations vs. hazard

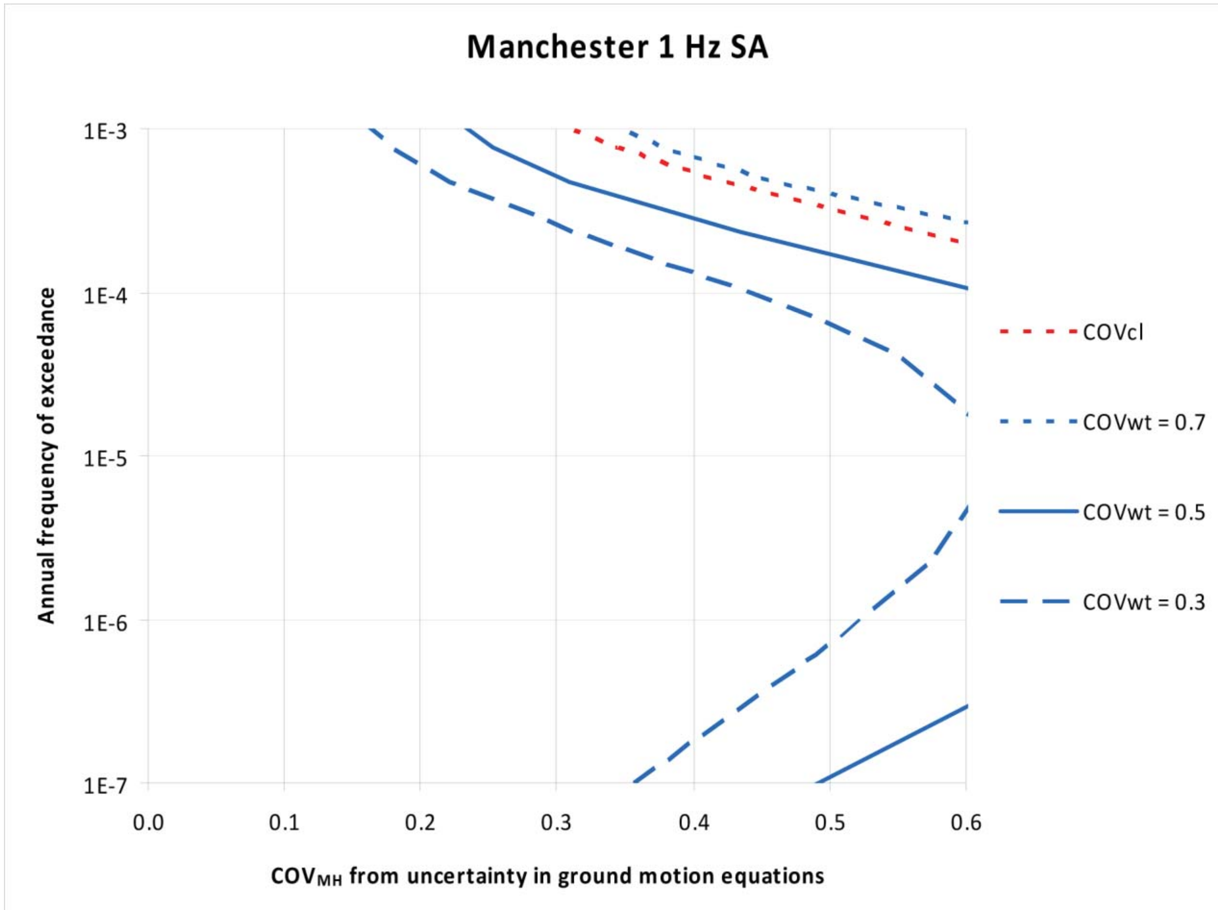

Figure 9.4-12
COV of 1 Hz hazard at Manchester site from ground motion equations vs. hazard

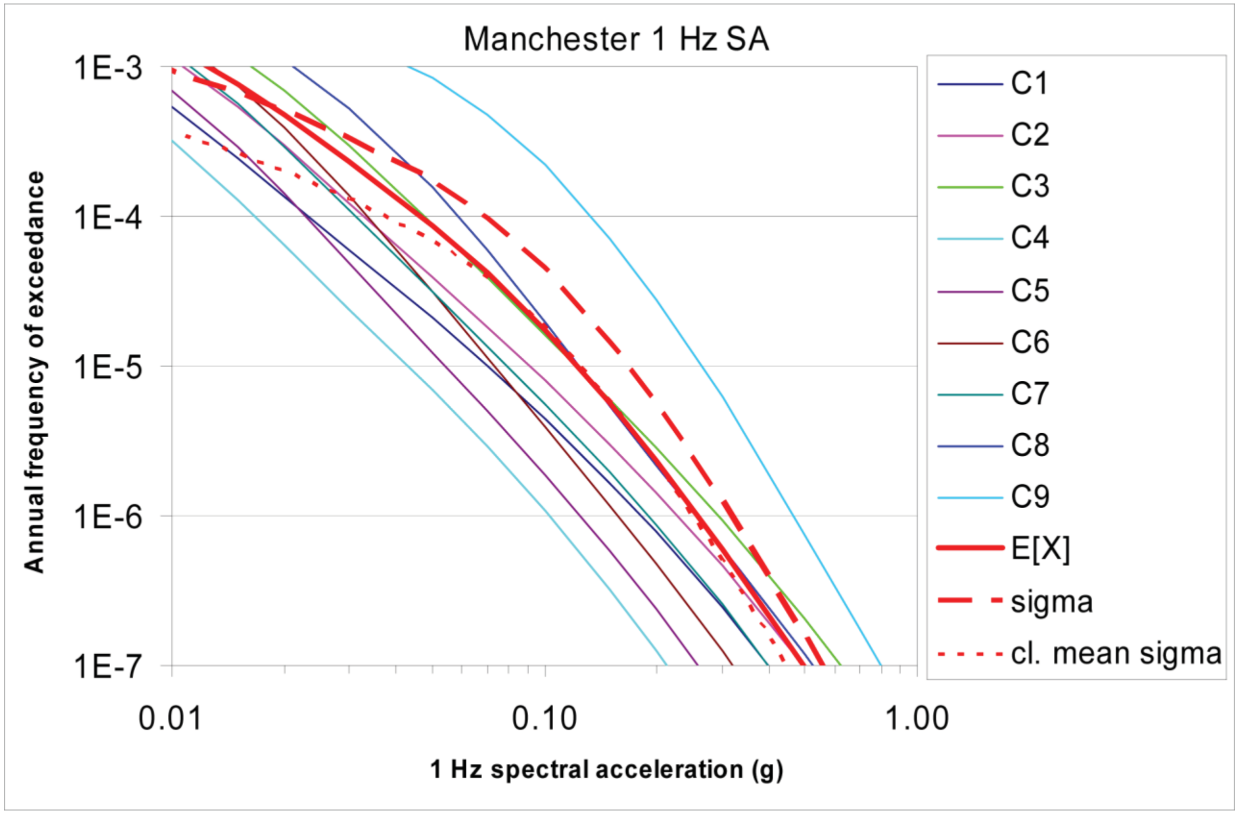

Figure 9.4-13
1 Hz spectral acceleration hazard curves for Manchester test site

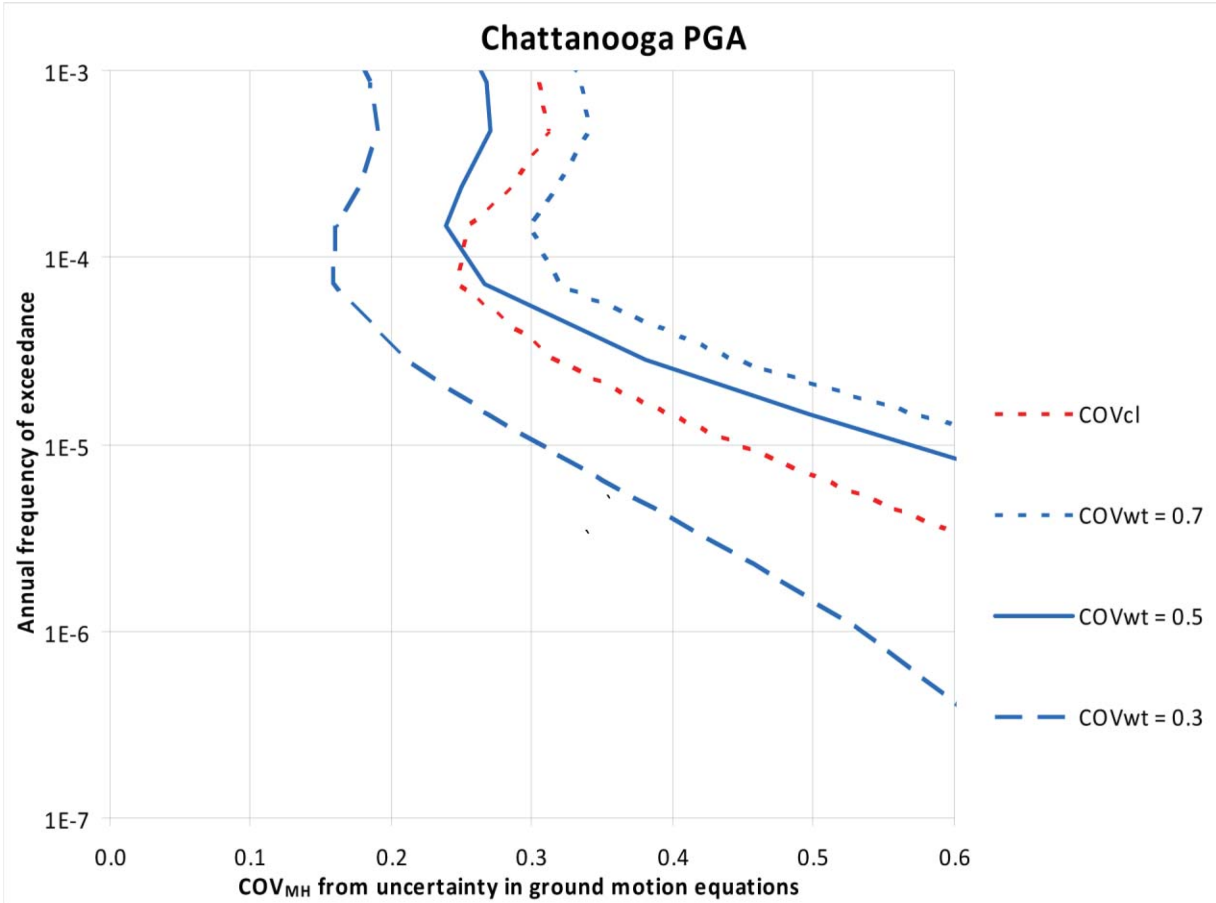

Figure 9.4-14
COV_{MH} of PGA hazard at Chattanooga from ground motion equation vs. hazard

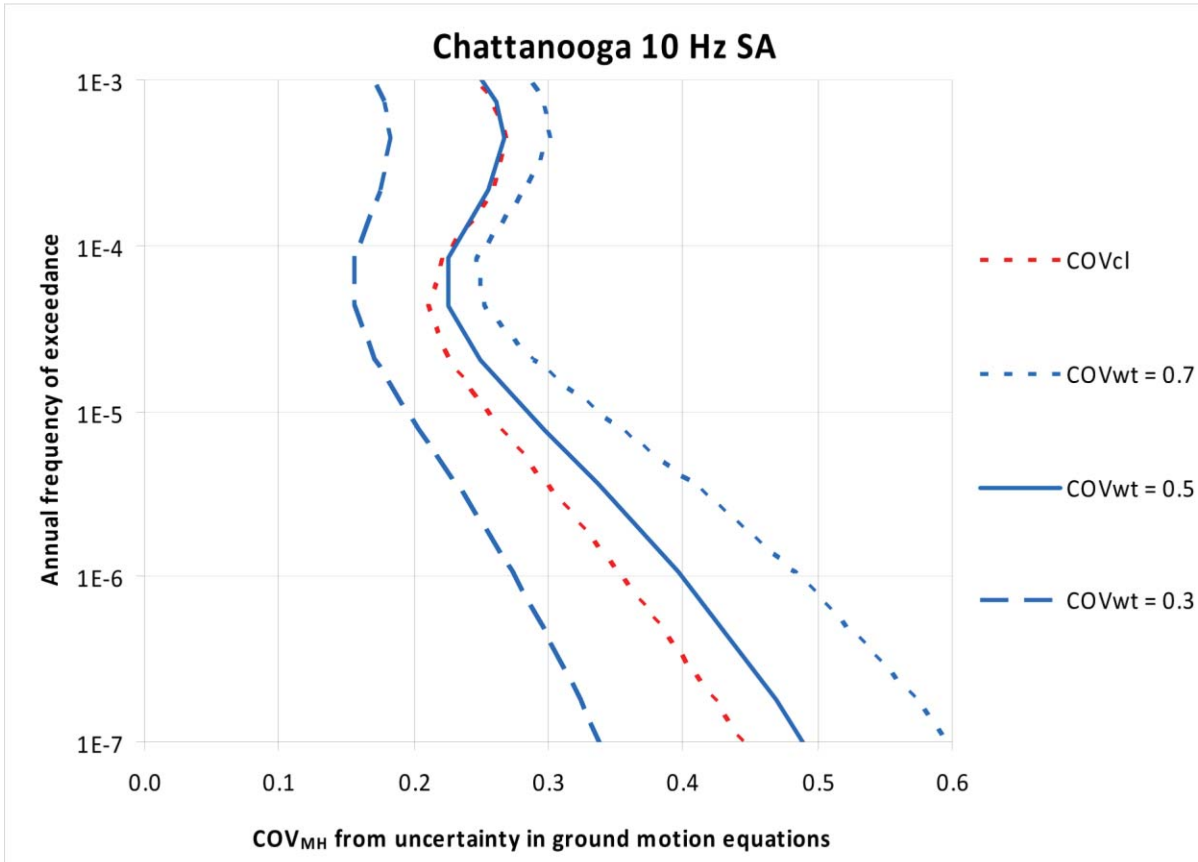

Figure9.4-15
COV_{MH} of 10 Hz hazard at Chattanooga from ground motion equation vs. hazard

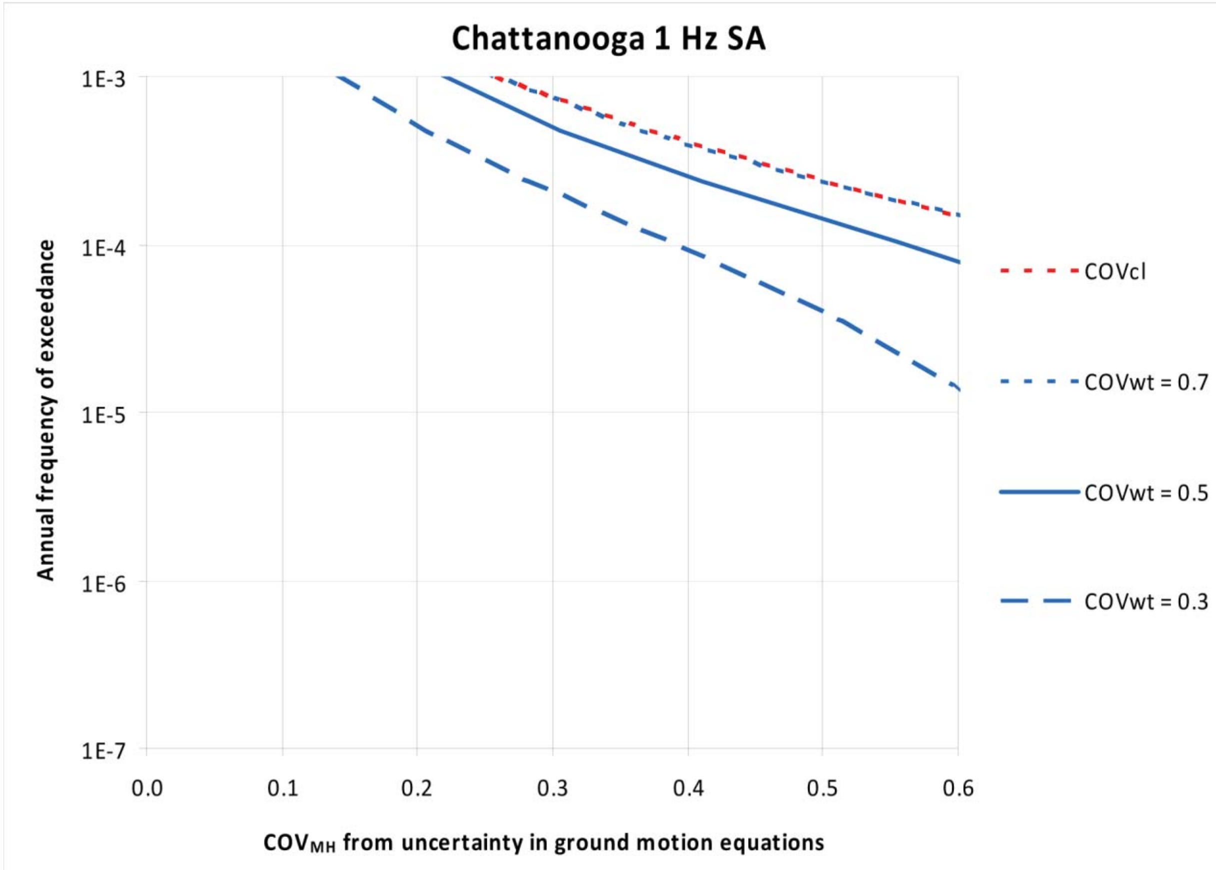

Figure 9.4-16
COV_{MH} of 1 Hz hazard at Chattanooga site from ground motion equation vs. hazard

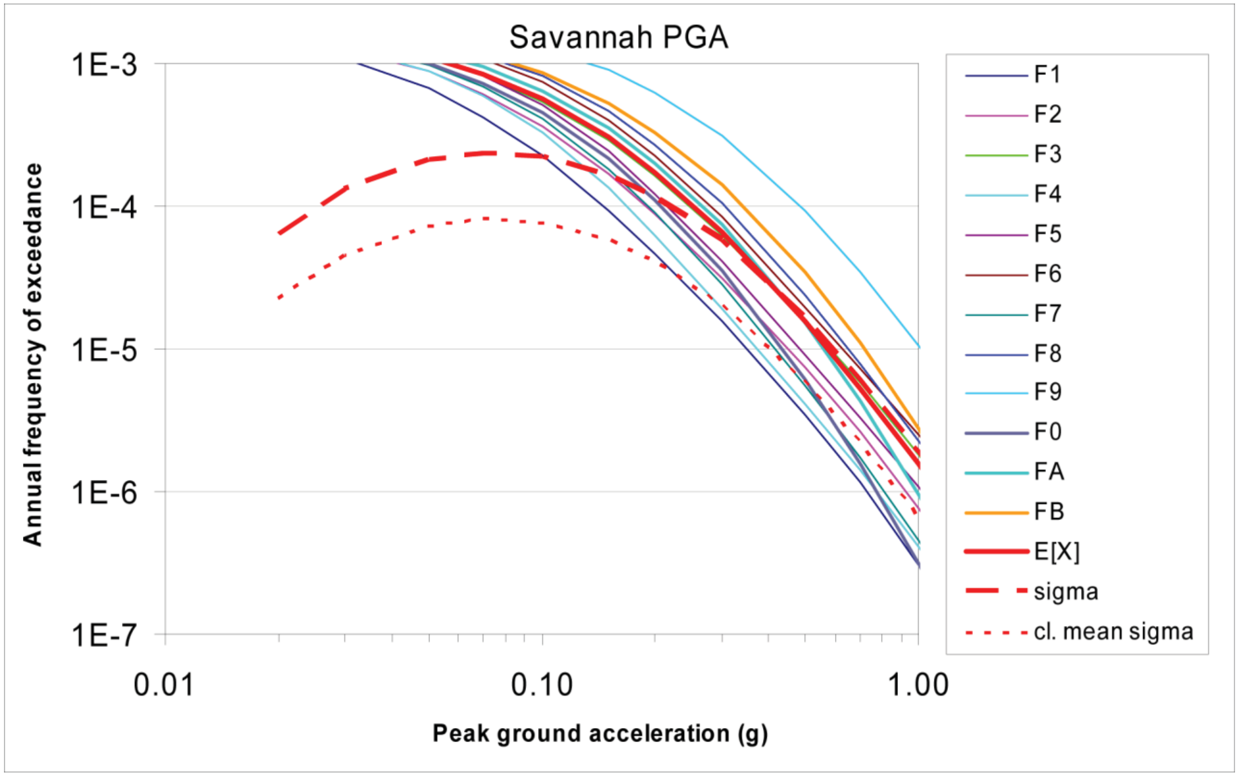

Figure 9.4-17
PGA hazard curves for Savannah test site

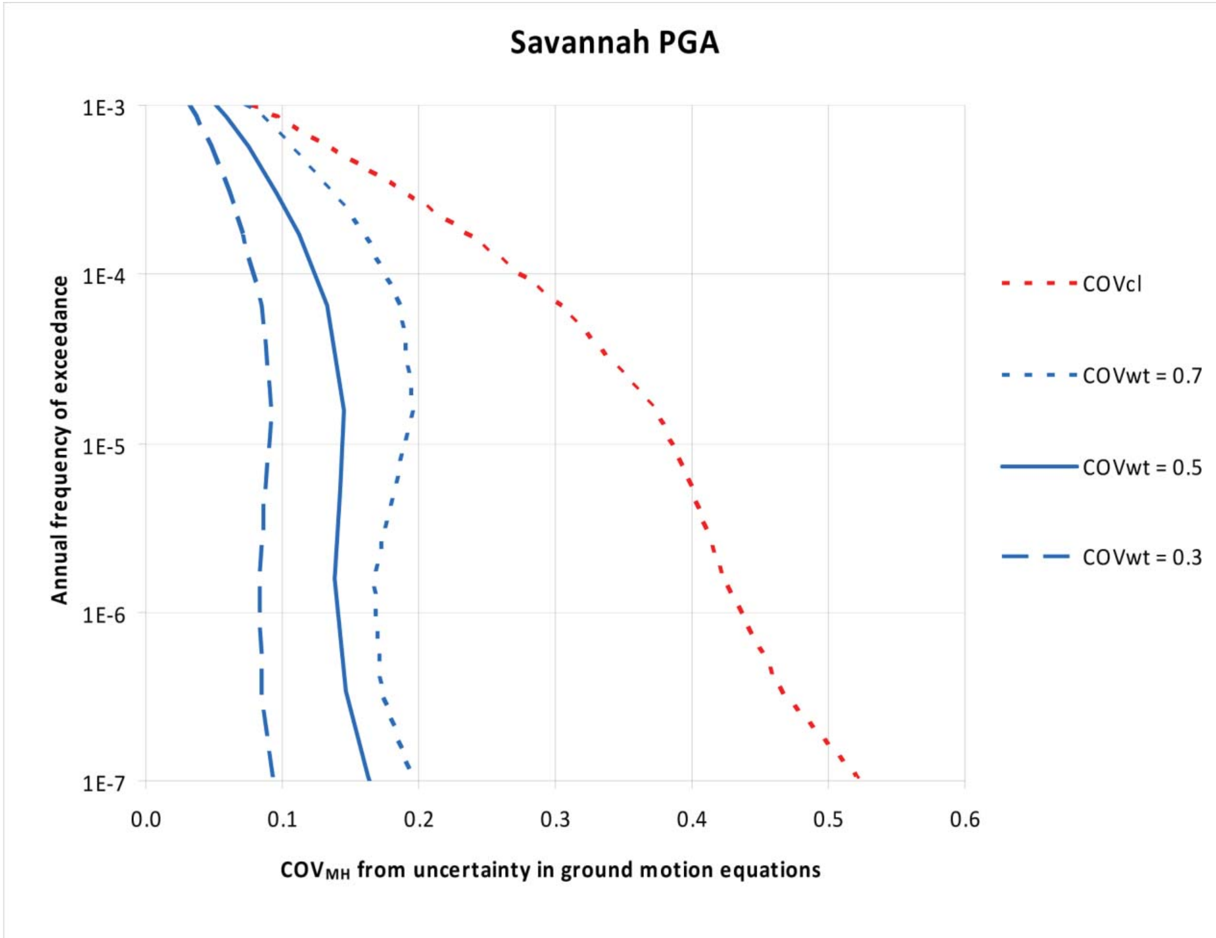

Figure 9.4-18
COV_{MH} of PGA hazard at Savannah site from ground motion equations vs. hazard

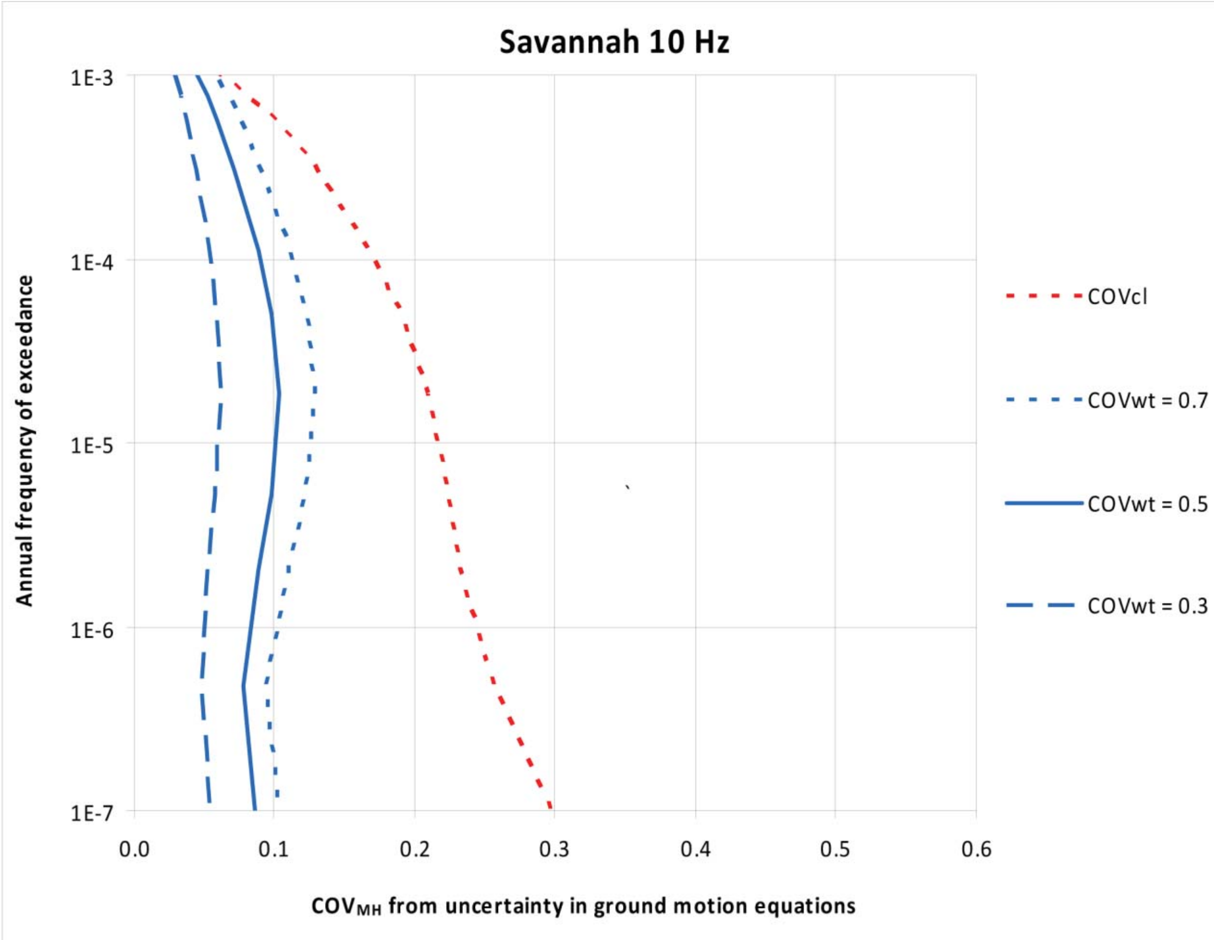

Figure 9.4-19
COV_{MH} of 10 Hz hazard at Savannah site from ground motion equations vs. hazard

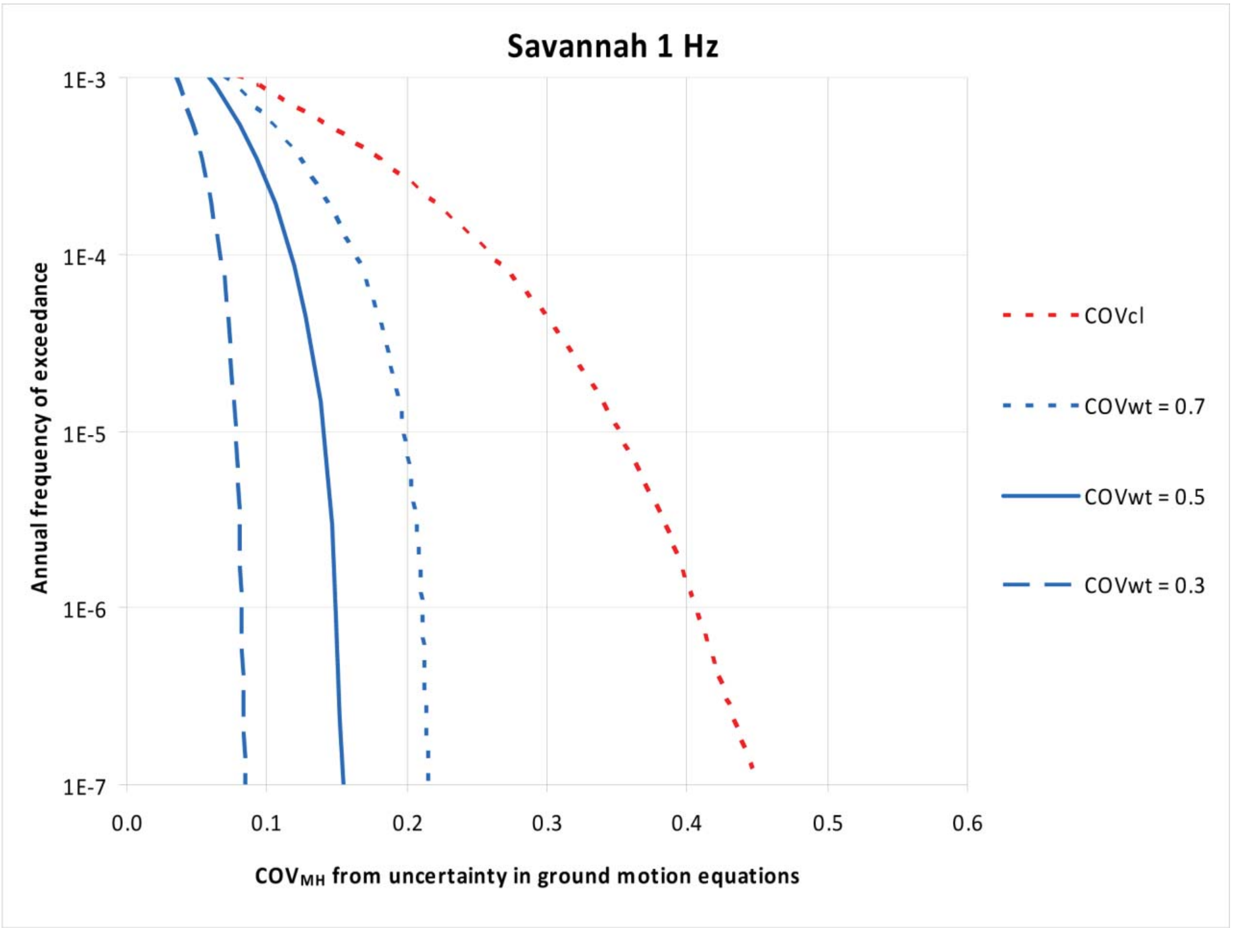

Figure 9.4-20
COV_{MH} of 1 Hz hazard at Savannah site from ground motion equations vs. hazard

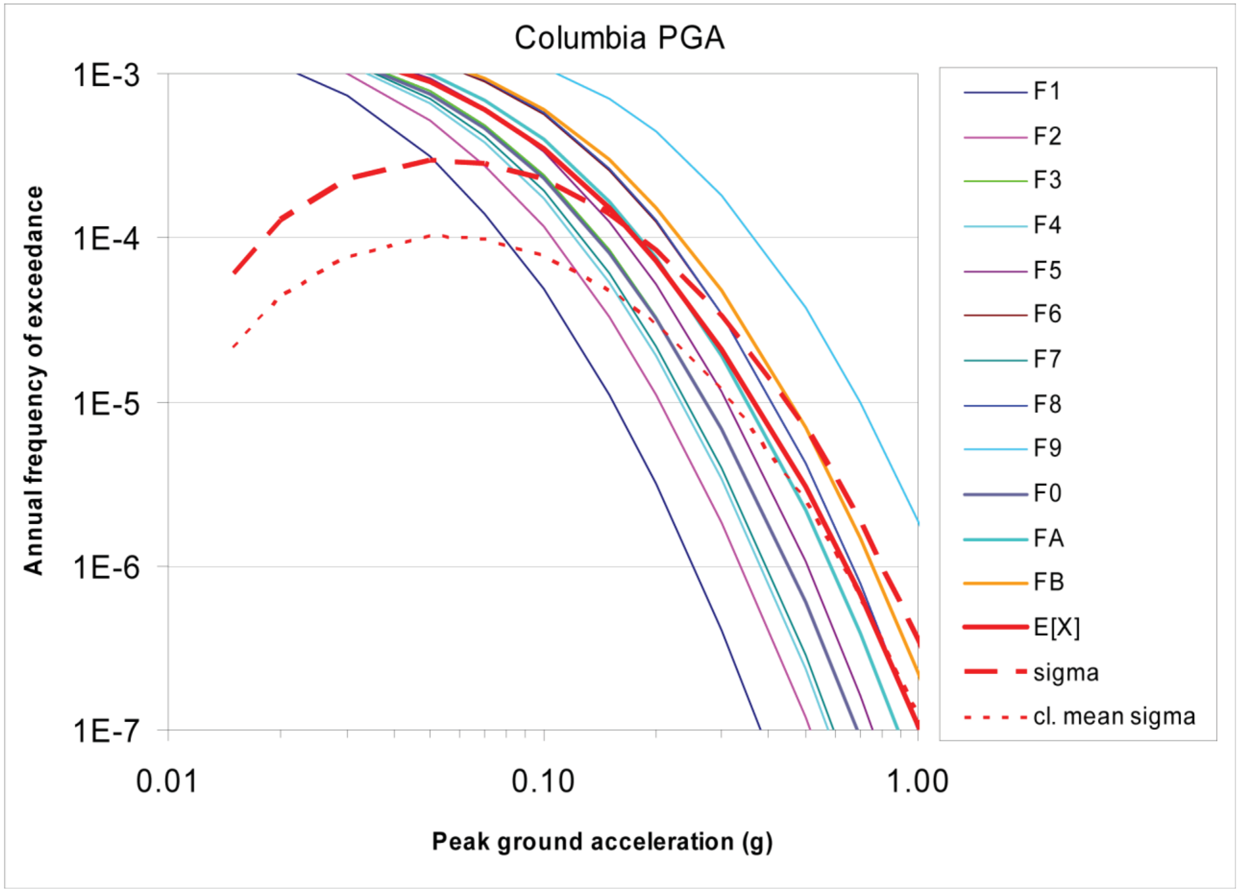

Figure 9.4-21
PGA hazard curves for Columbia site

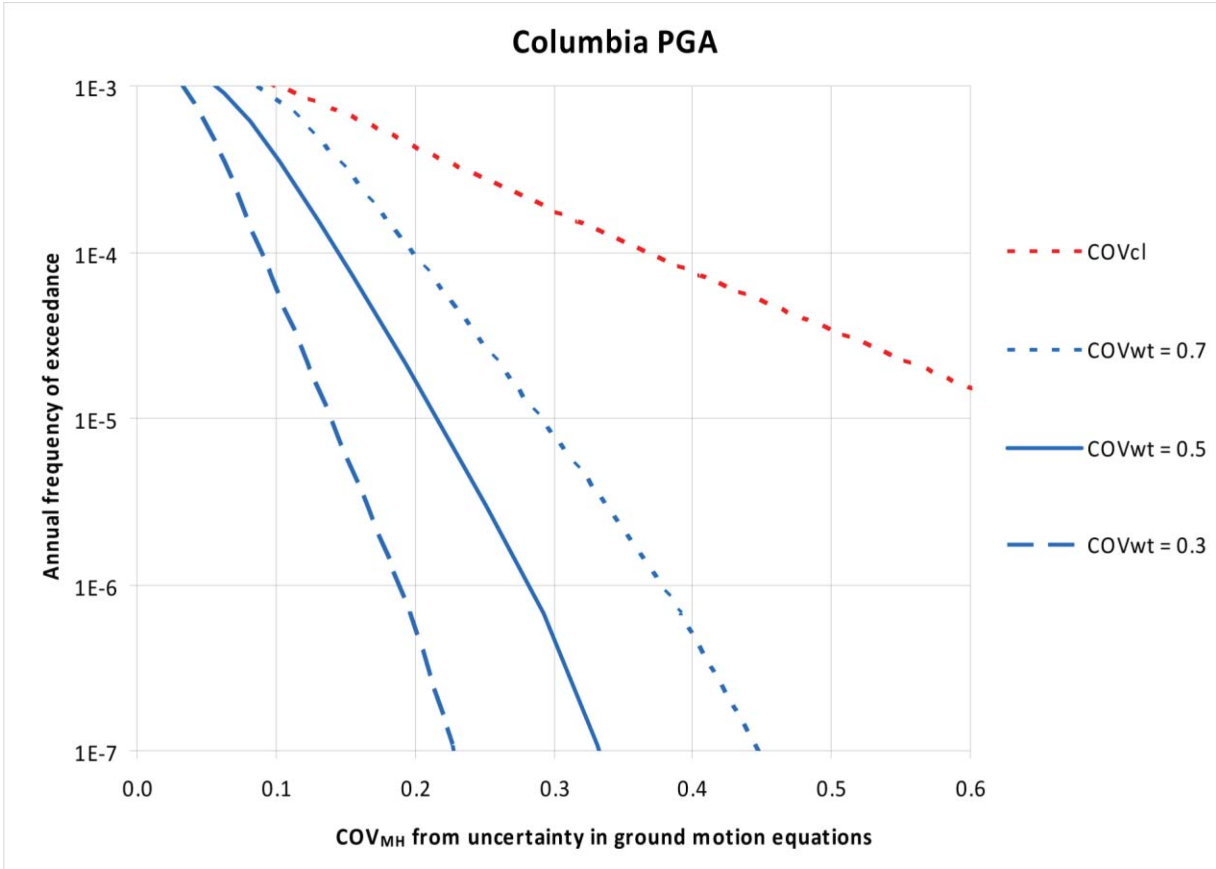

Figure 9.4-22
COV_{MH} of PGA hazard at Columbia from ground motion equations vs. hazard

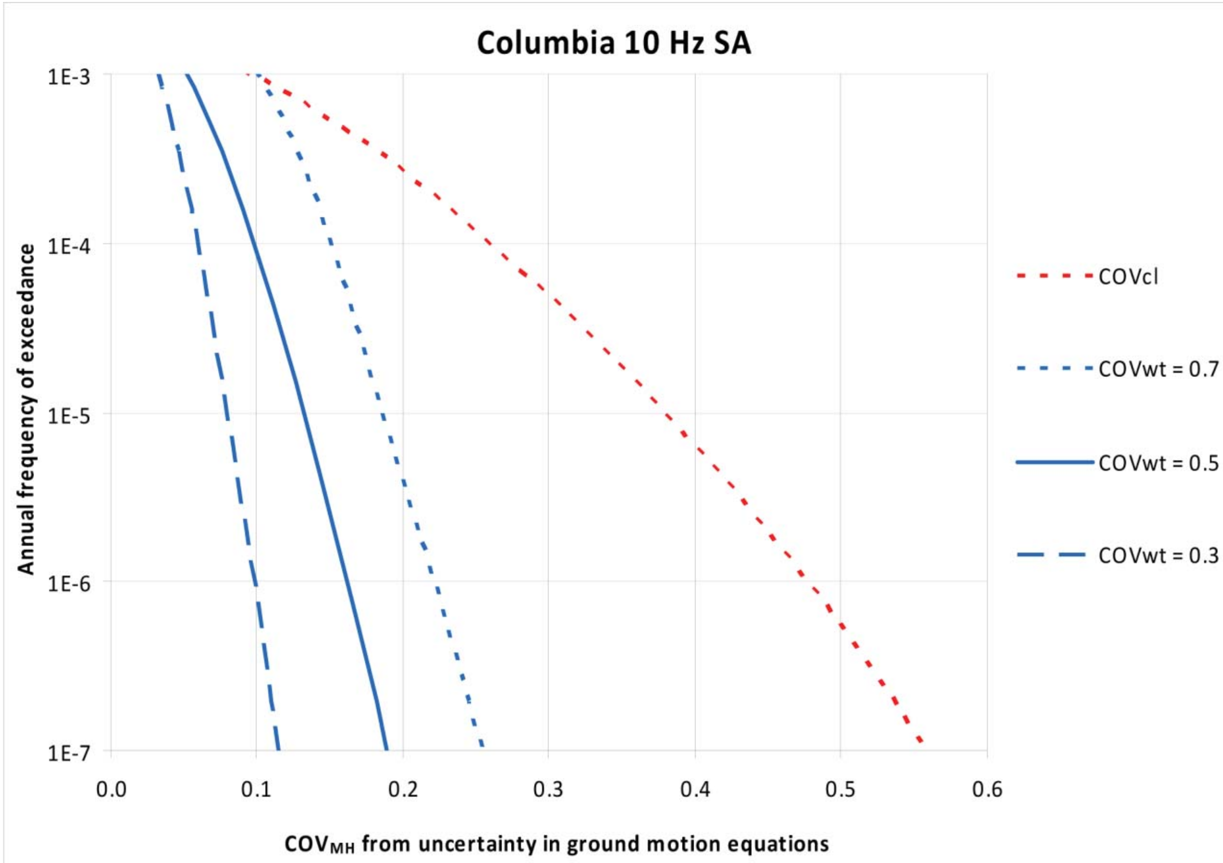

Figure 9.4-23
COV_{MH} of 10 Hz hazard at Columbia from ground motion equations vs. hazard

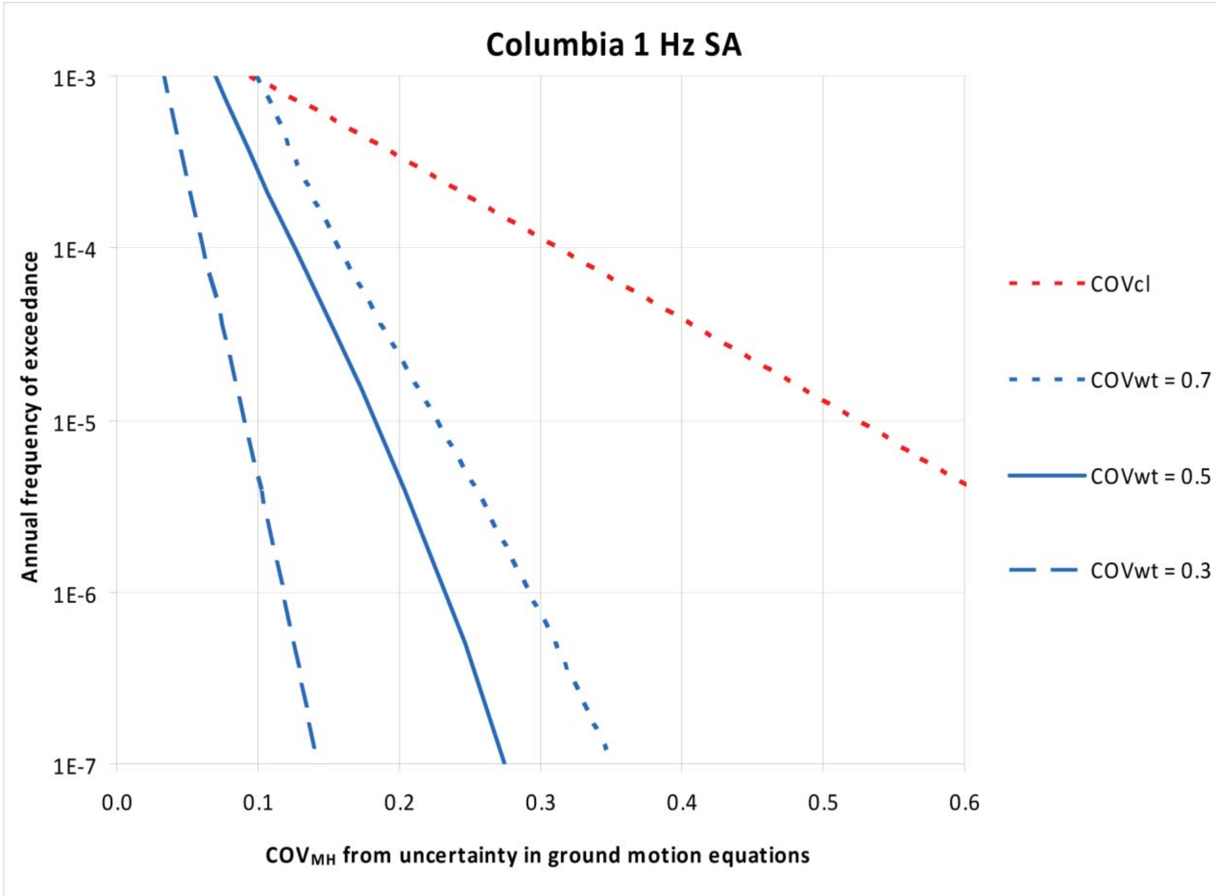

Figure 9.4-24
COV_{MH} of 1 Hz hazard at Columbia from ground motion equations vs. hazard

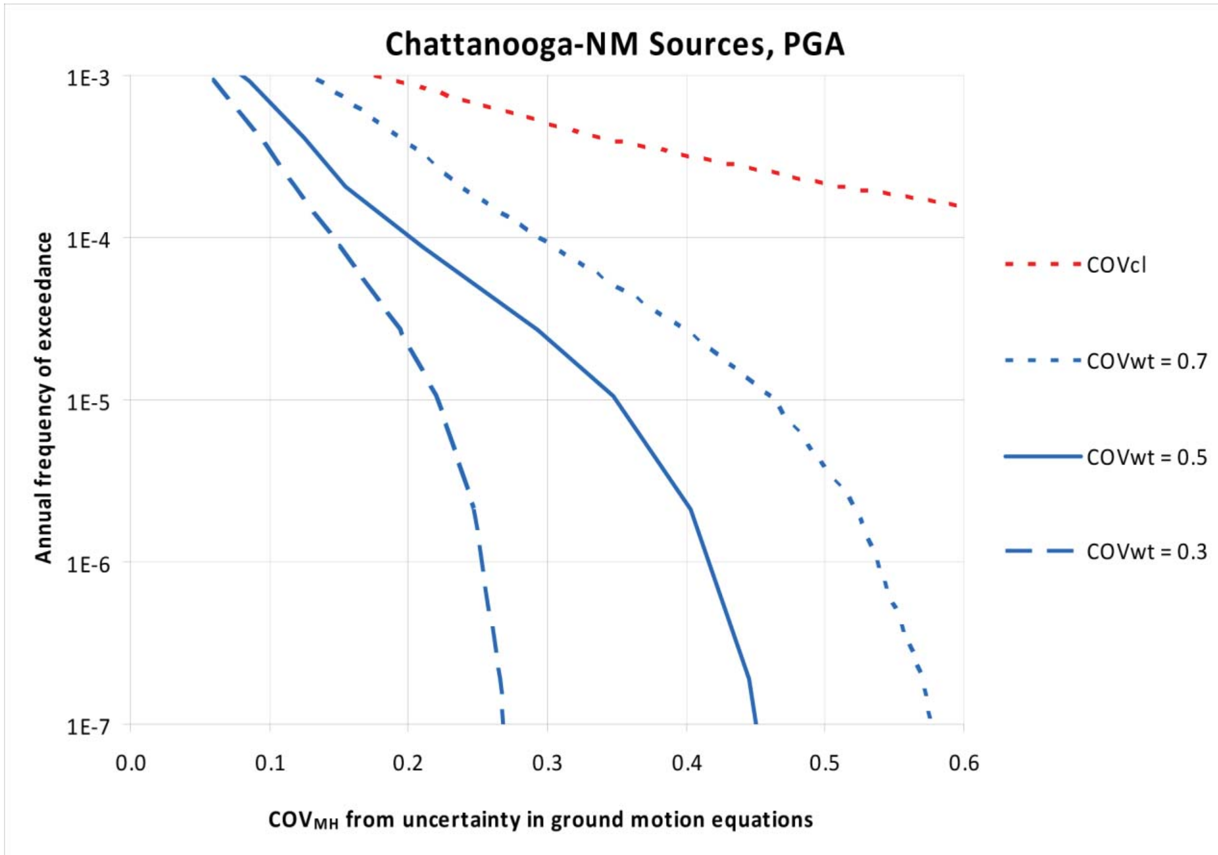

Figure 9.4-25
COV_{MH} of PGA hazard at Chattanooga (New Madrid only) vs. hazard

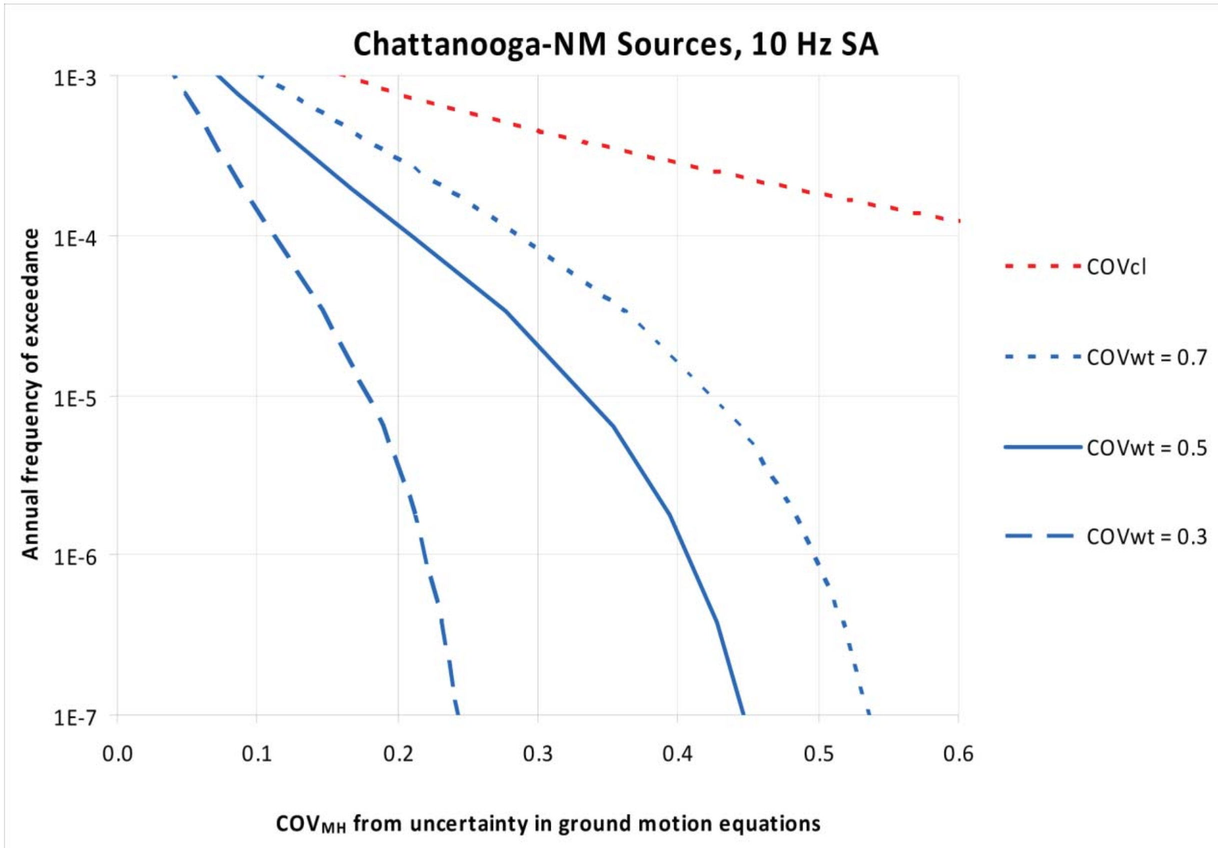

Figure 9.4-26
COV_{MH} of 10 Hz hazard at Chattanooga (New Madrid only) vs. hazard

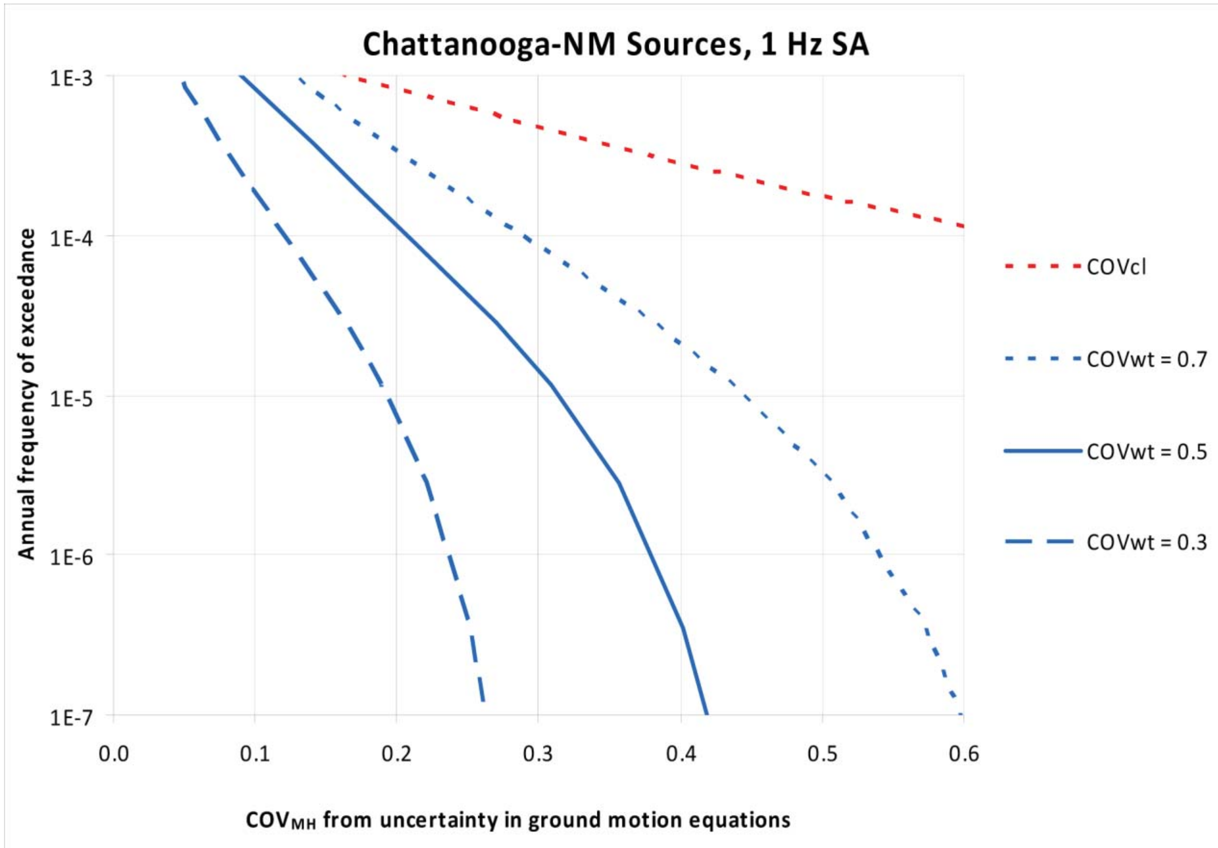

Figure 9.4-27
COV_{MH} of 1 Hz hazard at Chattanooga (New Madrid only) vs. hazard

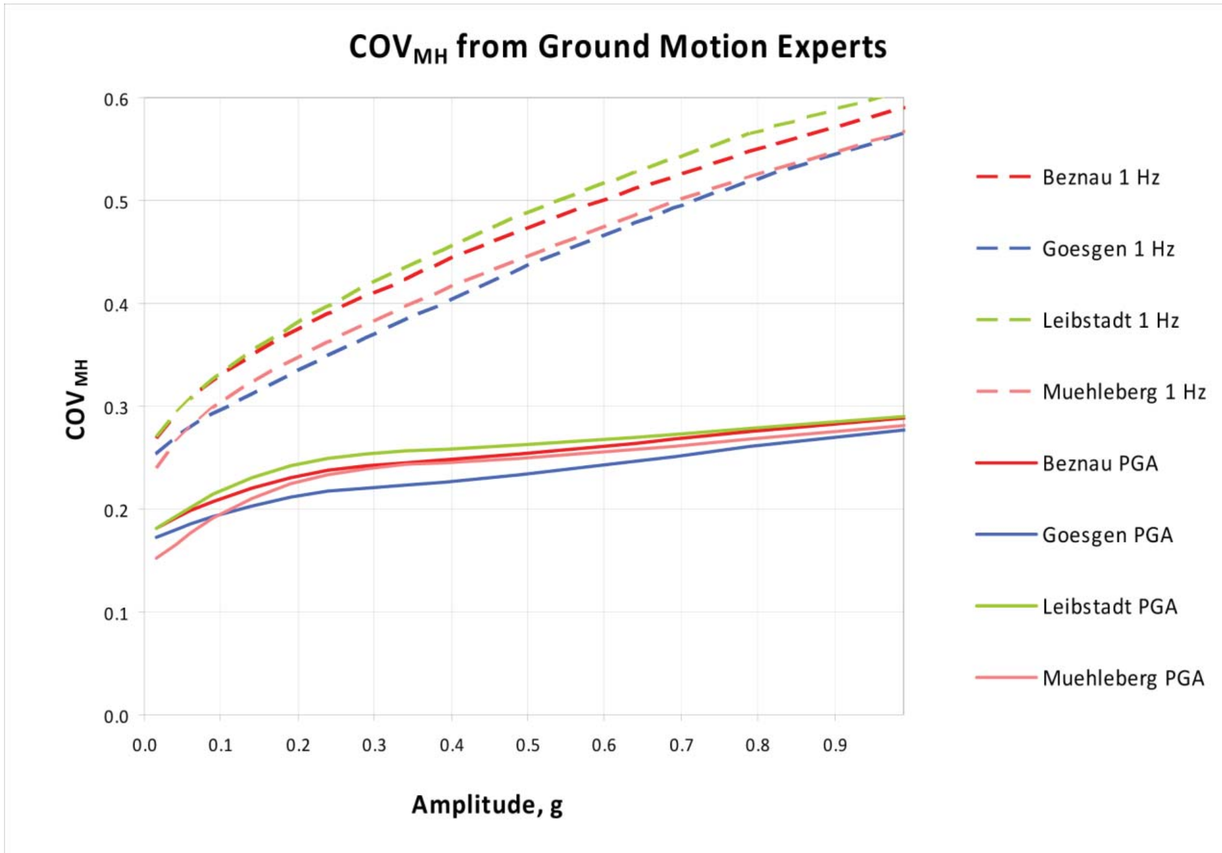

Figure 9.4-28
COV$_{MH}$ for PGA and 1 Hz SA vs. ground motion amplitude resulting from alternative ground motion experts, PEGASOS project

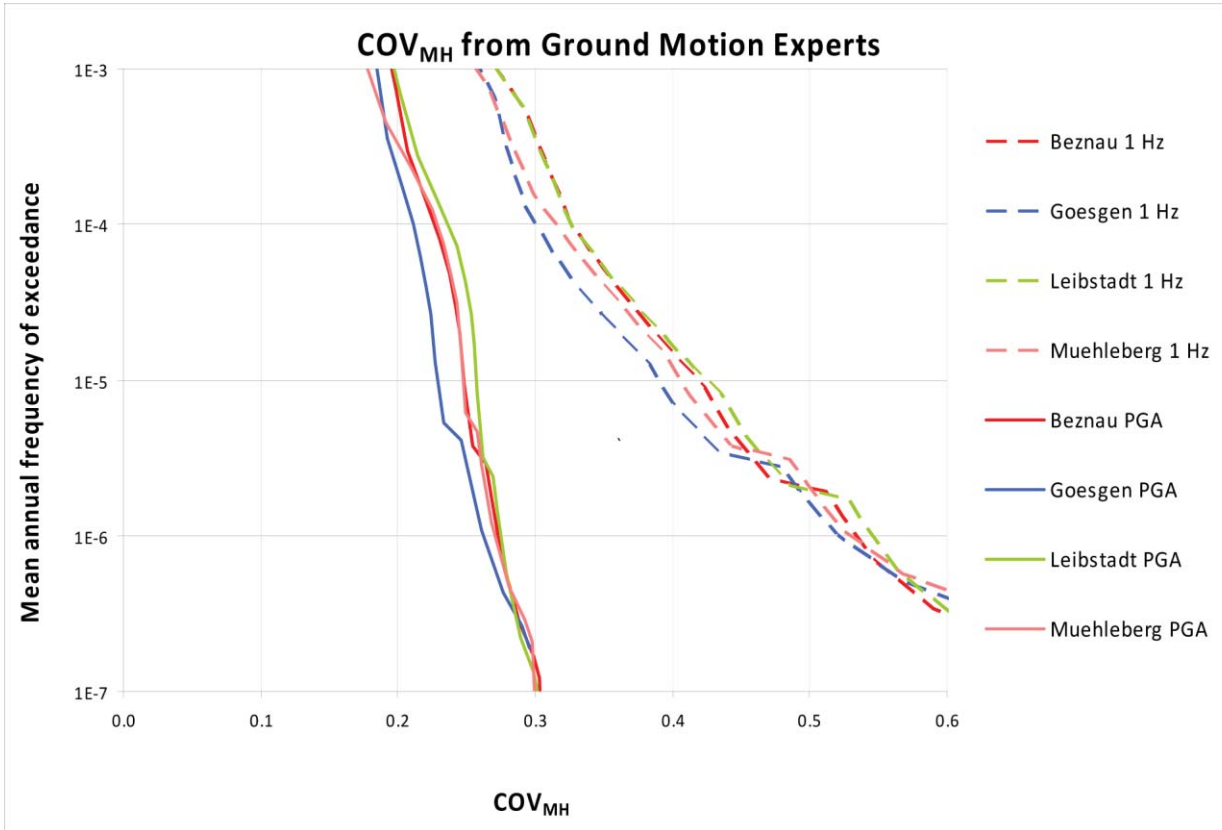

Figure 9.4-29
COV$_{MH}$ for PGA and 1 Hz SA vs. mean hazard from alternative ground motion experts, PEGASOS project

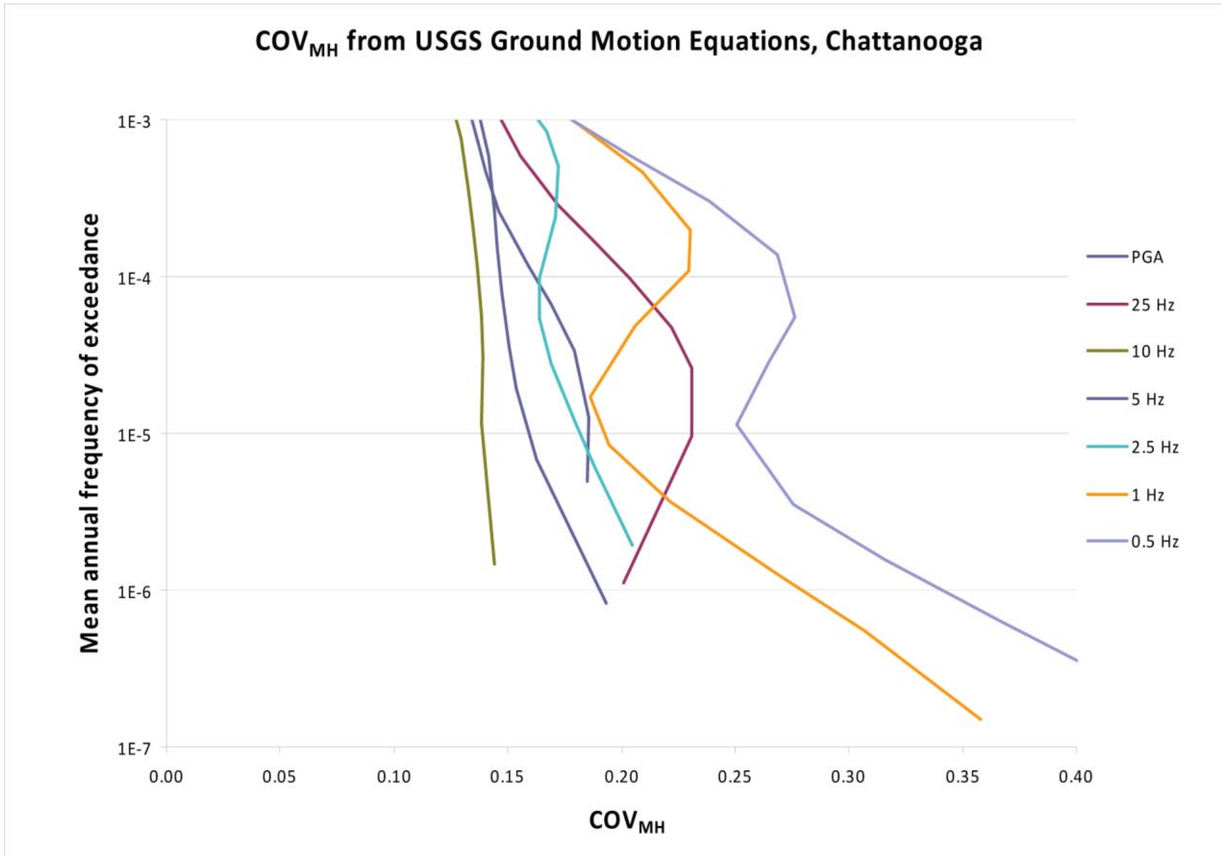

Figure 9.4-30
COV$_{HAZ}$ from ground motion equations vs. mean hazard for Chattanooga

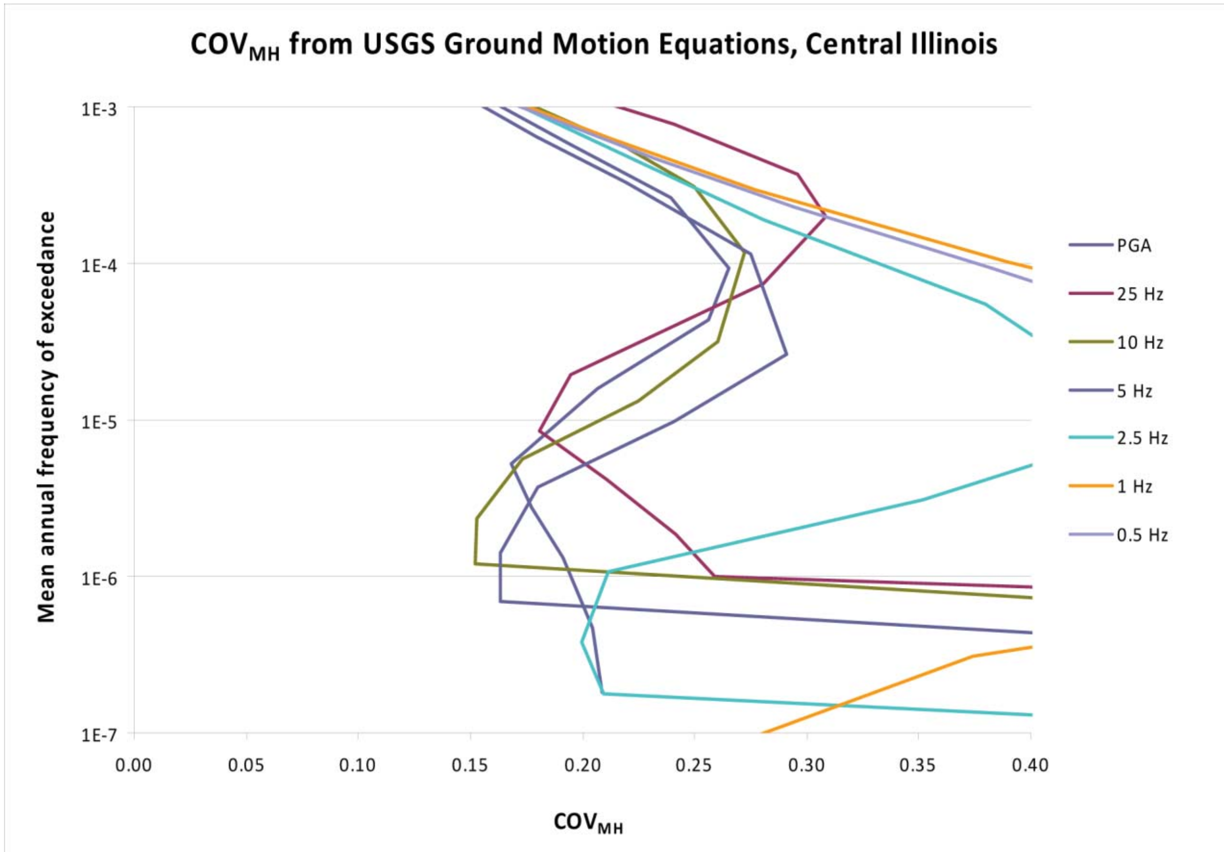

Figure 9.4-31
COV_{MH} from ground motion equations vs. mean hazard for Central Illinois

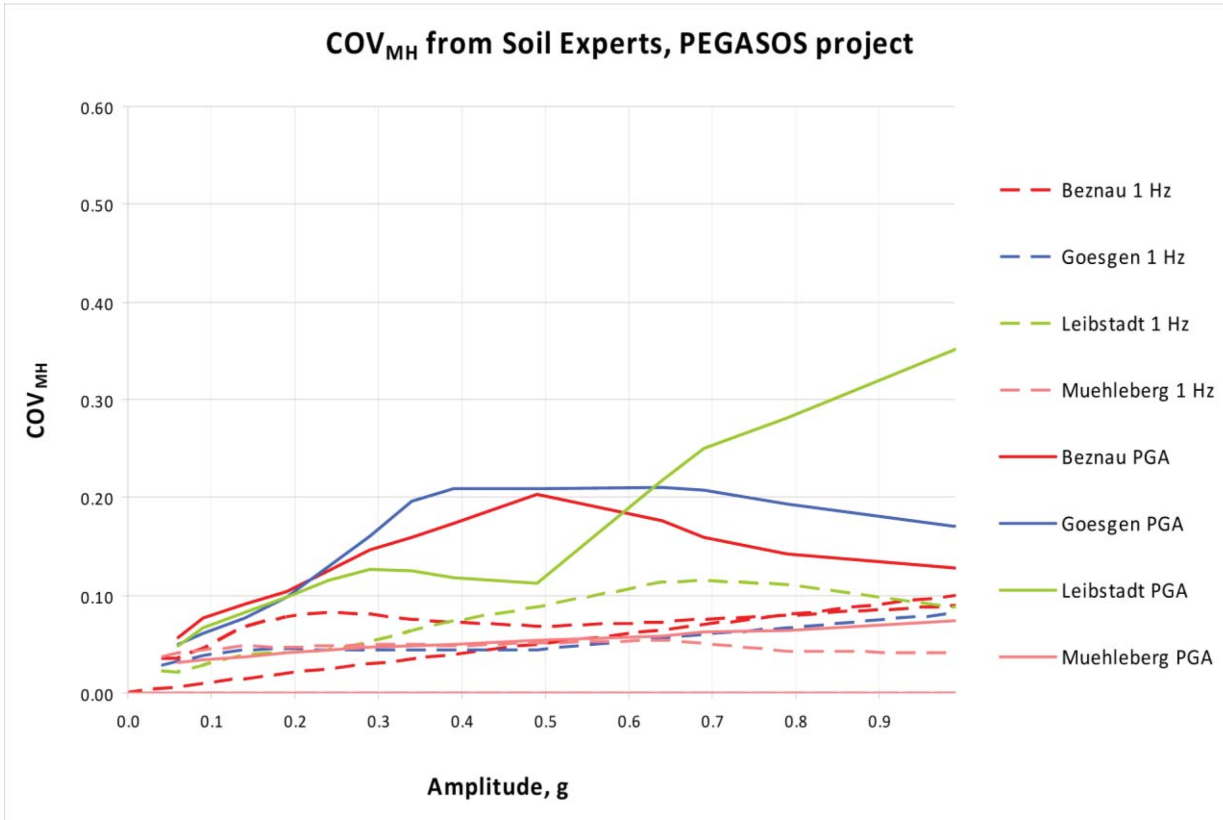

Figure 9.4-32
COV_{MH} from soil experts vs. PGA and 1 Hz SA, PEGASOS project

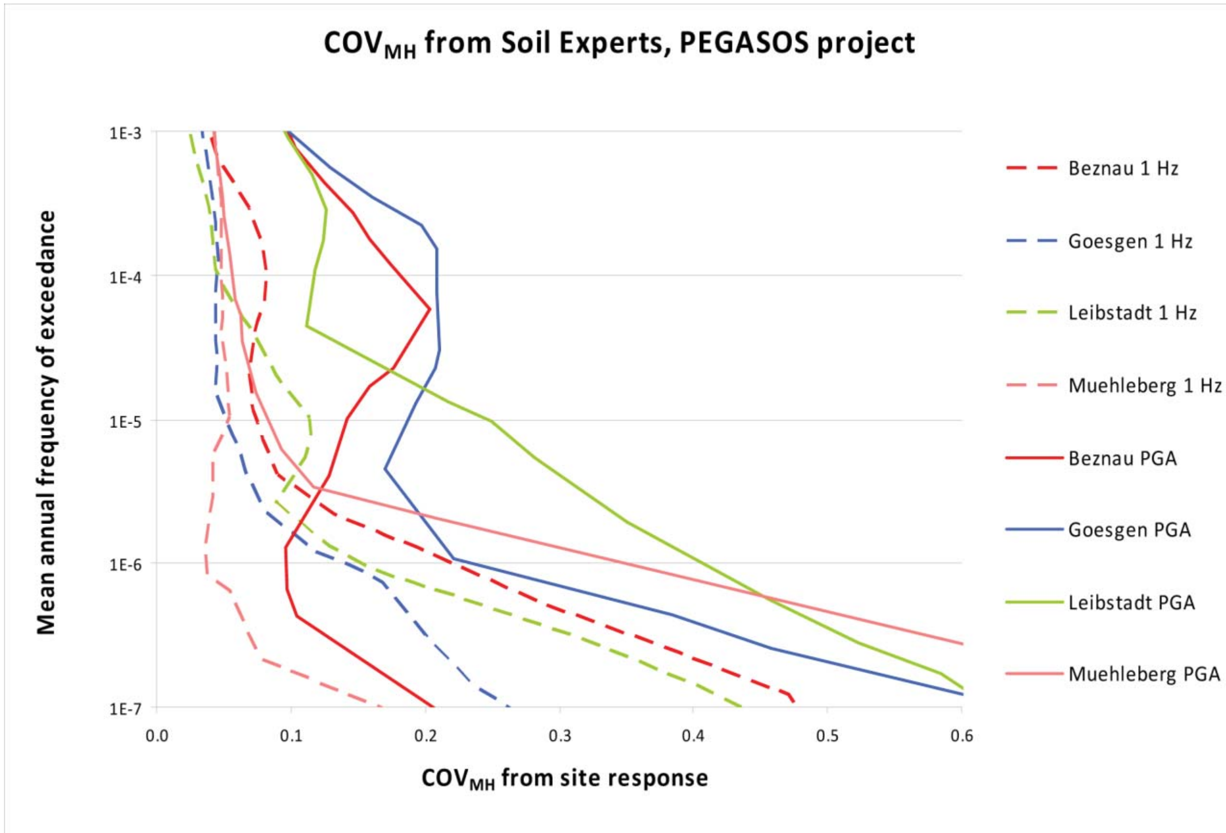

Figure 9.4-33
COV_{MH} from soil experts vs. mean hazard for PGA and 1 Hz SA, PEGASOS project

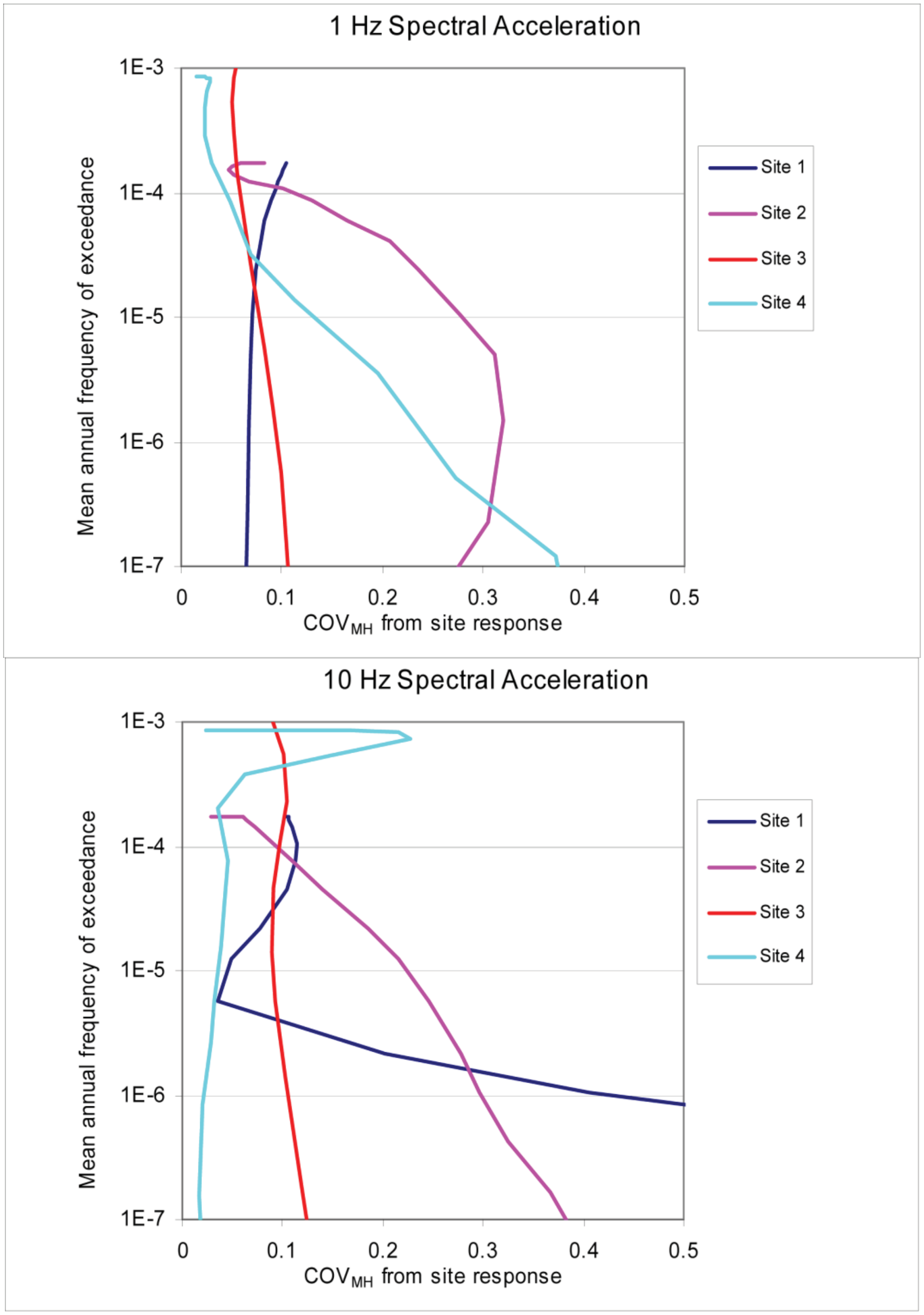

Figure 9.4-34
COV$_{MH}$ resulting from site response models vs. mean hazard for four sites, 1 Hz (top) and 10 Hz (bottom)